Optogenetics in striated muscle: defibrillation of the heart and direct stimulation of skeletal muscles with light

Dissertation

zur

Erlangung des Doktorgrades (Dr. rer. nat.)

der

Mathematisch-Naturwissenschaftlichen Fakultät

der

Rheinischen Friedrich-Wilhelms-Universität Bonn

vorgelegt von
Dr. med. Tobias Brügmann
aus
Gräfelfing

Bonn 2019

Angefertigt mit Genehmigung der Mathematisch-Naturwissenschaftlichen Fakultät der Rheinischen Friedrich-Wilhelms-Universität Bonn.

Die vorliegende Arbeit wurde in der Zeit von Oktober 2013 bis Oktober 2018 am Institut für Physiologie I der Rheinischen Friedrich-Wilhelms-Universität Bonn unter der Leitung von Prof. Dr. Philipp Saße angefertigt.

1. Gutachter: Prof. Dr. Philipp Saße
2. Gutachter: Prof. Dr. Evi Kostenis
Tag der Promotion: 23.5.2019
Erscheinungsjahr: 2019

Table of Contents:

1. Summary

Optogenetic depolarization of cells using the non-selective cation channel Channelrhodopsin-2 (ChR2) provides distinct advantages over electrical stimulation. Using light as stimulus enables precise control over the membrane potential of cells within a specific area of intact organs. Furthermore, the selective overexpression of light-gated proteins allows cell type-specific and pain-free stimulation which could be of great benefit for future scientific and therapeutic approaches.

In my thesis, I explored two potential applications of optogenetic methods in striated muscle: optogenetic defibrillation to terminate ventricular arrhythmia in intact mouse hearts and direct optogenetic stimulation of skeletal muscles. These new approaches could lead in the future to the development of optogenetic defibrillators and laryngeal pacemakers. Most experiments were performed with explanted hearts, isolated skeletal fibers and muscles or larynges from transgenic ChR2 expressing mice. To add translational perspectives, we also explored optogenetic defibrillation and intralaryngeal muscles stimulation after ChR2 gene transfer to wild type mice using adeno-associated virus (AAV).

To investigate defibrillation in explanted mouse hearts, I initially developed a new protocol to enable induction of sustained ventricular arrhythmia using lower extracellular K^+ concentration as well as adding the K_{ATP} channel opener Pinazidil and electrical burst stimulation. Optogenetic defibrillation by epicardial illumination was highly efficient in terminating ventricular arrhythmia in transgenic hearts with an average success rate of 97% when illuminating the whole anterior surface of both ventricles. The success rate of optogenetic defibrillation was depending on the pulse duration, the size of illumination and the light intensity. Importantly, we were also able to terminate ventricular arrhythmia in non-transgenic hearts even one year after AAV mediated gene transfer. The potential applicability of optogenetic defibrillation in the human heart was assessed in experimentally-calibrated computer simulations of a patient's heart with infarct-related ventricular tachycardia. Interestingly, these simulations suggested that the epicardial illumination only terminated the arrhythmia when myocytes at all myocardial depths were sufficiently depolarized to block the wave front propagation. This is in line with the required high light intensities for successful optogenetic defibrillation in the experiments because lower light intensities would only depolarize cells in the epicardial layer. Because optogenetic stimulation would be in principle pain-free in patients, the proof for its feasibility could lay the foundation for the development of a new treatment option for patients at high risk for ventricular arrhythmia. Furthermore our results propose that optogenetic defibrillation is a new tool to investigate the mechanism

underlying electrical defibrillation and could thereby help to improve current treatment strategies.

Direct optogenetic stimulation of skeletal muscle was first proven in isolated *Flexor digitorum brevis* fibers and in intact soleus muscles, which could both be stimulated using brief light pulses. I used isometric force measurements and sharp electrode recordings for in depth biophysical characterization and quantification of force development. The force of light-induced single twitches could be precisely controlled by varying the pulse duration and light intensity. During prolonged illumination (>1s), force declined to the basal level indicating the requirement of short repolarizations for the generation of tetanic contractions by the summation of Ca^{2+} transients. Thus we explored pulsed illumination using various repetition rates to induce maximum tetanic force. Optogenetic stimulation was most efficient with 10 ms long pulses at a repetition rate of 40 Hz reaching ~84% of the maximum force generated by electrical stimulation with 100 Hz. Increasing repetition rate of light pulses over 50 Hz resulted in weaker force because the used ChR2-H134R variant has rather slow off kinetics (~20ms). In line with this, we showed that light pulse rates above 50 Hz lead to continuous depolarization of muscle fibers.

Recurrent nerve paralysis is a severe complication of neck surgery, malignant processes or central neurological diseases and results in a fixed paramedian position of the vocal cords as well as life-threatening dyspnea in the case of bilateral paralysis. Current treatment options consist only of destructive surgery. Unfortunately the use of local electrical stimulation to restore laryngeal function faces severe technical limitations. Therefore I sought to explore direct optogenetic stimulation of intralaryngeal muscles in explanted larynges from ChR2 transgenic mice. Specific illumination of the individual intralaryngeal muscle groups led to an opening or closing of the vocal cords depending on the site of illumination. This proves the sufficient spatial resolution of light for selective stimulation of the intralaryngeal muscles groups. In addition, we were able to induce opening of the vocal cords in wild type mice after AAV-based gene transfer of ChR2 with light. Thus optogenetic stimulation could become a new treatment option for patients suffering from bilateral laryngeal paralysis.

In conclusion, optogenetic stimulation can overcome the severe limitations of electrical stimulation of the heart and skeletal muscles. The new technologies, I have developed and characterized in this thesis, allow for the design of completely new stimulation patterns to address open questions in muscle physiology. Furthermore, optogenetic stimulation of striated muscles could become a new treatment option for patients enabling selective and pain-free stimulation with few side effects.

2. Introduction

2.1 Excitability of muscle cells

Every eukaryotic cell has a membrane consisting of a lipid bilayer which separates and electrically isolates the cytosol from the extracellular space. Charged ions are thereby unequally distributed between the intracellular and extracellular compartment leading to the formation of electrochemical gradients across the cell membrane for each type of ion. Ions can only cross the membrane by active transport or passive conductance through ion channels. Ion channels are proteins within the membrane which form a pore, selective for specific kinds of ions and allow them to cross the membrane along their electrochemical gradient. Therefore, expression of the different types of ion channels, their open probability and single channel conductance determines the membrane potential. Every cell type has its characteristic expression pattern of ion channels and transporters. Normally, the membrane potential is determined by K^+ and Cl^- channels and is therefore negative (Figure 1). In addition, the opening and closing of ion channels can be under control of distinct physical or chemical stimuli leading to change in the current flow through the membrane and thereby the membrane potential over time.

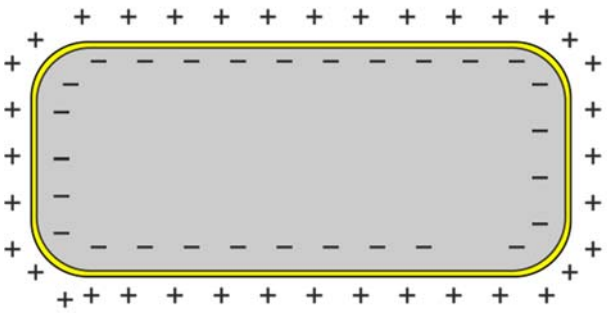

Figure 1: Schematic drawing of a cell and its membrane consisting of a lipid bilayer (yellow) which is impermeable for charged ions. Unequal distribution of ions between the intra- cellular (grey) and the extracellular compartment results in an electrochemical gradient across the membrane. The permeability of the membrane for each ion is depending on which ion channels are open and determines the membrane potential. At rest, the conductance is the highest for K^+ and Cl^- ions resulting in a negative membrane potential.

Neurons and muscle cells are excitable cells, which describes that they can be activated by an external stimulus. This results in a stereotypic sequence of opening and closing of distinct ion channels leading to a rapid change of the membrane potential, known as the action potential (AP). In skeletal and heart muscle cells, the excitation by APs triggers a series of intracellular events which eventually result in the contraction of cells, a process known as excitation-contraction-coupling.[1] Although the overall principle of this mechanism is similar in skeletal and heart muscle cells, the individual steps show variations in both cell types. Therefore I will describe the exact mechanism within both cell types separately in the next paragraphs.

Ventricular cardiomyocytes are normally inactive because of a very stable resting membrane potential which is maintained almost exclusively by the so-called inward rectifying K^+ currents (I_{K1}) through Kir2.1 channels. Therefore the resting membrane potential is close to the Nernst

equilibrium for K^+ at approximately −80 to −90 mV. To evoke an AP, ventricular cardiomyocytes normally require electrical activation from surrounding myocytes which are intercellularly coupled through ion conducting gap junctions. If a propagating excitable wave front arrives at a cardiomyocyte, the membrane potential becomes depolarized by current flow from the adjacent already depolarized cardiomyocytes until the AP threshold is reached. This initiates the AP (phase 0) with a very fast depolarization above +30 mV because of opening of voltage-gated Nav1.5 Na^+ channels. The AP threshold is therefore depending on the availability and the membrane potential required for opening the Na^+ channels and once they are activated, an AP with its stereotypic series of ion channel opening and closing is running automatically without requiring any further external input (Figure 2A and B): Within very few milliseconds (1-5ms), the Na^+ channels inactivate and transient outward Kv4 channels open briefly, leading to outward I_{to} current and a partial repolarization in phase 1 (Figure 2A and C). This is followed by phase 2 with the characteristic AP plateau sustained by inward Ca^{2+} currents through L-type Ca^{2+} channels (Cav1.2) (Figure 2A and B). The flow of Ca^{2+} ions increases the local Ca^{2+} concentration in a small intracellular space between the external cell membrane (the sarcolemma) and the internal membrane of intracellular Ca^{2+} stores, the sarcoplasmic reticulum. This triggers the opening of Ryanodine receptors type 2 and a large release of Ca^{2+} from the sarcoplasmic reticulum, a mechanism termed Ca^{2+}-induced-Ca^{2+}-release.[1] All together these events rise the intracellular Ca^{2+} concentration, a so called Ca^{2+} transient (Figure 2A), which initiates contraction of the cell. At the end of the AP (phase 4), Ca^{2+} channels close and the repolarizing K^+ hERG (I_{Kr}) channels and KvLQT (I_{Ks}) channels open leading to the return to the resting membrane potential and reactivation of I_{K1}(Figure 2A and C).[2,3]

The comparably long AP duration in cardiomyocytes (300-400 ms) resulting from the Ca^{2+} currents during phase 2 and the biophysical gating mechanism of Nav1.5 prevent a fast reactivation of the Na^+ channels because they are in an inactivated state until the membrane potential is repolarized below −50 mV. The time period during which myocytes cannot be activated because of this mechanism is called refractory period and ensures the rhythmic and concerted electrical activity of the heart important for sufficient cardiac output.

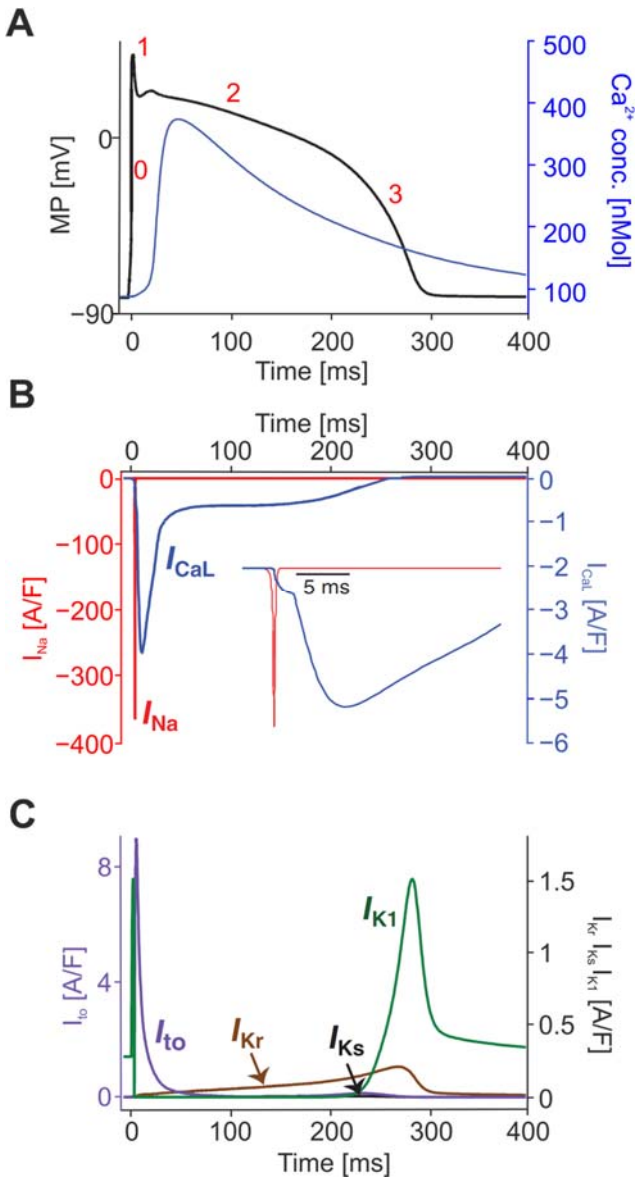

Figure 2: The cardiac AP and the underlying ion currents in a ventricular cardiomyocyte. (A) Overlay of the typical AP shape (black) with the AP phases marked in red and the corresponding intracellular Ca^{2+} transient (blue). (B) Corresponding timing of Na^{+} (red) and Ca^{2+} (blue) inward currents during the cardiac AP. Note the sequential occurrence highlighted in the insert. (C) Overlay of the repolarizing K^{+} outward currents I_{to} (purple), I_{Kr} (brown), I_{Ks} (black) and I_{K1} (green) during the different phases of the cardiac AP (corresponding to A). Figure has been modified from Bartos DC et al., Comprehensive Physiology 2015.[3] MP: membrane potential; I: current density.

In contrast to the electrically well-coupled cardiomyocytes, skeletal muscle fibers do not express gap junctions and are electrically isolated from each other. This allows them to be individually activated by their respective motor neurons. In addition, each skeletal muscle is comprised of different types of muscle fibers. The slower contracting type generates less force but is also less prone to fatigue development during continues activation. This is why the slow muscle fiber types are normally activated first, especially when steady contraction over prolonged time period is desired. In contrast, faster muscle fiber types can generate more force but only during shorter time periods and become therefore activated only if high force generation for short time periods is required. For skeletal muscle contraction, an AP must be evoked in a motor neuron and propagated along the axon to the presynaptic end where it results in an opening of neuronal Ca^{2+} channels. The elevated Ca^{2+} concentration in the presynaptic

terminal is leading to exocytosis of vesicles containing the neurotransmitter acetylcholine. Within the neuromuscular junction, acetylcholine activates nicotinic acetylcholine receptors at the postsynaptic side, which is the so called motor endplate of the skeletal muscle fiber. This results in opening of the non-selective nicotinic acetylcholine receptors leading to Na^+ inflow and little depolarization. Subsequently an AP starts by activation of large and fast Na^+ currents through $Na_v1.4$ channels. To ensure that every neuronal stimulus successfully triggers an AP, the $Na_v1.4$ channel density is 3-7 times higher around the motor endplate implying lower excitability at the other parts of the muscle fiber. Depolarization subsequently activates the skeletal isotype of L-type Ca^{2+} channels ($Ca_v1.1$) which act primarily as voltage sensors and directly activate Ca^{2+} release via ryanodine receptors type 1 from the sarcoplasmic reticulum leading to a rise in Ca^{2+} concentration and contraction. Because the skeletal L-type Ca^{2+} channels do not contribute significantly to the AP shape,[4] the skeletal muscle fibers repolarize very quickly within 1-4 ms after the AP onset. The fast repolarization is due to the fast inactivation of the Na^+ channels and supported by repolarizing K^+ and Cl^- currents.[5] For the K^+ currents, a slow and fast type of voltage activated delayed outward K^+ channels has been described in slow fibers whereas only the fast channel type is present in fast fibers in rats.[6] In contrast to cardiomyocytes, the resting membrane potential of skeletal muscle fibers is 70% due to conductance of Cl^- ions and only 30% is attributed to K^+ currents.[5,7] Due to the fast repolarization of the AP, the refractory period for re-excitation is much shorter than the duration of the Ca^{2+} transients. Thus a closely timed second stimulus can evoke a second AP leading to the summation of Ca^{2+} release events. This results in increased force generation during so called tetanic contractions of skeletal muscles,[4] a feature which is not present in the heart muscle.

Taking together, ventricular cardiomyocytes and skeletal muscle fibers are normally inactive unless they are electrically excited by surrounding cardiomyocytes or neuronal input, respectively. Once the voltage threshold for Na^+ channel activation is reached, a free-running AP triggers cytosolic Ca^{2+} increase and thereby contraction. Despite an overall similar principle, details within the excitation-contraction coupling machinery are different between both cell types with a profound impact on their electrical excitability.

2.2. Electrical stimulation

The first description of electrical stimulation of muscle cells was made in the 18th century by Luigi Galvani. In his opus "*De viribus electricitatis in motu musculari"*, he reported that the muscles of frogs' legs start contracting when they were getting in touch with an electrical spark. Not only did these observations lead to the development of electrical stimulation of muscles

per se, they also laid the foundation for the whole field of electrophysiology and electrochemistry.[8] Electrical stimulation of excitable cells can be performed in two ways: either a current is injected directly into the cytosol of one cell via an intracellular electrode or an extracellular electrical field is generated by two electrodes placed outside of the cells or the tissue. Both methods rely on sufficient depolarization above the threshold to evoke a free-running AP. However, there are important technical and mechanistic differences which are described in detail in this chapter.

2.2.1 Intracellular stimulation

Intracellular stimulation relies on the patch clamp technique and requires the access of the patch pipette to the cytosolic part of the cell. Glass pipettes with a silver electrode inside and very small openings (typically 1-3 mm diameter) are brought adjacently to the cell membrane in order to establish a tight seal with GΩ resistance between the membrane and edge of the pipette. By applying negative pressure, the cell membrane is disrupted within the pipette opening. The cytosol is now directly connected to the pipette solution in the so-called whole-cell-mode and is thus electrically coupled to the pipette electrode with a series resistance in the range of 10 MΩ. This allows measuring the membrane potential in the current clamp mode and its tight control by current injection into the cytosol.[9]

Unfortunately getting access to the cell is technically challenging, requires one electrode per cell and is typically limited to a maximum of two cells which can be investigated and stimulated simultaneously. In addition, the pipettes are made of glass which complicates its use in contracting single muscle cells and in moving organs such as the beating heart or contracting skeletal muscles. In excitable cells, the injected current charges the membrane uniformly leading to depolarization until the threshold of Na^+ channels for generation of a free-running AP is reached. Because of the relatively high membrane resistance, the amount of current required to excite isolated muscle cells is considerably low and the current injection to evoke APs in single cells is rather unproblematic. Importantly, this approach allows in principle precise control of the membrane potential of the whole cell without spatial differences (Figure 3). Measuring simultaneously the membrane potential enables feedback control and allows keeping the cells at a chosen membrane potential throughout the whole cell (voltage clamp mode) with minor risk of so-called loss-of-voltage-control, at least in small cells.[10]

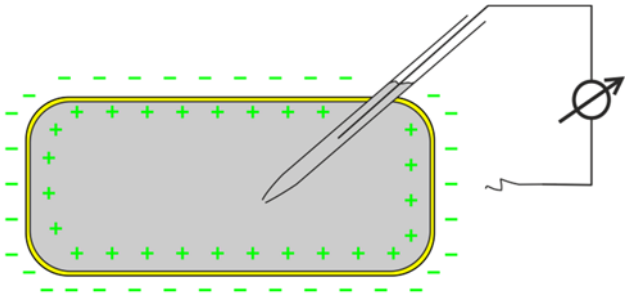

Figure 3: Intracellular electrical stimulation of a cell. To get access to the intracellular compartment, the patch pipette is attached to the cell surface and the membrane within the opening of the pipette is disrupted. Thereby the cytosol is directly connected to the electrode allowing homogenous voltage control by current injection.

In contrast, a spatially uniform control over the membrane potential is not possible in larger cells or electrically coupled syncytium of cells such as the much longer adult skeletal muscle fibers[11] or the well-coupled cardiomyocytes in the intact heart, respectively. Because of the hole in the cell membrane and the relative large solution volume in the patch pipette, the intracellular fluid is rapidly dialyzed. While this effect can be utilized to adjust the concentration of some intracellular compounds, it also leads inevitably to wash out of many important cytosolic components resulting in a "run down" of channel activity and limitation of the experiment time to several minutes.[12] In conclusion, intracellular electrical stimulation can be used to trigger APs in excitable cells and allows fine-grain and sustained control of the membrane potential but requires the use of electrodes affecting the cytosol and is restricted to isolated single cells.

2.2.2 Electrical field stimulation of single cells

Extracellular field stimulation of single muscle cells can be performed using two electrodes in the extracellular solution surrounding the cells. Within the electrical circuit, the electrodes and the extracellular solution have different electrical behavior. The electrodes carry the current by electron transfer and the solution carries charge by ion movement. Because of this physical difference, current injection into the electrical circuit leads to building of an interphase between the electrodes and the external solution to enable transfer of the charges to close the electrical circuit. This charge transfer between electrodes and solution can happen by two different mechanisms in dependence of the amount of electrical energy fed into the circuit. If the current injection is small and short, the current passes through the solution by redistributing charged ions within the fluid without real electron transfer from the electrode to the solution. This process is called the non-faradic or capacitive reaction because the interphase between the electrode and the solution can be regarded as capacitator. Importantly, this process is fully reversible and considered to be harmless. Above a certain threshold, electrons are exchanged between the ions within the solution and the electrodes by chemical reactions. This second mechanism is called faradaic reaction consisting of redox processes which are predominantly non-reversible. Unfortunately, the resulting end-products like reactive oxygen species, O_2, Cl_2

and H_2 diffuse away from the electrode and can be toxic to the cells.[13] Therefore the duration of electrical pulses is limited to the millisecond range (3-5 ms maximum), and also pulsed stimulation of cells over prolonged time periods is technically very challenging because it requires constant exchange of the extracellular fluids to wash out the toxic reagents.

At a certain distance from the electrodes and the interphases, the so called far-field, the energy of the electrical field is the same and influences the cells indirectly due to the redistribution of ionic charges on the extracellular side. Because positively charged ions (cations) are attracted towards the negatively charged electrode, this electrode is termed cathode and the positively charged electrode is the anode (Figure 4, symbols on the electrodes). Within the electric far field, each cell is exposed to the different poles of the electrical field, which results in a variation of the external potential parallel to the orientation of the electrical field (Figure 4, symbols outside the cell). As a result, the intracellular parts of the cell near the cathode (Figure 4, green) are relatively depolarized and the parts facing the anode become relatively hyperpolarized (Figure 4, red). The extracellular redistribution of charges activates different voltage-dependent ion channels in the distinct parts and in excitable cells an AP is evoked once the whole cell is depolarized above the AP threshold.[14] Importantly and in clear contrast to intracellular stimulation, extracellular field stimulation is not able to hold the membrane potential at a chosen level. Furthermore, the electrical stimulation is severely affecting parallel electrical recordings by inducing large artefacts.[15]

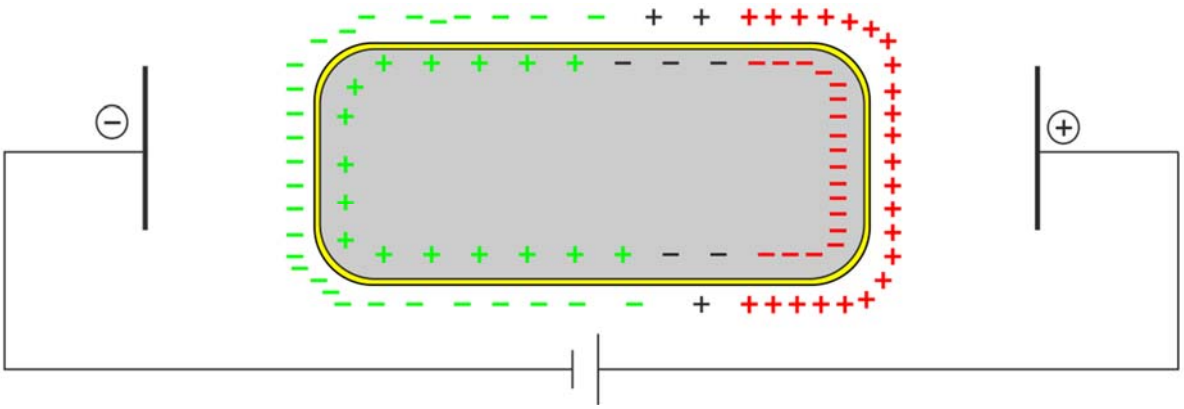

Figure 4: Electrical field stimulation of a single cell. Within the electrical far field from the electrode, distribution of the charged ions is changed leading to depolarization at the end facing the cathode (-) and hyperpolarization at the site next to the anode (+).

In sum, extracellular field stimulation can be used to trigger AP in excitable cells but cannot be used to clamp the cells at a certain membrane potential. It also co-induces hyperpolarization in some parts of the cells, results in stimulation artefacts in electrical recordings and can lead to the production of toxic reactions.

2.2.3 Electrical field stimulation of muscle tissue

Electrical field stimulation of muscle tissue has to be considered quite differently compared to stimulation of single muscle cells. The intracellular compartment and the extracellular solution are highly anisotropic due to varying ion channel expression in different parts of the membrane, intracellular resistances and the complex architecture of muscle tissue, respectively. Therefore, electrical field stimulation always induces simultaneously depolarization, called the virtual cathode, and hyperpolarization, called the virtual anode around the stimulating cathode placed within or next to the muscle tissue. The size and amplitude of the effects of the electrical field stimulation are not only determined by the physical features of the stimulus amplitude but also by the structural architecture and electrophysiological behavior of the tissue. Because these are both very different for myocardium and skeletal muscle, the electrical field stimulation will be separately described.

2.2.3.1 Electrical stimulation of the heart

The myocardium has a very distinct structure with varying orientations of cell bundles adjacent to each other.[16,17] Within these bundles, each cardiomyocyte has a rectangular shape and is approximately 200 µm long with a diameter of 20 µm. The cytosolic parts of the cardiomyocytes are coupled electrically to each other by gap junctions. Thus the whole heart can be considered as an electrical syncytium of single cells. Therefore for electrical pacing of the heart, it would be in principle sufficient to trigger an AP in one cardiomyocyte and the rest of the myocardium will be activated in an avalanche-type of cell-to-cell excitation. However, more electrical energy is required to depolarize one cardiomyocyte within an electrical syncytium of cells towards the AP threshold. This is because the induced current (source) in one cardiomyocyte will be distributed through gap junctions to all adjacent cells which are all adding repolarizing I_{K1} currents, counteracting the depolarization and can be considered as sink. This principle is called sink-source relationship and explains why much more inward current is required to depolarize one well-coupled cardiomyocyte within the heart compared to an isolated single cardiomyocytes.

Importantly, the amount and localization of de- and hyperpolarization and their expansion within myocardial tissue cannot be controlled using electrical stimulation due to the specific anatomical and physical features: Because gap junctions have higher resistance than the cytosol of cells, they lead to an additional resistance within the intracellular compartment which is not present in the extracellular space. Furthermore, the intercellular resistance between cardiomyocytes is crucially determined by the amount of gap junctions formed between the

cells. Gap junctions are most prominent at the intercalated disks at the short end of the cardiomyocytes which results in better electrical coupling in the longitudinal than the transversal direction of fiber orientation.[18] This intercellular anisotropy within the intracellular compartment is causing the effect within myocardial tissue that depolarization expands more in the transversal than the longitudinal direction of the muscle fiber orientation[19] resulting in a dog bone shape of the virtual cathode.[20] The virtual anode is the hyperpolarized tissue which is simultaneously induced perpendicular to the virtual cathode and parallel to the fiber orientation.[21] Furthermore within the extracellular compartment, blood vessels, endocardial structures such as trabeculae and papillary muscles, extracellular cleft spaces as well as varying fiber orientations are adding up to structural inhomogeneity which has a great influence on the electrotonic coupling between the cardiomyocytes. All these effects are causing a high regional variability and inhomogeneity in the electrical sink, which is why the regional anatomy has a significant impact on excitability, refractoriness and thus ability to successfully capture a local electrical stimulus.[22]

In conclusion, electrical field stimulation of myocardial tissue simultaneously triggers depolarization as well as hyperpolarization around the stimulating electrode. Unfortunately it is almost impossible to control and predict the extent of these virtual electrodes in the electrical syncytium of the heart due to the anisotropic electrical conductivity as well as the structural heterogeneity of the myocardium.

2.2.3.2 Electrical stimulation of skeletal muscles

In contrast to the myocardium, skeletal muscles consist of muscle fibers up to several centimeters long oriented parallel to the macroscopic muscle and in the direction of force generation. Importantly all myofibers are electrically isolated from each other while this allows fine-grain control of the generated muscle force because individual motoric units can be separately activated, all muscle fibers have to be individually stimulated to induce maximum force. The excitability of the skeletal myofiber varies between the fiber types and along the membrane.[5] Because each fiber is not spanning from end to end of the whole muscle, all fibers together have to form a complex structure including nerves, vessels and connective tissue.[23] This structural architecture explains why direct electrical stimulation of the whole skeletal muscles requires high energy[24-26] to efficiently excite all fibers at the different loci within the muscle. This need for high electrical energy leads to co-stimulation of adjacent muscles and nerves as well as generation of toxic gases.[13] In addition, both slow and fast muscle fibers are activated equally without the above mentioned important physiological recruitment patterns.

Skeletal muscles can also be activated by indirect electrical stimulation either of the innervating motoric nerve outside the muscle or of the presynaptic nerve endings of the neuromuscular endplate within the muscles. Importantly, such indirect nerval stimulation requires over 200 times less energy[25] and thus has far fewer side-effects compared to the direct electrical stimulation of the muscle fibers. However, co-activation of other neurons in the vicinity leads to simultaneous stimulation of other muscles as well as many other neurogenic effects. In addition, the electrically stimulated motor neurons are non-selectively activated recruiting simultaneously the fast and slow muscle fibers which is also in contrast to the physiological recruitment and leads to increased fatigue development during prolonged stimulation periods.[27,28] Furthermore, the indirect stimulation requires intact motoric nerves and unaltered AP generation and propagation within the neuron as well as functional signal transmission at the neuromuscular endplate. Therefore indirect electrical stimulation of skeletal muscle is limited to the all-or-nothing principle of single AP propagation and quantal synaptic transmission and thus does not allow continuous or subthreshold stimulation of the muscle fiber itself.

Taken together, the direct electrical stimulation requires very high energy and is thus practically unusable in intact muscles. Indirect electrical stimulation via the innervating nerves can be used to excite skeletal muscles with much less electrical energy but requires intact neuronal function, provides only low spatial resolution and allows only generation of short AP in the muscle fiber.

2.2.4 Electrical stimulation in patients

Since the first implantation in the 1950s,[29] cardiac pacemaker became the most successful application of electrical stimulation in clinical routine. Subsequently, it was detected that higher electrical energy can be used to terminate cardiac arrhythmia leading to the invention of cardioversion and defibrillation. Other possible applications of electrical stimulation such as laryngeal or gastric pacemaking have remained stagnant in early developmental stages for decades. All of these approaches suffer from similar intrinsic technical problems using electrical stimulation but with varying impact on their applicability.

Patients with bradycardia suffer from low beating rate of the heart leading to reduced cardiac output and insufficient blood and oxygen supply of the body, which can be a life-threatening condition. Cardiac pacemakers for electrical stimulation are currently the first option to treat bradycardia by electrical stimulation of the heart. Restoring normal heart rate by electrical stimulation has proven to be a safe and very efficient treatment.[30] This is mainly because the electrical energy required to stimulate the heart is relatively low and does not induce sensation

or pain because the beating of the heart is not perceived by the patient under physiological conditions and the myocardium itself is relatively insensitive to pain except during ischemia.[31] Therefore cardiac pacemakers are well-tolerated by patients. The main risks of cardiac pacemakers arise from surgical implantation of the device and the requirement for electrical leads to be impaled into the myocardium causing infections. After the implantation, the battery lasts on average no longer than 10 years and the electrode leads can dislocate from the myocardium as well as fibrosis can form around the electrode reducing the efficiency of electrical stimulation.[32] All these complications require an invasive correction or re-implantation with the additional risk for infections.

Ventricular tachycardia and fibrillation are arrhythmic states of the ventricles characterized by rapid regional excitation of the cardiomyocytes leading to uncoordinated and ineffective beating and thus a complete loss of cardiac output. This results in an acute drop in arterial blood pressure, syncope and eventually sudden cardiac death. The only primary therapy for these acutely life-threatening arrhythmias is electrical defibrillation with the aim to reestablish the normal heart rhythm.[33] Unfortunately, the electrical energy required for defibrillation to terminate ventricular arrhythmia is several orders of magnitude higher than for electrical pacing. This is because electrical pacing relies on stimulating one small area of the myocardium with intrinsic conduction of electrical activity through gap junctions to the remaining heart but defibrillation requires the synchronous depolarization of a large mass of ventricular tissue.[34] Therefore the term electrical shock for defibrillation was introduced as the required high energy leads to many undesired side effects, in particular massive co-excitation of nerves and skeletal muscles and severe pain.[35]

Besides the use of external defibrillators during acute cardiopulmonary resuscitation, patients with a predictable high risk to develop ventricular arrhythmia can be treated with implantable cardioverter/defibrillators (ICD).[33] These devices monitor online the electrical activity of the heart and apply high energy electrical shocks with implanted electrodes once a tachyarrhythmia is detected. To apply the high energy shock, ICD must charge internal capacitators which requires several seconds.[36] Therefore most patients with severe ventricular arrhythmia are already unconscious during the electrical shock and are thus not aware of the massive pain. However, arrhythmia detection algorithms have to be made very sensitive to assure that every ventricular arrhythmia is detected. This implies the risk of unjustified application of electrical shocks in conscious patients because of false positive arrhythmia detection. In fact, such inappropriate shocks have been reported to constitute one third of all shocks and more than 10% of ICD patients have encountered the very traumatic experience of an inappropriate shock.[37]

For this reason, implantation of cardiac defibrillators is associated with a high risk for anxiety and depressive disorders as well as post-traumatic stress syndrome.[38] Furthermore, electrical shocks are so strong that they can physically damage the myocardium[39] and it has been shown that there is a drop in contractility and cardiac output after electrical shocks.[40] For these various reasons detailed statistical analysis revealed that despite being acutely live-saving, applying electrical shocks is associated with an increased mortality over long term.[41] Taken together, electrical stimulation of the heart is used in clinical routine and electrical pacemakers are safe and efficient in treating bradycardia. Electrical shocks for defibrillation are acutely life-saving but the required high electrical energy induces massive pain, damages the heart and is associated with increased mortality.

Direct electrical stimulation of skeletal muscles is not accepted by patients due to the unavoidable induction of massive firing in sensible and pain neurons and many other side effects.[25] Indirect electrical stimulation through the motoric nerve requires less power[25] and can be thus much better tolerated. Hence, indirect electrical stimulation has been suggested to restore skeletal muscle function after spinal cord injuries[42] and to improve training and to restrengthen muscles in injured patients.[43,44] Recent publications have shown the benefit of electrical stimulation of the hypoglossal nerve to prevent relaxation of the tongue and subsequent closure of the airway in patients suffering from obstructive sleep apnea.[45]

Similarly, electrical stimulation of the phrenic nerve was tested in patients to restore normal ventilation by diaphragm contraction[46] which could improve outcomes during long term mechanic ventilation in comatose patients or after lung transplantation. However, the indirect electrical stimulation of the innervating nerve in distance to the muscle itself is restricted to motor nerves which innervate only one muscle. In other anatomical situations, all other muscles innervated by the same nerve would be co-stimulated which is in contrast to the physiological concerted movement of hands or legs and is an absolute requirement for normal behavior. In addition, indirect stimulation cannot be performed in diseases affecting the motor nerve or the neuromuscular junction, such as amyotrophic lateral sclerosis or myasthenia gravis.

2.3 Optogenetic stimulation

2.3.1 History of optogenetic tool development

Optogenetics is a new technique consisting of genetic modification of a certain cell type of interest in order to control the membrane potential, intracellular signaling or other cellular processes with light. This approach provides several significant advantages over traditional electrical or pharmacological strategies: Genetic targeting allows expression of light-sensitive proteins only in a specific cell type of interest and thereby only these cells will be directly influenced by the illumination. Cell type-specific stimulation was identified by neuroscientists to be of special interest because it enables the stimulation of a specific subset of neurons to determine their respective function within the intact brain. Furthermore light can be focused on a certain region with high precision and fine-grain control of intensity. These two advantages were first shown by the group of Gero Miesenböck in 2002, who demonstrated that genetic expression of a three-gene *Drosophila* phototransduction cascade in neurons allowed the control of neuronal activity by illumination.[47] However, this system required three proteins to be overexpressed and suffered from rather low temporal kinetics because of the involvement of a slow G protein signaling cascade. Therefore, the search continued for a light-gated ion channel which would provide greater temporal resolution depending solely on the channel gating kinetics.

Since the 19th century, it was known that algae like *Chlamydomonas reinhardtii* were light sensitive.[48] Upon illumination with low light intensity, the cells swim towards the light source whereas higher light intensities trigger escape reactions. Because it was found much later that illumination with light evoked this behavior within very few milliseconds, it was proposed that photon energy would directly interact with an ion channel.[49] Thus light sensitive proteins were searched encoded within the genome of algae. This genomic search was facilitated by the knowledge gathered from the discovery[50] and detailed investigations[51,52] of the light-inducible proton pump bacteriorhodopsin since the 1970s, which allowed to search for sequence homologies within the genome. Importantly, overexpressing bacteriorhodopsins, as well as the Cl^- transporting pump 19urgeries19sin in oocytes of *Xenopus laevi* was established for their detailed electrophysiological characterization from the 1990s on.[53,54] This method became very useful when Peter Hegemann and his group discovered two new gene sequences for large microbial-type rhodopsins in a cDNA library from *Chlamydomonas reinhardtii* in the early 2000s because it immediately enabled the proof by Georg Nagel and Ernst Bamberg that these two genes encoded in fact light-gated ion channels.[55,56] The first gene encoded for a proton channel but the second gene encoded for a light sensitive non-selective cation channel, which

was called Channelrhodopsin-2 (ChR2). ChR2 consists of seven transmembrane helices, binds covalently retinal as chromophore and changes it conformation upon illumination with blue light opening its pore. Under physiological conditions in mammalian cells, ChR2 is predominantly permeable for monovalent cations, which leads to inward currents and depolarizes the cell membrane. Because of its fast on- and off kinetics of few milliseconds, ChR2 seemed to be well-suited for optogenetic approaches. This was also due to its simplicity consisting of only 315 amino acid and requiring only all-trans retinal as co-factor which is cheap and easy to add in *in vitro* experiments and already present in most mammalian tissue *in vivo*.[57] In addition, there is no constitutive activity without illumination such that no ChR2 current is present in the dark. Finally ChR2 overexpression is well tolerated in all tested cell systems. For these reasons, the first optogenetic applications were reported shortly after the discovery of ChR2 independently by five different groups. The group of Karl Deisseroth and Hirumo Yawo proved the high temporal precision by demonstrating the feasibility to evoke APs by simple LED flashes in neurons *ex vivo* in a light pulse-to-AP manner.[58,59] The first *in vivo* applications were shown by Stefan Herlitze and his group controlling the burst activity of neurons within the spinal cord of chicken embryos[60] as well as by the group of Georg Nagel and Alexander Gottschalk by light-induced contractions in the muscles of *Caenorhabditis elegans* nematodes.[61] Almost at the same time, the group of Zhou-Hua Pan demonstrated that inscribing light sensitivity by ChR2 expression in surviving inner retinal neurons of blind mice can be used to restore the ability to react to light.[62] This pioneering work established the idea that optogenetic stimulation could also be eventually used for therapeutic approaches (see chapter 2.3.4). Ever since, optogenetic stimulation has gained increasing importance especially in the field of neuroscience allowing for the first time the analysis of connections between specific subtypes of neurons and brain regions as well as the investigation of the specific neuronal causes for whole animal behavior *in vivo*.

Besides light-induced depolarization via ChR2, the optogenetic toolbox was soon expanded. Light-inducible H^+ and Cl^- pumps from bacteria and fungi enabled the export of positive H^+ ions or the import of negative Cl^- ions, respectively. This can be used for light-induced membrane hyperpolarization to inhibit electrical activation.[63,64] However, their transport rate is rather low and they require ~10 times higher light intensities compared to ChR2 for full activation. Recently, Cl^- selective ChR2 variants[65,66] have been developed by amino acid exchange and novel natural anion conducting light gated channels have been discovered.[67] Their ability to silence electrical activity in excitable cells depends strongly on the Nernst potential for Cl^- and for example in cardiomyocytes with a relatively high intracellular Cl^-

concentration their activation leads to depolarization.[68] In the recent years, many other optogenetic approaches have been developed which aim to make intracellular signaling cascades light-inducible. The spectrum ranges from light-switchable G protein coupled receptors,[69-75] light inducible enzymes including adenylyl cyclases,[76,77] guanylyl cyclases[78-80] and phosphodiesterases[81] to light-inducible tools to modulate gene expression[82] and induction of apoptosis.[83]

Optogenetic stimulation has developed rapidly since its initial inception in the early 2000s thanks primarily to the concerted effort of the neuroscience research community. This can be explained by the enormous potential this new technique has to offer both for basic research as well as future clinical approaches. While a variety of different tools exist nowadays, ChR2 is still currently the best suited candidate for light-induced depolarization. Because of its distinct advantages and simplicity, optogenetics entered quickly the field of basic research and gathered special importance in the investigation of the brain and its function.

2.3.2 The light-sensitive cation channel Channelrhodopsin-2

The natural ChR2 protein is composed of seven transmembrane helices and an additional cytosolic C-terminal appendix which is not necessary for its channel function[56] and therefore excluded for optogenetic approaches.[84] Within the hydrophobic center of core protein, retinal is bound to helix 7 via a lysine with a Schiff base linkage.[85,86] Absorption of blue light by retinal with a peak at 485 nm leads to its isomerization from the all-trans to 11-cis state which triggers a conformational change of the whole protein including tilting of helix 2 and opening of an ion conducting pore (Figure 5A).[87]

This signal transduction from photon absorption to ion conductance occurs very quickly with a rise time of the photocurrent as fast as 200 µs when using supramaximal illumination. During continuous illumination, the peak current declines quickly to a steady state[88] current which persists unaltered during illumination.[56] After termination of illumination, the ChR2 current deactivates with a decay constant (τ_{off}) of approximately 10 ms (Figure 5B).[64] The diameter of ion conducting pore is slightly larger than the pore in voltage gated Na^+ channels allowing to pass monovalent cations depending on their size ($H^+ >> Gd^+ > Li^+ > Na^+ > K^+$) and to a much lesser extent bivalent cations ($Ca^{2+} > Sr^{2+} > Ba^{2+} \gg Zn^{2+}$). Because of this non-selective monovalent cation conductance, ChR2 photocurrents reverse at physiological ion concentrations around 0 mV resulting in inward currents and depolarization at negative membrane potentials and in outward currents and hyperpolarization at positive membrane potentials (Figure 5C).[56] The currents through ChR2 are therefore strongly dependent on the

membrane potential with a slight inward rectification. Although ChR2 currents within the whole cell are large in the range of several pA/pF, the single channel conductance is so small (<50 fS) that it cannot be directly measured and was estimated by noise analysis experiments.[56,85,89] Thus, the fact that ChR2 leads to significant whole cell currents is mainly due to its massive and non-harmful expression level even in mammalian cells.

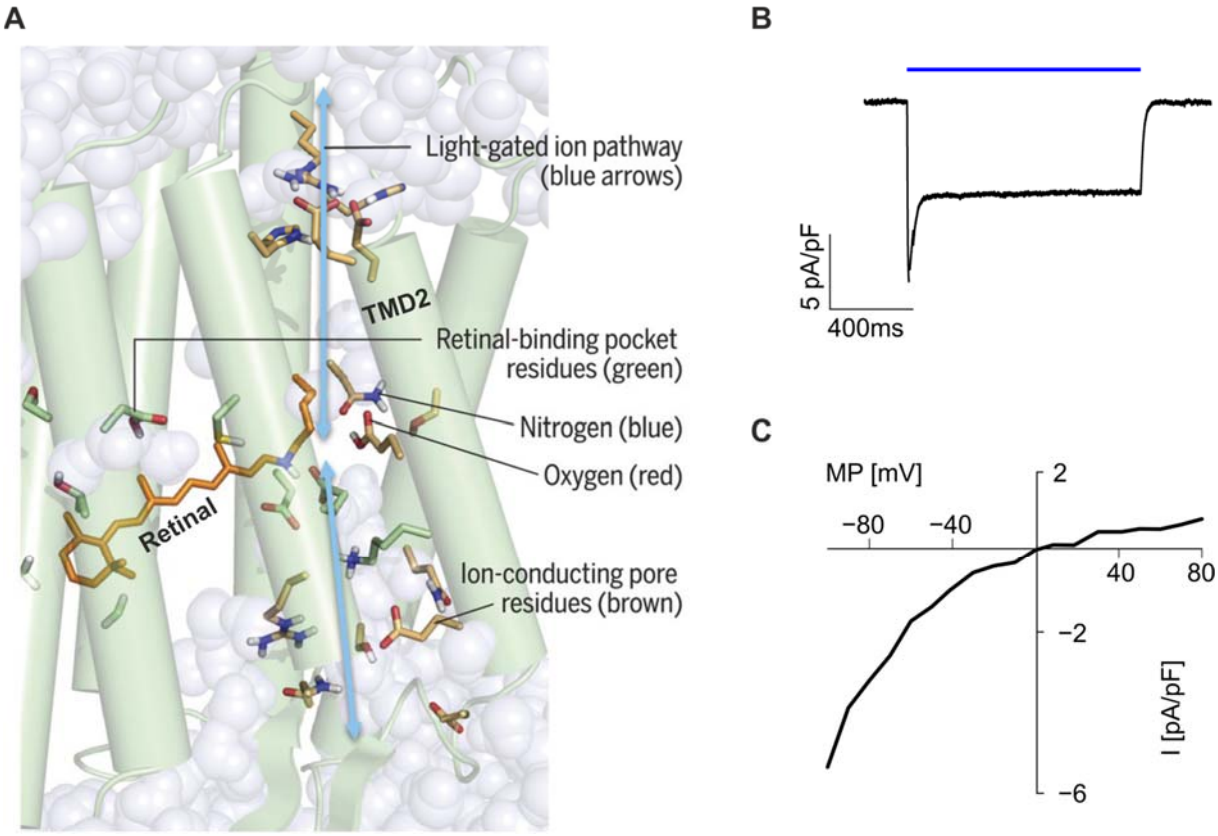

Figure 5: Light-induced pore opening and currents in ChR2. (A) Picture of structure of ChR2 from a molecular dynamics simulation displaying the retinal binding and the probable ion conducting pore (blue arrows) opened by tilting of transmembrane domaine 2 (TMD2) after light-absorption and conformation change of the retinal. Picture is taken from K. Deisseroth and P. Hegemann, Science 2017.[90] (B) Illumination with blue light (470 nm, 5 mW/mm^2) induces inward currents at a negative membrane potential (−40 mV). Figure is adopted and modified from Lapp H. et al., Scientific Reports 2017. (C) Current (I) to voltage (MP: membrane potential) relationship of ChR2 H134R in a cardiomyocytes. Note the typical inward rectification. Figure is taken and modified from Bruegmann T. et al., Nature methods 2010.[91]

After the identification of the natural ChR2, many mutations were performed and other natural Channelrhodopsins (ChR) from different species were investigated to create new superior variants.[64] The first mutant was generated by a single amino acid exchange from a Histidine to an Arginine at position 134 (ChR2 H134R), anticipated from prior experiments with bacteriorhodopsin. This gain-of-function mutation led to lesser desensitization and larger stationary photocurrents compared to wild type ChR2 but had a slightly slower deactivation kinetics ($\tau_{off} \sim 20$ms).[61] Interestingly, the ChR2 H134R variant is still the most commonly used

ChR variant because of its well defined expression within the membrane and the good biophysical properties.

Many new ChR variants have been described with varying ion selectivity, gating kinetics, larger currents and distinct wavelength characteristics.[64] CatCh was generated by a single point mutation (L132C) and was reported to have an enhanced Ca^{2+} permeability leading to more efficient depolarization at lower light intensities with faster kinetics.[92] While CatCh was indirectly faster due to activation of K^+ channels by the subsarcolemmal Ca^{2+} increase, other variants such as ChETA,[93] ChIEF[89] or Chronos[94] showed biophysically faster off-kinetics of the photocurrent itself. Other approaches were undertaken to slow down the closing of ChR2 in order to make the channel bi-stable. These so-called step-functional opsins can be activated by a short light pulse of one wavelength, stay open thereafter and can be inhibited by a short pulse of another, typically longer wavelength.[95-97] In experiments in which continuous depolarization over long periods is required, such step-functional opsins allow for a large reduction of the required photons over time. Interestingly, comparing many ChR variants revealed that there is a strong correlation between the light sensitivity of the variant and its deactivation kinetics.[64] In addition to ChR variants with altered gating kinetics, efforts were undertaken to change the wavelength specificity by single point mutations, generating chimeric proteins and analysis of natural ChR variants.[96,98-100] The most red-shifted ChRs are the ChRimson variant[94] derived from the species *Chlamydomonas noctigama* and ReaChR[99] which was created from different parts of Channelrhodopsin-1, ChR2[89] and ChR from *Volvox cateri*.[88] The advantage of this wavelength shift is that red light is less absorbed and therefore much less toxic and penetrates much deeper through biological tissue than blue light.[101] In fact, the use of ReaChR allowed to trigger spiking within the motor cortex in awake mice with red light even through the intact skull.[99]

Genetic modification as well as the discovery of new natural ChRs has led to a huge variety of light-gated channels which differ in their ion permeability, wavelength specificity, gating kinetics as well as their light sensitivity. While the H134R variant is still by far the most used ChR, other variants can be selected for specific purposes. However it has to be taken into account that good expression and toleration by the cells are the most important factors for optogenetic experiments.

2.3.3 Light-induced depolarization of muscle cells

Expressing ChR2 in cells allows depolarization by illumination. The great advantages of this approach are the possibility of cell-specific stimulation with precise spatial and temporal

resolution as well as fine-grain control over the extent of depolarization. Cell-specific stimulation can be obtained because only cells expressing ChR2 will be depolarized by light whereas non-expressing cells are usually not light sensitive. For this purpose, ChR2 must be expressed under the control of a promotor which is only active in the subtype of cells-of-interest. This allows not only to decipher the exact role and function of the individual cell type within the whole organ or organism but also to prevent unwanted side effects of the light stimulation. Importantly, in contrast to electrical stimulation, co-excitation of nociceptive and pain neurons can be excluded if ChR2 is not expressed in these cells. Fortunately, ChR2 stimulation does not require high light intensities which could lead to heat generation during continuous illumination.[102,103]

The spatial resolution of the stimulation is defined by the ChR2 expression itself and the illumination. The ability to control the site of stimulation by ChR2 expression is of particular interest because ChR2 expression can also be restricted to distinct compartments or organelles within the cell[104-106] to investigate the role of individual organelles or specific parts of the cell membrane. Without such targeted expression, ChR2 is equally distributed over the whole sarcolemma.[91] Thus uniform illumination of the whole cell will result in homogenous depolarization over the whole cell (Figure 6A). Importantly, the amount of depolarization depends on the applied light intensity, the ion selectivity and inward rectification of ChR2 as well as the endogenous counterbalancing and repolarizing currents. In tissue and organs, light can be precisely focused to defined regions of the surface. The actual depth of stimulation depends thereby on the light intensity and physical penetration of the light (Figure 6B).

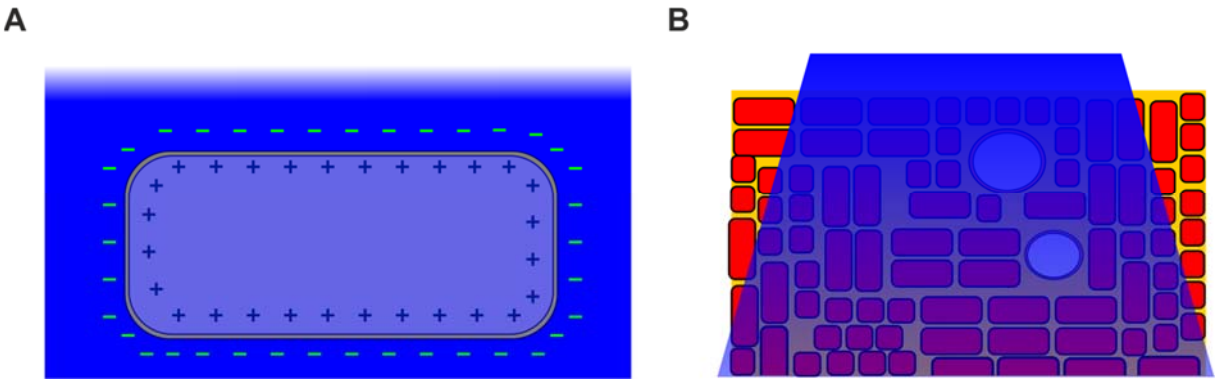

Figure 6: Light induced depolarization in ChR2 expressing cells. (A) Uniform illumination depolarizes the membrane homogenously which can be used to control the voltage without disturbing the cell membrane. (B) Illumination depolarizes all cells within the illuminated area primarily irrespective of the architecture of the tissue.

The amount and location of cardiac tissue which will be depolarized by the illumination within an organ can be much better controlled than using electrical stimulation because optogenetic is primarily independent of the regional architecture of the tissue and does not induce virtual

anodes with hyperpolarized areas. The temporal precision of light-induced depolarization via ChR2 is determined predominantly by the on- and off-kinetics of ChR2 itself and to some part by the counterbalancing and repolarization ion currents of the cell under investigation. In clear contrast to electrical field stimulation, optogenetic depolarization can be used almost indefinitely because the steady state current of ChR2 is stable over seconds and minutes. Therefore optogenetic stimulation enables fine-grain control of the membrane potential without temporal limitations and high spatial resolution. Importantly, optogenetic stimulation enables to expand the possibilities of intracellular stimulation to the tissue level because of the advantageous physical properties of light.

2.3.3.1 Optogenetic pacing of the heart

While optogenetic stimulation very quickly entered the field of neurosciences, it took some years until its first applications could be demonstrated in cardiovascular research.[107] In the first publication,[91] we were able to show optogenetic stimulation of cardiomyocytes *in vitro* as well as the intact heart *ex vivo* and *in vivo*. In ChR2 expressing cardiomyocytes differentiated from transgenic murine embryonic stem cells or isolated from transgenic adult mouse hearts, light induced inward currents and evoked APs and contractions. Importantly, we proved that prolonged illumination can be used for sustained depolarization: At low light intensities, continuous illumination induced an acceleration of spontaneous beating in vitro, which we attributed to subthreshold depolarization in the pacemaking cells. High light intensities prolonged the AP resulting in a sustained depolarization at a membrane potential of approximately −30 mV (Figure 7A). Because this level of depolarization should be sufficient to keep Na^+ and Ca^{2+} channels in the refractory state, we anticipated that optogenetic stimulation could be also used to block electrical activation in cardiomyocytes. This was proven by experiments with a spontaneously beating monolayer of cardiomyocytes in which localized illumination blocked the electrical activity selectively within the illuminated region (Figure 7B). All together these findings were pointing towards the potential of optogenetic stimulation to terminate tachyarrhythmias.[108] In addition to these *in vitro* experiments, we aimed to explore optogenetic stimulation in the intact heart and generated transgenic mice expressing ChR2 H134R in ventricular and atrial cardiomyocytes. To enable high expression in muscle cells, we used the chicken-β-actin promotor. Importantly, we searched for unwanted side-effects by the ChR2 expression alone because a potential dark current or high expression within the membrane could alter the basic electrophysiological properties. However, we found no signs of cardiac hypertrophy or heart failure. Also ChR2 expression did not affect basic

electrophysiological parameters because the AP duration, resting membrane potential or the membrane resistance were not altered.

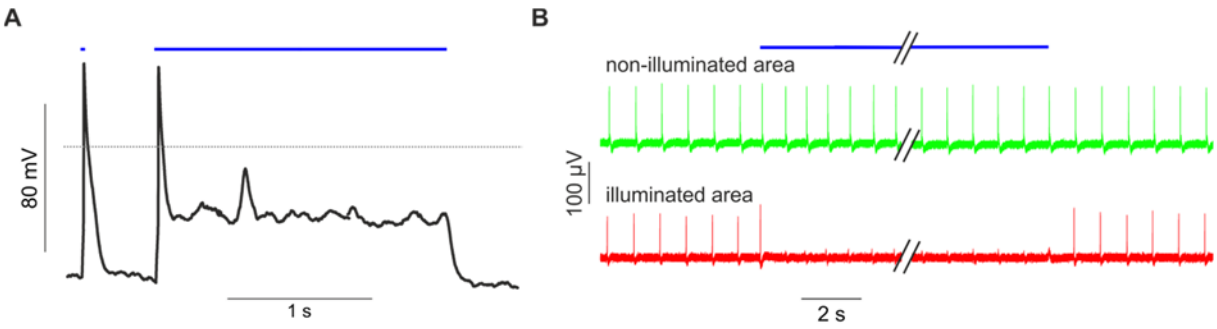

Figure 7: Continuous illumination of cardiomyocytes. (A) Membrane potential recording from a ChR2 expressing cardiomyocyte. Short illumination induced a free-running AP (left) whereas continuous illumination kept the cardiomyocytes depolarized. Grey dotted line indicates 0 mV. (B) Field potential recordings (cellular ecg) from two sites of a spontaneously beating monolayer of cardiomyocytes plated on a multi-electrode array: Prolonged illuminated of one region blocks the electrical activity selectively while the rest of the monolayer is unaffected and continues to beat spontaneously. Figure is adapted from Bruegmann T et al., Nature methods 2010.[91]

To locally trigger supraventricular and ventricular extrasystolic beating, we used localized illumination of the atrium and ventricles of intact hearts, respectively. Interestingly, we were able reduce the illuminated area down to 0.05 mm^2 for successful optogenetic pacing of the heart.[91] These experiments laid out the tantalizing prospect that the spatial precision of optogenetic stimulation can be used to determine the number of cardiomyocytes which are required to generate extrasystolic beating within intact ventricles. This important question could only be addressed by computer simulations so far.[109] Zaglia et al. expanded upon this idea by investigating the distinct requirements for the generation of extrasystolic beating within the conduction system compared to the working myocardium by using cardiomyocytes subtype specific ChR2 expression and varying illumination sizes.[110] Almost at the same time of our initial publication, Arrenberg et al. reported successful optogenetic stimulation of the heart in embryonic zebra fish larvae.[111] Besides optical pacing using ChR2, they employed the light-inducible Cl^- pump Halorhodopsin to inhibit electrical activity. In a series of elegant experiments, patterned illumination by a digital mirror device was used for precise spatial control of electrical inhibition to pinpoint the origin of the electrical automaticity during different developmental stages.

After the initial reports expressing ChR2 directly in cardiomyocytes,[91,111] another strategy was demonstrated *in vitro* using a cell-delivery technique. HEK293 cells expressing ChR2 were co-cultured with wild-type neonatal rat cardiomyocytes. Because both cell types can electrically couple through gap junctions, the light-induced inward currents in the HEK293 cells can excite and pace the cardiomyocytes.[112] This cell-cell coupling approach was further expanded using

fibroblasts expressing ChR2 or the light-gated H^+ pump ArchT for pacing or electrical silencing of gap-junctional coupled wild-type cardiomyocytes.[113] For optogenetic stimulation of hearts, the cell-delivery approach would have the advantage that only cell transplantation but no genetic modification of the myocardium is required. Computer simulations suggested that this approach might be suitable for optical pacing of a human heart.[114] However, stable long term and effective cell engraftment of ChR2 expressing cells has never been proven and is highly questionable.[115,116] Furthermore transplantation of non-excitable cells could lead to local fibrosis, electrical isolation and altered electrical properties of the host cardiomyocytes which is highly pro-arrhythmic in fibrotic heart tissue.[117]

Viral gene transfer to express ChR2 directly within cardiomyocytes seems to be the better suited alternative for optogenetic stimulation of wild type hearts and maybe suited even for patients in the future. Viral transduction for cardiac optogenetics was first shown *in vitro in* adult guinea pig cardiomyocytes using adenovirus[118] and in neonatal rat cardiomyocytes using lentivirus.[119] These experiments were used to construct and validate a computer model for ChR2 in cardiomyocytes[118] and to terminate arrhythmia-like rotating spiral waves in a monolayer *in vitro* suggesting the potential use of optogenetics to treat cardiac arrhythmia.[119] Unfortunately lentiviral transduction in humans can have detrimental side effects including malignant leukemia.[120] In clear contrast, gene transfer using adenoassociated virus (AAV) has been demonstrated to generate high cardiomyocyte transduction rates with administrative safety in several clinical trials[121,122] and the persistence of gene expression could be shown for more than 2 years in the hearts of patients.[123] Excitingly, several subtypes of AAV vectors were identified to have high tropism towards specific cell types enabling selective transduction with systemic injection.[124] Among these, AAV encapsulated with proteins from the serotype 9 showed a strong tropism towards cardiomyocytes, at least in rodents.[125] Therefore, we injected systemically AAV particles and observed robust ChR2 expression within the ventricles up to 10 weeks after the injection (Figure 8A). This enabled reliable optical pacing in approximately 75% of all hearts, both *in vivo* and in explanted hearts *ex vivo* (Figure 8B). By investigating hearts with different cardiomyocyte transduction rates, we were able to suggest that at least 40% ChR2 expressing cardiomyocytes are required for optical pacing of the heart.[126] This underlies the power of cardiac optogenetics to investigate electrical coupling between cells within the myocardium. In addition, the group of Lior Gepstein tested intramyocardial injection of AAV in rats and suggested that optical pacing from two distinct sites can be used to resynchronize the ventricular activity. Such an approach would be similar to current biventricular electrical pacing which is advantageous in heart failure patients with a bundle

branch block.[127] Finally, it was estimated that optogenetic pacemakers would require less energy that could prolong the battery lifespan of implantable devices and reduce re-implantation 28urgeries.[112,128]

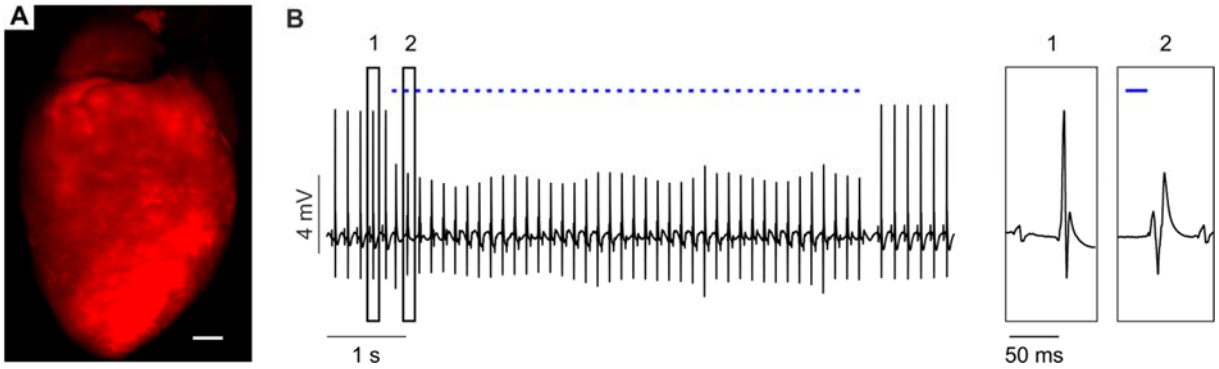

Figure 8: Optogenetic pacing of wild type hearts after AAV mediated gene transfer. (A) Epicardial view of a mouse heart four weeks after systemic injection of AAV encapsulated with proteins from the serotype 9 for expression of ChR2 in fusion to the red fluorescence protein mCherry. Fluorescence signals (red) indicate ChR2 expression (bar = 1 mm). (B) Pulsed illumination (indicated by blue lines: 470 nm, 20 ms, 0.5 mW/mm^2) focused on the anterior part of the ventricles (25 mm^2) allows stable optical pacing *in vivo*. Inserts show the different QRS shape of extrasystoles and the retrograde p-wave during optical pacing (2) in contrast to the sinus rhythm (1). Figures are adapted and modified from Vogt CC et al., Cardiovascular Research 2015.[126]

In conclusion, optogenetic stimulation of cardiomyocytes and the intact heart has been demonstrated several times and allows completely new experiments to address unsolved questions in cardiac electrophysiology. In addition, AAV based gene transfer could enable in principle optogenetic stimulation in human hearts and presents a potential new treatment option.

2.3.3.2 Optogenetic stimulation of skeletal muscle

Indirect optogenetic stimulation of skeletal muscle through the motor neuron system was demonstrated by illumination of ChR2 expressing neurons in the motor cortex which triggered movement of the whiskers[129] and locomotion in freely moving mice.[102] Soon afterwards, it was reported that optogenetic stimulation of the phrenic motor neuron restored movement of the diaphragm and was able to restore breathing in rats after spinal cord injury.[130] Furthermore indirect optogenetic stimulation of skeletal muscles was also achieved by illuminating peripheral ChR2expressing nerves in transgenic animals[131] and in wild type mice after AAV injection[132] or after transplantation of ChR2 expressing embryonic stem cell derived neurons.[133] Interestingly, optogenetic technology was also used to prevent AP propagation and inhibit muscle activation by expressing the Cl^- pump Halorhodopsin in motor neurons.[134] Thus indirect control of skeletal muscles was demonstrated by stimulating all parts of the motor nerve tract.[24]

However, such indirect stimulation cannot be used to investigate excitation contraction coupling in skeletal muscles or to analyze possible feedback mechanisms from skeletal muscles to the innervating nerves. The first direct non-neuronal stimulation of skeletal muscles was demonstrated in the nematodes *Caenorhabditis elegans*:[61]ChR2 was expressed within the body wall and the egg-laying muscles and illumination of the whole animal simultaneously induced contraction of the whole body including egg expulsion. In mammalian system, direct stimulation of skeletal muscles was first demonstrated *in vitro* in C2C12 cells, which are immortalized myoblasts from mice. After differentiation and cell-fusion, C2C12 cells can form myotubes with some contractile function.[135,136] Pulsed illumination of ChR2 expressing C2C12 myotubes was shown to induce contractions. Global illumination results thereby in a homogenous depolarization of the cell membrane.[137] Focusing light on only small parts of the membrane was used to test the excitability at this site and to analyze how local membrane depolarization propagates along the sarcolemmal surface.[138] Interestingly, long term optogenetic stimulation induced preliminary maturation in C2C12 myotubes detected by a higher percentage of myotubes with sarcomeric structures, contractility and a slight reduction of the resting membrane potential.[139] In addition, optogenetic stimulation of C2C12 myotubes can improve movements of robotic actuators because it enables fine grain control of force and selective stimulation of different parts within the robotic muscle tissue.[140] The concept of optogenetic muscle actuators for robotic movement was demonstrated by two recent studies: The first study demonstrated bidirectional movement of bioactuators and the advantage that the generated force can be controlled over a wide range.[141] The second study showed the generation of a complete artificial fish-like robot built from dissociated ChR2 expressing rat cardiomyocytes engrafted into a microfabricated gold skeleton. A tightly controlled sequence of illumination patterns even allowed to guide the robotic fish through an obstacle course by phototactic steering.[142] Taken together, direct stimulation of skeletal myotubes could be demonstrated *in vitro* but the feasibility and especially efficacy to stimulate intact skeletal muscles has never been tested.

2.3.4 Optogenetic technologies for therapeutic approaches

The ability of optogenetics to perform cell-specific stimulation with high spatial control has soon led to tantalizing proposals for treatment of patients. The general feasibility of several approaches has been demonstrated in small animal models including restoration of vision,[62] cochlear implants,[143] pain inhibition in peripheral nerves,[103] control of blood glucose levels,[144,145] as well as restoring urinary bladder contraction[146] and treating erectile

dysfunction.[80] Among these, the most promising approach that was soon suggested after the discovery of ChR2 was to restore visual perception in cases of Retinitis pigmentosa,[62] a disease which leads to irreversible degeneration of the directly photosensitive cells in the retina. Ever since, many groups have tried different approaches towards this ambitious aim[147-150] and in 2017 the first clinical trial was approved by the food and drug administration of the United States (FDA).

All therapeutic approaches face similar challenges. A safe way to express the light-sensitive protein in cells of interest is most important. Until today, it remains unresolved whether the overexpression of the non-human ChR2 proteins *in vivo* will be detected by the immune system and could trigger an immune response. In fact, injection of AAV to express ChR2 in the retina of rats led to antibody production against the AAV as well as against ChR2.[151] However this was not associated with histological changes or loss of vision. Taking into account that the eye is an immunological privileged region, these results cannot be transferred to other applications. Once ChR2 expression is solved, sufficient illumination in situ is required but can be technically challenging especially in regions of the body which are moving. For this purpose, several biotechnological advancements in the recent years have resulted in promising options. Among these are cell-scale injectable LEDs[152-154] which can be integrated in stretchable integumentary membranes[155] or the development as well as the application of μLED arrays.[156] Taken together, optogenetic stimulation and its intrinsic technical advantages propose new strategies for clinical treatments. However implantation of light emitting devices, the required gene transfer and the expression of previously extraneous proteins are major obstacles which have to be solved before entering clinical trials.

3. Optogenetic defibrillation

3.1 Prologue

Currently, defibrillation by electrical shocks is the only acute therapeutic option to rescue patients from life-threatening ventricular tachyarrhythmia. However the mechanism responsible for the termination of the arrhythmia by the electrical shock is still poorly understood. This is mainly because the effects of electrical stimulation cannot be predicted within the heart with its complex structure and electrical anisotropy resulting in de- and hyperpolarized areas. Thus most mechanistic investigations on defibrillation are restricted to analyses of correlative observations or computer simulations of the heart.[157] Several principles have been suggested to be the underlying mechanism for successful defibrillation by depolarization such as filling of the excitable gap,[158,159] prolongation of the refractory period[160]

and conduction block.[161] Furthermore, also the hyperpolarization has been discussed to play a crucial role.[162] To unravel the importance of each suggested mechanism, a novel method is required which can evoke de- and hyperpolarization separately in specific areas with well-defined timings. Optogenetic stimulation would allow such experiments and the advantage of this technology for the investigation of defibrillation has already been demonstrated *in vitro*. We have shown that regional illumination of a spontaneously beating monolayers induces a conduction block.[91] Others have used optogenetic depolarization to reduce the excitability, slow conduction and thereby terminate re-entrant wave fronts in a monolayer of rat cardiomyocytes.[119] In addition, specific illumination patterns were used to inscribe excitation waves, to control the direction of conduction and to destabilize the reentry wave fronts in cardiomyocyte monolayers.[163] Finally, initial computer simulations of a human heart suggested optogenetic defibrillation with red light sensitive ChRs and illumination from the endo- and epicard.[164] While all these *in vitro* and *in silico* experiments delivered tantalizing results, they are unsuited to predict the feasibility of optogenetic defibrillation within the intact heart. The main question was whether the light could penetrate through all layers of the myocardium to depolarize a sufficient amount of cardiac tissue. Computer simulation were performed to predict the physical penetration of light estimating the residual light intensities for the myocardial layers in dependence to the applied light intensity at the epicardium.[165] However in addition to light scattering and attenuation, the resulting depolarizing effect could only be roughly estimated because of the unpredictable influence of the electrical coupling and the local anatomical structure. Furthermore, the amount and local extent of depolarization required for successful optogenetic depolarization is not known. Besides addressing the mechanism of defibrillation, optogenetic defibrillation would provide a tempting outlook for the treatment of ventricular arrhythmia because in contrast to electrical shocks, optogenetic stimulation could be performed pain-free and would be less damaging. Therefore, we explored the practicability and requirements of optogenetic defibrillation in intact hearts of mice. In addition, we translated the results generated in mouse hearts to a computer simulation of an infarcted human heart to identify the requirement for therapeutic applications of optogenetic defibrillation by epicardial illumination.

3.2 Original publication

The Journal of Clinical Investigation RESEARCH ARTICLE

Optogenetic defibrillation terminates ventricular arrhythmia in mouse hearts and human simulations

Tobias Bruegmann,[1,2] Patrick M. Boyle,[3] Christoph C. Vogt,[1] Thomas V. Karathanos,[3] Hermenegild J. Arevalo,[3] Bernd K. Fleischmann,[1] Natalia A. Trayanova,[3] and Philipp Sasse[1]

[1]Institute of Physiology I, Life and Brain Center, and [2]Research Training Group 1873, University of Bonn, Bonn, Germany. [3]Institute for Computational Medicine and Department of Biomedical Engineering, Johns Hopkins University, Baltimore, Maryland, USA.

Ventricular arrhythmias are among the most severe complications of heart disease and can result in sudden cardiac death. Patients at risk currently receive implantable defibrillators that deliver electrical shocks to terminate arrhythmias on demand. However, strong electrical shocks can damage the heart and cause severe pain. Therefore, we have tested optogenetic defibrillation using expression of the light-sensitive channel channelrhodopsin-2 (ChR2) in cardiac tissue. Epicardial illumination effectively terminated ventricular arrhythmias in hearts from transgenic mice and from WT mice after adeno-associated virus–based gene transfer of ChR2. We also explored optogenetic defibrillation for human hearts, taking advantage of a recently developed, clinically validated in silico approach for simulating infarct-related ventricular tachycardia (VT). Our analysis revealed that illumination with red light effectively terminates VT in diseased, ChR2-expressing human hearts. Mechanistically, we determined that the observed VT termination is due to ChR2-mediated transmural depolarization of the myocardium, which causes a block of voltage-dependent Na^+ channels throughout the myocardial wall and interrupts wavefront propagation into illuminated tissue. Thus, our results demonstrate that optogenetic defibrillation is highly effective in the mouse heart and could potentially be translated into humans to achieve nondamaging and pain-free termination of ventricular arrhythmia.

Introduction

Ventricular tachycardia (VT) and ventricular fibrillation (VF) are malignant arrhythmias, which are characterized by fast and uncoordinated electrical excitations of the myocardium, resulting in pump failure and leading to sudden cardiac death. The current state-of-the-art therapy for these life-threatening disorders is defibrillation by the delivery of high-energy electrical shocks. Patients at risk for developing ventricular arrhythmia receive implantable automatic defibrillators. Clinical studies have demonstrated the life-saving potential of this therapeutic approach; however, it is also associated with significant adverse effects, such as structural damage of cardiac tissue worsening the underlying cardiac disease, severe pain due to nonselective excitation of nerves and muscles with subsequent psychological trauma, and increased mortality (1–4). Thus, there is a need for alternative approaches that enable pain-free and less deleterious termination of lethal arrhythmia.

Optogenetics is an emerging technology that enables modulation of electrical function with light in cells overexpressing light-sensitive proteins. The light-activated cation channel channelrhodopsin-2 (ChR2) has been used to directly pace the heart with brief (1–10 ms) blue light pulses in vivo (5–8). However, these results do not imply the feasibility of optogenetic defibrillation, because cardiac pacing entails only a brief depolarization in a few cardiomyocytes with subsequent intrinsic excitation of the whole heart through gap-junctional electrical coupling. In contrast, defibrillation requires the simultaneous depolarization of a large mass of ventricular tissue (9), and therefore the energy required for a defibrillating shock is dramatically larger than that of a typical pacing stimulus. Optogenetics enables the selective depolarization of ChR2-expressing cardiomyocytes only, making it an attractive pain-free alternative to electrical shocks. An additional strength over electrical shocks is that optogenetics allows uniform and sustained depolarization by continuous illumination. Although this advantage has been exploited in vitro to achieve fine-grain control of excitation waves in cardiomyocyte monolayers, including reentry destabilization (10), slowing of conduction (11), and suppression of electrical activity (5), the feasibility of optogenetic defibrillation in intact hearts has never been demonstrated experimentally.

Herein, we report a new protocol to induce sustained ventricular arrhythmia in mouse hearts and provide experimental evidence that optogenetic defibrillation by illumination of the epicardial surface is a highly reliable approach. In addition, we investigate the translational potential of optogenetic defibrillation by epicardial illumination with a novel in silico approach using a model of the heart of a patient with a propensity for infarct-related VT.

Results

Optogenetic defibrillation via epicardial illumination in intact hearts of transgenic mice. First, we explored optogenetic defibrillation via epicardial illumination in hearts of transgenic mice expressing ChR2 in all cardiomyocytes (5). Because of the small size of the

Authorship note: T. Bruegmann and P.M. Boyle contributed equally to this work.
Conflict of interest: The authors have declared that no conflict of interest exists.
Submitted: June 3, 2016; **Accepted:** August 4, 2016.
Reference information: *J Clin Invest*. doi:10.1172/JCI88950.

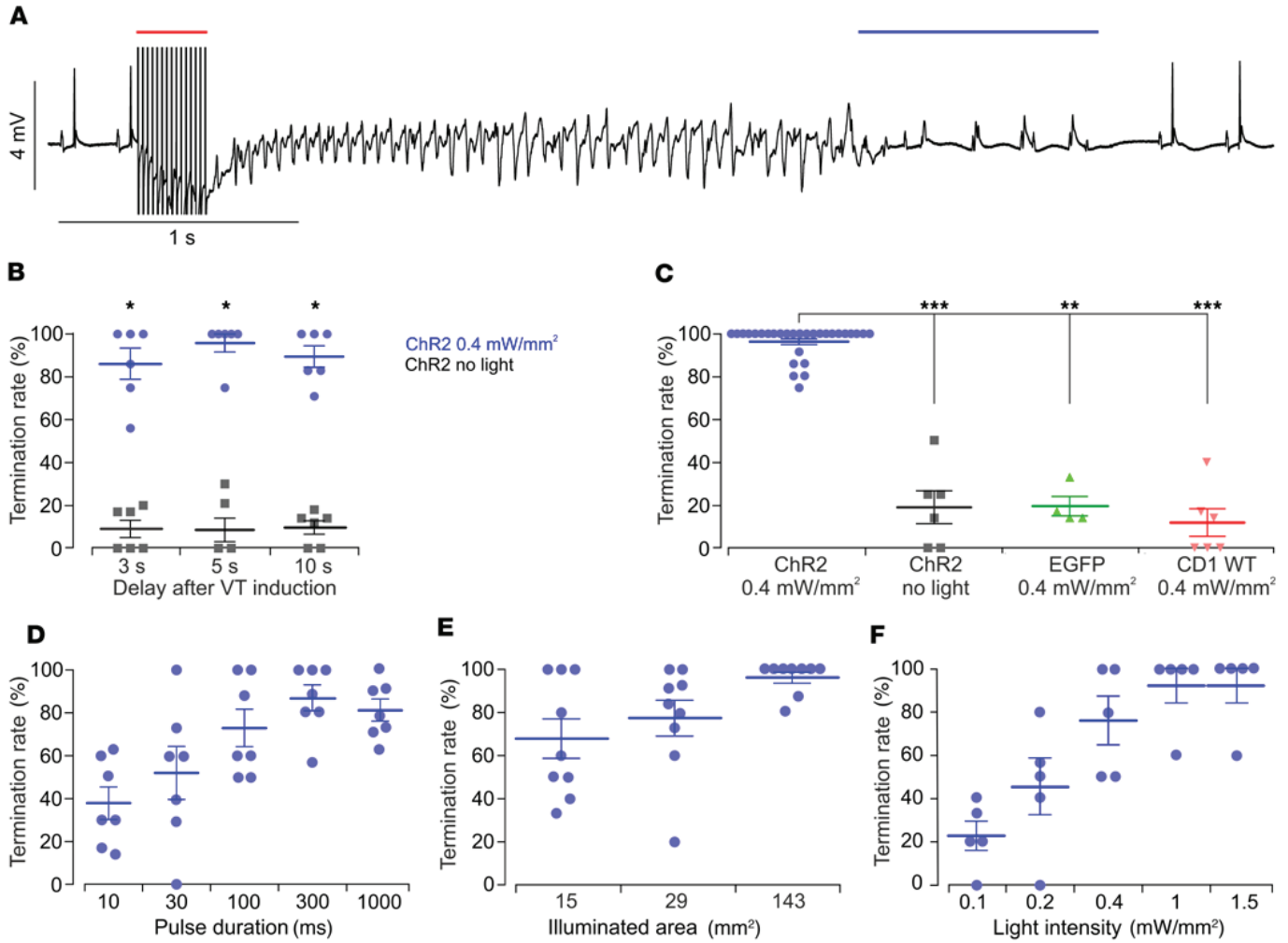

Figure 1. Optogenetic defibrillation in transgenic hearts. (**A**) Representative ECG (black) from an explanted heart expressing ChR2. Sustained VT was induced by electrical burst stimulation (50 Hz, red bar) and terminated by epicardial illumination with blue light (blue bar, 470 nm, 1 second, 0.4 mW/mm², 143 mm², n = 36). (**B**) Arrhythmia termination rate in ChR2 hearts after one 1-second-long light pulse (0.4 mW/mm², 143 mm², blue) applied 3, 5, and 10 seconds after induction of arrhythmia compared with control conditions (i.e., no illumination, black) in the same time window (see Supplemental Figure 1B for experimental protocol; Wilcoxon matched pairs test, $P < 0.04$, n = 6). (**C**) Arrhythmia termination rate in response to a 4-light-pulse protocol (Supplemental Figure 1C) in ChR2 mouse hearts with illumination (1 second, 0.4 mW/mm², 143 mm², blue) and without illumination (black), as well as in hearts expressing only EGFP (green) and in CD1 WT hearts (red) with illumination (Kruskal-Wallis test, $P < 0.0001$, with Dunn's multiple-comparison post-test; ChR2 light: n = 29; ChR2 no light: n = 6; EGFP: n = 4; CD1 WT: n = 6). (**D**–**F**) Influence of illumination duration (**D**, 0.4 mW/mm², 29 mm², n = 7, P = 0.0007), area (**E**, 1 second, 0.4 mW/mm², n = 9, P = 0.031), and light intensity (**F**, 1 second, 15 mm², n = 5, P = 0.013) on arrhythmia termination rate (Friedman test). Each point shows the percentage of successful optogenetic defibrillation attempts in 1 heart. Data are shown as the mean ± SEM.

mouse heart, electrically induced ventricular arrhythmias in vivo are often self-terminating after several cycles (12), rendering the analysis of defibrillation efficacy impossible. Therefore, we developed a novel protocol and obtained sustained ventricular arrhythmias evoked by electrical burst stimulation or S1-S2 protocols from the base of the right ventricular wall at a point with minimal effective refractory period (ERP) in hearts perfused ex vivo with low-K^+ (2 mM) Tyrode's solution and the K_{ATP} channel activator pinacidil (100 μM; Supplemental Figure 1A; supplemental material available online with this article; doi:10.1172/JCI88950DS1). Termination of ventricular arrhythmia was achieved by illumination of the anteroseptal epicardium with blue light (470 nm) in all hearts tested (n = 36; Figure 1A). These results reveal that uniform light-induced depolarization is sufficient for cardiac defibrillation. Quantitatively, application of 1 single light pulse (1 second, 0.4 mW/mm², 143 mm²; Supplemental Figure 1B) resulted in arrhythmia termination with an average success rate of about 85%, independent of the preceding arrhythmia duration (3, 5, or 10 seconds; Figure 1B, blue). Control experiments without illumination showed that the rate of spontaneous arrhythmia termination in the same time window was very low (<15%, $P < 0.04$; Figure 1B, black). To further enhance optogenetic defibrillation efficacy, we developed an illumination protocol involving 4 consecutive light pulses (1 second, 0.4 mW/mm², 143 mm²; Supplemental Figure 1C), which yielded a very high success rate of 97% ± 0.01% (n = 29; Figure 1C, blue). Importantly, when the identical illumination protocol was applied to hearts without ChR2 expression from EGFP-expressing or CD1 WT mice, the arrhythmia termination rate in the same time window was approximately 20% (Figure 1C, green and red). This value is similar to the spontaneous termina-

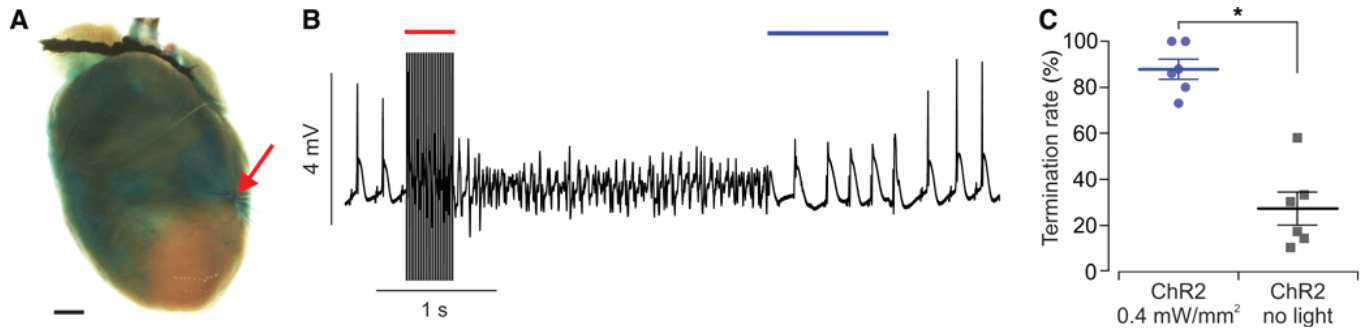

Figure 2. Optogenetic defibrillation of infarct-related ventricular arrhythmia in ChR2-expressing hearts. (**A**) Image of the whole heart after ligation of the left anterior descending coronary artery (red arrow) and dye perfusion (blue), highlighting the nonperfused infarct area. (**B**) Representative ECG (black) after ligation. Note the prominent elevation of the ST segment during normal sinus rhythm. Ventricular arrhythmia was induced by electrical burst stimulation (50 Hz, red bar) and terminated by epicardial illumination with blue light (blue bar, 470 nm, 1 second, 0.4 mW/mm^2, 143 mm^2, n = 10). (**C**) Arrhythmia termination rate in infarcted hearts induced by one 1-second-long light pulse (0.4 mW/mm^2, 143 mm^2, blue) applied 5 seconds after induction of arrhythmia compared with control (i.e., no illumination, black) within the same time window (see Supplemental Figure 1B for experimental protocol; Wilcoxon matched pairs test, P = 0.031, n = 6). Scale bar: 1 mm. Data are shown as the mean ± SEM.

tion rate in the absence of illumination in transgenic ChR2 hearts (Figure 1C, black). Thus, neither illumination of ChR2-negative hearts nor ChR2 expression in the absence of illumination caused or facilitated arrhythmia termination.

To determine how different illumination parameters affect defibrillation success rates, sequential protocols with light stimuli of varying duration, intensity, and size of illuminated area were tested (Supplemental Figure 1, A and C). This revealed a significant influence of light stimulus duration, and the defibrillation rate was low for durations less than 100 ms (Figure 1D), suggesting that illumination lasting for at least the duration of the entire VT cycle (~80 ms) was required for successful arrhythmia termination. Decreasing the illuminated area to 15 mm^2 also reduced efficacy (Figure 1E), and in this situation the light intensity needed to effectively defibrillate increased from 0.4 to 1 mW/mm^2 (Figure 1F). This suggests that optogenetic depolarization of a critical portion of myocardium was necessary to successfully defibrillate.

Optogenetic defibrillation after acute myocardial infarction. To experimentally assess the feasibility of optogenetic defibrillation in a scenario clinically more relevant to the underlying causes of life-threatening arrhythmia in humans, we determined whether infarct-related arrhythmia could be terminated by light. Therefore, hearts from ChR2 mice were perfused ex vivo with standard Tyrode's solution, and the left anterior descending coronary artery was ligated (Figure 2A, arrow). This led to acute myocardial ischemia, which was proven by ST-segment elevation in the ECG (Figure 2B) and by the lack of local perfusion documented by dye injection after the experiment (Figure 2A). Prolonged ventricular arrhythmia could be induced by electrical pacing in 6 of the 12 hearts investigated. In these 6 hearts we found that a single light pulse (1 second, 0.4 mW/mm^2, 143 mm^2) could terminate arrhythmia (Figure 2B) with a success rate of 88% ± 0.04% in contrast to the significantly lower rate of spontaneous termination in the absence of illumination (27% ± 0.07%, P = 0.03; Figure 2C).

Optogenetic defibrillation in WT hearts after gene transfer. After establishing the feasibility of optogenetic defibrillation in transgenic mice, we sought to test the same approach in nontransgenic hearts after gene transfer in vivo, since this would be required for therapeutic applications in humans. We previously used adeno-associated virus (AAV) with tropism toward cardiomyocytes systemically injected into WT mice and found ChR2 expression in approximately 58.2% of cardiomyocytes 4 to 8 weeks later, enabling optogenetic cardiac pacing (6). With the same approach, 1 year after AAV injection we found uniform ChR2 expression throughout the ventricles (Figure 3A) and in all myocardial layers (Figure 3B), localized to the sarcolemma and the T-tubule system of cardiomyocytes (Figure 3C). In vivo optogenetic pacing experiments (5, 6) in these hearts demonstrated stable ventricular pacing 1 year after the AAV injection with a threshold of 0.64 ± 0.20 mW/mm^2 (Figure 3D; 10 ms pulse duration, 15 mm^2 illuminated area, n = 3). This value is similar to our previously reported data for optogenetic pacing 4–8 weeks after injection of AAV (6). Importantly, we also tested optogenetic defibrillation ex vivo 1 year after the AAV injection. Therefore we induced ventricular arrhythmia after low K^+ (2 mM) and pinacidil perfusion and found that illumination (1 second, 0.4 mW/mm^2, 143 mm^2) of the anteroseptal epicardium reliably terminated ventricular arrhythmia in all 3 tested mice (Figure 3E).

Optogenetic defibrillation via epicardial illumination in a model of a patient heart. In order to explore whether our findings in mice could be translated to human hearts for potential clinical applications, we conducted computer simulations of optical defibrillation by epicardial illumination in the heart of a patient suffering recurrent VT. The model (Supplemental Figure 2) was reconstructed from a late gadolinium enhancement MRI scan of a patient with myocardial infarction and VT episodes that required defibrillator implantation. Consistent with clinical observations, rapid electrical pacing from the ventricular apex in this model induced infarct-related, sustained VT (cycle length: ~350 ms; Supplemental Figure 3 and Supplemental Video 1), which was evident in the pseudo-ECG (Figure 4A). Based on expression levels in our previous reports on AAV gene transfer (6), we simulated expression of ChR2 in 58.2% of the cardiomyocytes (Supplemental Figure 4) using an optogenetic modeling framework (13) validated by comparison with in vitro recordings from ChR2-expressing cardiomyocyte syncytia (14). The ChR2

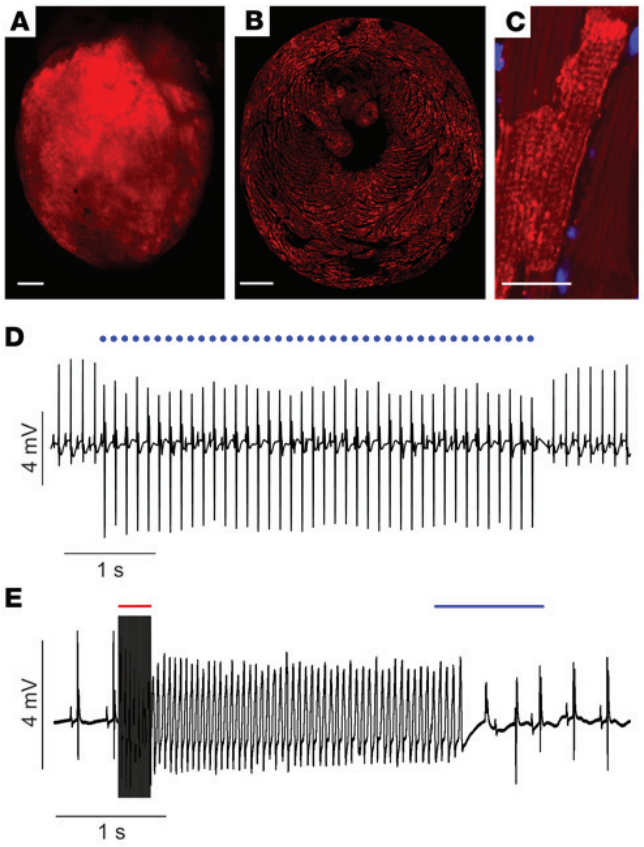

Figure 3. Optogenetic pacing and defibrillation in hearts 1 year after in vivo gene transfer. (**A**) Epicardial mCherry fluorescence signal of a mouse heart 16 months after systemic injection of ChR2-mCherry AAV. (**B**) Section through the left ventricle showing transmural mCherry fluorescence. (**C**) Membrane-bound ChR2-mCherry signals in a ventricular cardiomyocyte. (**D**) Pulsed illumination (blue dots, 470 nm, 10 ms, 0.36 mW/mm^2, 15 mm^2, n = 3) of the left ventricle in vivo induced ectopic ventricular pacing, as shown in the ECG (black). (**E**) VT episode was terminated by epicardial illumination (470 nm, 1 second, 0.4 mW/mm^2, 143 mm^2, n = 3) of the ventricles. Scale bars: 1 mm (**A** and **B**) and 20 μm (**C**); nuclear staining in blue.

photocurrent model (15) was calibrated to match measurements from AAV-transfected mouse cardiomyocytes (6).

We have recently shown in computer stimulations that for optogenetic defibrillation of a structurally normal heart by simultaneous epicardial and endocardial illumination, red light and increased opsin light sensitivity (increased 2.2-fold vs. normal ChR2) are needed (16). These changes are consistent with the biophysical properties of red-shifted ChR2 variants (17, 18) and the CatCh variant of ChR2 (19), respectively. Accordingly, to assess the feasibility of light-based defibrillation in the more complex setting of a patient heart with structural and electrophysiological heterogeneities, we performed simulations with the same optogenetic parameters. However, epicardial-only illumination was simulated, because the feasibility of endocardial illumination is questionable. Our simulations revealed that exclusive illumination from the epicardium with red light (1 second, 10 mW/mm^2, 669 nm) effectively terminated the sustained VT (Figure 4, B and C, and Supplemental Video 2).

Critical biophysical determinants for optogenetic defibrillation. Next, we investigated the critical factors underlying successful optogenetic defibrillation by analyzing membrane potential (V_m) traces from epicardial, midmyocardial, and endocardial sites during simulated illumination (Figure 5A). Our analysis revealed simultaneous transmural excitation upon illumination, followed by strong diastolic depolarization (~–40 mV) that affected all layers (Figure 5B) and completely abrogated Na^+ channel excitability, even in the endocardial layer (Figure 5C). Therefore, action potential initiation during illumination became purely Ca^{2+} current–dependent (Figure 5C), resulting in a critical decrease in the excitability of the illuminated myocardial wall. Importantly, the deepest layer in which red light depolarized at least 75% of all cardiomyocytes beyond the threshold to inactivate 90% of Na^+ channels (V_m = –65.8 mV) was 6 mm from the epicardium (Figure 5D, red arrow). Consequently, the wavefront emerging from the isthmus of the re-entrant circuit, located in the nonilluminated ventricular septum, could not propagate through the optogenetically depolarized right ventricular free wall, thereby leading to VT termination (Figure 5E and Supplemental Video 3).

To verify that transmural depolarization is critical for optogenetic defibrillation, we simulated epicardial illumination with blue light, which is much more attenuated by heart tissue (Supplemental Figure 5) (20). In fact, blue light (488 nm) triggered an initial epicardial excitation, which propagated transmurally and induced the above-defined degree of depolarization to block Na^+ channels only within 1 mm of the epicardial surface (Figure 5D, blue arrow, and Supplemental Figure 6A). Therefore, the excitation wavefront emerging from the septum was able to propagate through the endocardial layer of the right ventricular free wall, sustaining re-entrant propagation (Supplemental Figure 6, B and C, and Supplemental Video 2 and 3).

Modeling of pericardial illumination. Since illumination of the pericardium, rather than direct application of light to the epicardium, will be practically more feasible, we performed additional calculations to assess how the tissue layers surrounding the human heart would attenuate light. First, we considered layers of epicardial fat and pericardium assuming uniform thickness based on values previously reported for these layers in humans (4.1 and 1.7 mm, respectively) (21, 22). We found that the intensity of a pericardial light stimulus would need to be 4.7-fold higher than the target intensity on the epicardium in order to overcome attenuation in the fibrous and adipose layers covering the heart (Supplemental Figure 7A). Since individual and regional variability in epicardial fat thickness has been reported (21), we analyzed the consequences and found a required increase in pericardial light stimulus strength from approximately 2-fold in the absence of fat to approximately 10-fold when the adipose tissue layer was 8 mm thick (Supplemental Figure 7B).

Discussion

Herein we demonstrate effective optogenetic defibrillation in the intact mouse heart by epicardial illumination. To enable these experiments, we had to establish a new approach to reliably induce sustained ventricular arrhythmia in the small mouse heart, which normally lasts only a few seconds in vivo (12). Our approach is to perfuse explanted mouse hearts with low-K^+ solution, which is known to promote arrhythmias (23), and pinacidil, which activates

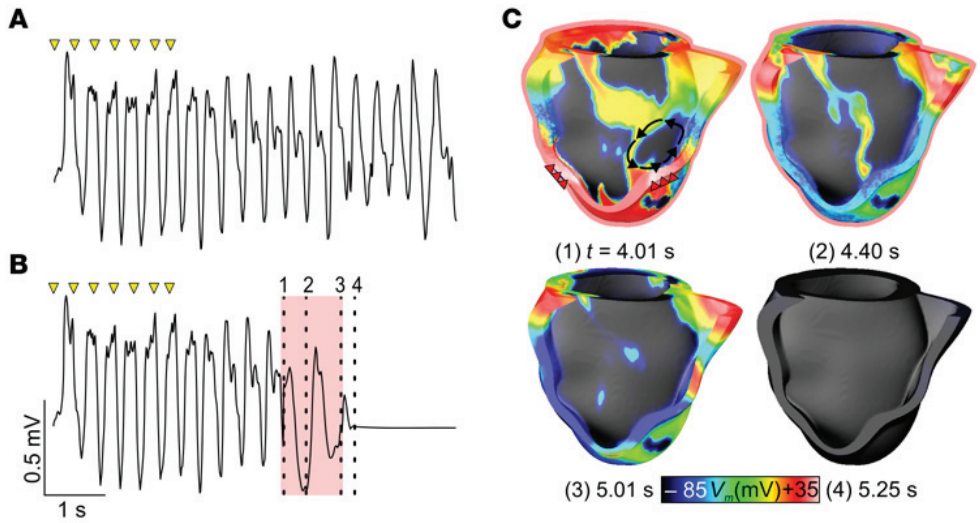

Figure 4. Optogenetic defibrillation in a model of a patient heart with infarct-related VT. (**A** and **B**) Pseudo-ECG signals for model configurations with no illumination (**A**) and epicardial illumination with red light (669 nm, 10 mW/mm^2, 1 second, red box, **B**). VT was induced by electrical stimulation (yellow triangles). (**C**) Snapshots of V_m distribution during the response to red light. Timings (from start of simulation) correspond to dashed lines in **B**. The right ventricular free wall is cut away to facilitate visualization. Black arrows indicate propagation of reentry during VT (see also Supplemental Figure 3 and Supplemental Videos 1 and 2); red triangles indicate initial excitations induced directly by optogenetic stimulation.

the ventricular Kir6.2/SUR2A K_{ATP} channels (24) and thus mimics pro-arrhythmic effects of ischemia, including action potential shortening and dispersion of repolarization and refractoriness (25). The ex vivo retrograde perfusion of the coronary arteries in the Langendorff configuration has the distinct advantage of constant oxygen and nutrition supply even during long episodes of sustained ventricular arrhythmia, enabling multiple defibrillation attempts for systematic analysis of defibrillation success rate.

Epicardial illumination proved to be highly efficient in all ChR2-expressing mouse hearts tested in terminating ventricular arrhythmias, the ECG patterns of which resembled those of VT, torsades de pointes, and VF. By comparing light-induced and spontaneous arrhythmia termination in ChR2-expressing hearts and by investigating control hearts without ChR2, we proved unequivocally that neither illumination nor ChR2 expression per se is sufficient for arrhythmia termination. Instead, optogenetic defibrillation is achieved by light-induced depolarization of ChR2-expressing cardiomyocytes. We found that optogenetic defibrillation required higher light intensities, longer durations, and larger illumination sizes compared with optogenetic pacing (5), reflecting the clear mechanistic difference between pacing, for which local depolarization is sufficient, and defibrillation, which requires depolarization of a much larger tissue volume (9). This requirement of defibrillation was proven in earlier work by selective coronary injection of potassium chloride, demonstrating that VF in canines could only be terminated when a critical amount of myocardium was depolarized (9). Our findings are consistent with these experiments because diminishing the illumination area reduced the efficacy of optogenetic defibrillation.

Although our experimental work here demonstrated the efficacy of optogenetic defibrillation after acute myocardial infarction and after AAV-based ChR2 gene transfer of WT mice, it is difficult to extrapolate these results to the human heart. Thus, the next step will be the extension of this technology to preclinical large-animal models with electrical and structural defects comparable to the human heart. As a preliminary proof-of-concept exploration in humans, we simulated optogenetic defibrillation in a human model of infarct-related VT (26). Our group has recently demonstrated the in silico approach to simulate this type of arrhythmia and its predictive power and clinical relevance, by predicting, with high accuracy and reliability, postinfarction risk of sudden cardiac death in a cohort of 41 patients (27). Here, in contrast to our recent modeling of optogenetic defibrillation in structurally normal ventricles (16), we exclusively illuminated the epicardial surface. This is because intracavitary optogenetic stimulation of the endocardium would be extremely challenging because of the presence of light-absorbing blood, the need for anticoagulation, and the difficulty of implanting light-emitting diodes (LEDs) within the densely trabeculated endocardium of the beating heart without compromising ventricular function or hemodynamic stability. Conversely, illumination of the epicardium in the human heart could be achieved by leveraging new developments in optoelectronics, such as light sources integrated in cell-scale injectable devices (28) or stretchable integumentary membranes, which have been proven useful for illumination of the heart (29). Moreover, because direct epicardial implantation of light sources will be associated with risks of infection, pericarditis, friction, or coronary artery damage, we anticipate that illumination in the human heart would be more feasible from the pericardial surface. Thus, we performed mathematical analysis to approximate the extent of light attenuation in the pericardium and epicardial fat and found that the intensity of light applied to the pericardium would need to be increased approximately 5-fold compared with direct epicardial illumination. However, excessive epicardial fat would greatly attenuate light and thus diminish the effectiveness of optogenetic defibrillation by pericardial illumination.

The new mechanistic insights presented here suggest that ventricular arrhythmia can be terminated not only by electrical shock–induced brief excitation, but also by a steady-state optogenetic modulation of electrical activity involving transmural depolarization and Na^+ channel inactivation. Importantly, our simulations clearly demonstrate that transmural depolarization depends critically on effective light penetration. This parameter is influenced greatly by the wavelength dependency of light penetration and, to a lesser degree, by ChR2 light sensitivity, photocurrent, or expression levels. Thus sufficient transmural depo-

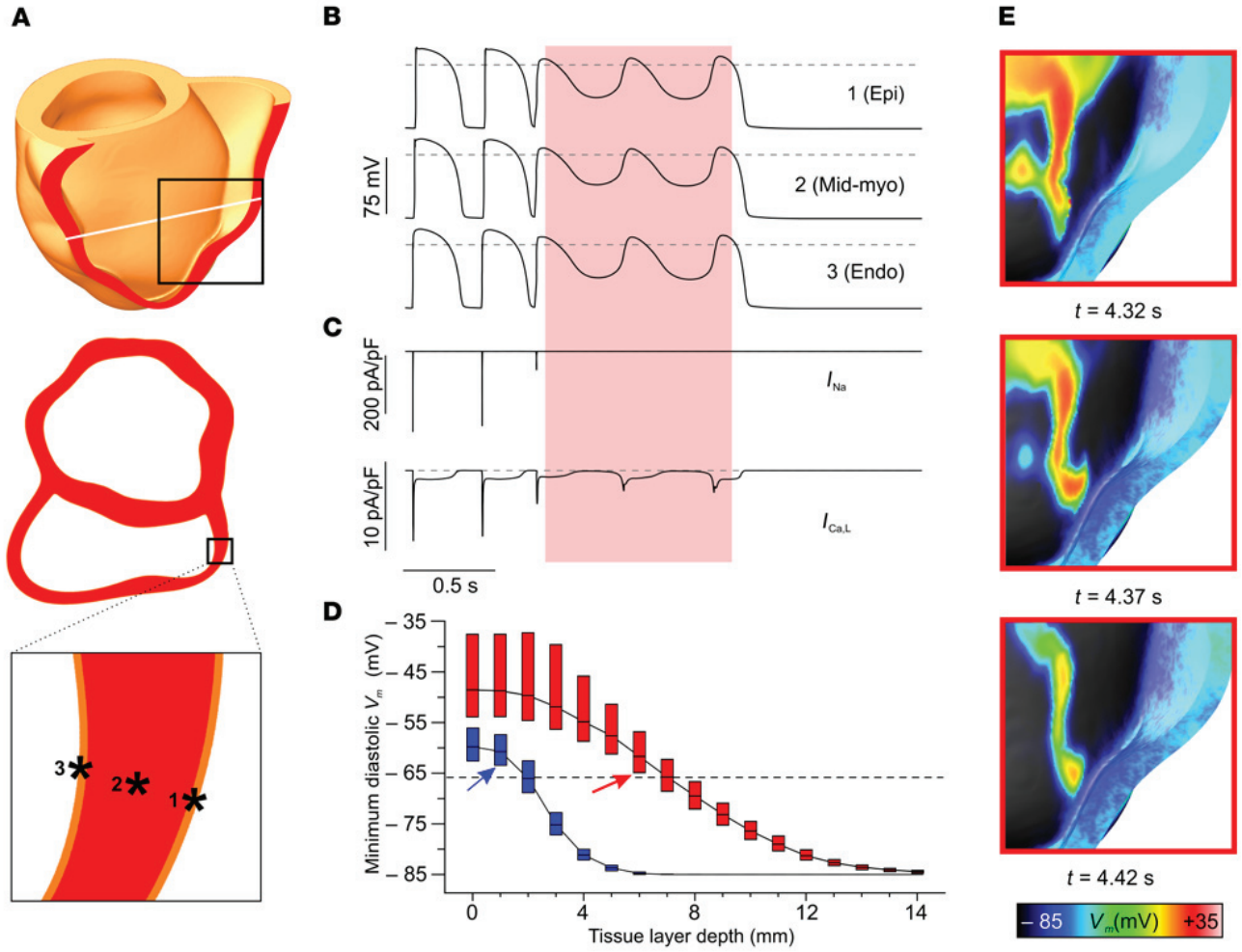

Figure 5. Mechanism of optogenetic defibrillation in the human heart. (**A**) Illustration of the locations of sites 1–3 on the right ventricular posteroseptal wall. (**B**) V_m traces from sites 1–3 during epicardial illumination with red light (669 nm, 1 second, 10 mW/mm^2, red box) Dashed lines indicate V_m = 0. (**C**) Ionic Na^+ (I_{Na}) and L-type Ca^{2+} ($I_{Ca,L}$) currents underlying V_m from endocardial site 3 in **B**. (**D**) Minimum diastolic V_m values during illumination with blue (488 nm) and red light as a function of depth in the ventricular free walls. Upper quartile, median, and lower quartile values are shown. Blue and red arrows indicate the deepest tissue layers in which more than 75% of cardiomyocytes had a minimum diastolic V_m exceeding the threshold for 90% inactivation of Na^+ current (V_m = –65.8 mV, dashed line). (**E**) Zoomed-in snapshots of V_m distribution during the illumination at the indicated time points from start of simulation (see also Supplemental Video 3). Snapshots were taken from the region shown in **A** (black rectangle, in top panel).

larization at low light intensities will be facilitated by exploiting recent advances in optogenetics, like red-shifted and hypersensitive ChR2 variants (17–19).

The fact that optogenetic defibrillation in human diseased hearts is feasible using only epicardial illumination and that cardiac gene expression via AAV in humans is safe (30) suggests the tantalizing possibility that clinical applications might be feasible. Importantly, we were able to demonstrate effective pacing and defibrillation of mouse hearts by epicardial illumination even more than 1 year after the gene transfer. The great advantage of optogenetic defibrillation is that this would be, in contrast to electrical shocks, pain-free, because ChR2 expression would be restricted to cardiomyocytes by cardiomyocyte-specific AAV vector capsids (30) or promoters (31). Notably, AAV-mediated transduction will result in spatial heterogeneity of ChR2 expression, which is not expected to be pro-arrhythmic per se since ChR2 has neither a leak current in the absence of illumination nor does it affect the electrophysiological properties of cardiomyocytes (5). During illumination, however, non-uniformities in either ChR2 expression or light application could result in heterogeneous excitation patterns, which might have secondary pro-arrhythmic consequences (e.g., reinitiation of VT/VF) in addition to the primary effect of optogenetic defibrillation. Fortunately, in contrast to electrical shocks, light stimuli used for optogenetic defibrillation have a much higher degree of flexibility, because spatially and temporally shaped light patterns minimizing secondary pro-arrhythmic effects could be used. Moreover, unlike defibrillation shocks, sequential light pulses can be applied repetitively, as these do not require the charging of a capacitator to generate high-voltage fields. In fact, our experimental results in mouse hearts showed that 4 consecutive light pulses instead of 1 increased the termination rate from 85% to 97%. Importantly, the optogenetic modeling approach presented here makes it possible to predict in silico the effectiveness of novel red-shifted ChR2 variants, gene transfer strategies, or illumination technologies before conducting large animal experiments in vivo and before proposing individualized clinical trials,

e.g., for therapy-resistant patients who experience frequent painful electrical shocks from implanted defibrillators.

Methods

Animals. Experiments on transgenic ChR2-expressing mice were performed with 23 males (aged 4–15 months, median 6 months) and 27 females (aged 3.5–14.5 months, median 4.5 months) from a previously established mouse line (5) expressing ChR2 with the H134R mutation (32) under the control of the chicken β-actin (CAG) promoter and backcrossed at least 10 generations onto a CD1 genetic background. The CAG-EGFP mouse line was reported before (5), backcrossed at least 10 generations onto a CD1 genetic background, and we used five 2.5- to 3.5-month-old females. From the CD1 WT strain (Charles River) we used 7 female mice 6.5 to 12 months old as controls and three 10-week-old female mice for ChR2 gene transfer by systemic injection of AAV.

Optogenetic defibrillation. Mice were heparinized and sacrificed by cervical dislocation. Hearts were explanted and perfused in Langendorff configuration with Tyrode's solution containing (in mM) 140 NaCl, 5.4 KCl, 1.8 $CaCl_2$, 2 $MgCl_2$, 10 glucose, and 10 HEPES (pH 7.4, adjusted with NaOH). A bipolar cardiac electrogram was recorded with a silver chloride electrode placed at the right atrium and a metal spoon under the apex of the heart using a bio-amplifier recording system (PowerLab 8/30, Animal Bio Amp ML 136, LabChart 7.1 software, AD Instruments). Electrical stimulation (1–10 mA, 2 ms) was applied via a bipolar silver chloride electrode (<3 mm distance) placed epicardially. The local effective refractory period (ERP) was determined using an S1-S2 protocol, with 6 stimuli at a cycle length of 150 ms (S1) followed by a premature stimulus (S2) with a variable delay (<150 ms) that was decreased in 5-ms increments. The shortest delay for successful S2 pacing was defined as the local ERP. The electrode was relocated until an epicardial site with a low local ERP (<55 ms) was identified, because we observed that pacing from such locations was the most reliable way to induce ventricular arrhythmia in mouse hearts. Application of either electrical burst stimulation (50 Hz, 20–50 pulses) or an S1-S2 protocol with an S2 delay exceeding the local ERP by less than 5 ms evoked free-running ventricular arrhythmia. In standard Tyrode's solution, arrhythmia episodes often terminated spontaneously after less than 15 seconds. Because sustained arrhythmias are required to test optogenetic defibrillation, we lowered the potassium concentration to 2 mM and added 100 μM pinacidil, which enabled induction of sustained (>30 seconds) ventricular arrhythmia. Notably, optogenetic defibrillation was attempted in all cases at least 3 seconds after induction, which led to inclusion of sustained arrhythmia only and exclusion of self-terminating VTs, most of which were shorter than 3 seconds. Illumination of the anterior ventricular epicardium (Supplemental Figure 1A) was performed with a macroscope (MVX10, Olympus) equipped with a 1× objective (MVPLAPO1x, numerical aperture 0.25) using 470-nm LEDs (LEDC5 and LEDD1, Thorlabs, or GCS-0470-50-A0510 and BLS-13000-1, Mightex) attached to the epifluorescence port. LED pulse duration and intensity were controlled and sampled with the bio-amplifier recording system. The spatial extent of the illuminated area was varied using the zoom function of the macroscope (Supplemental Figure 1A). Light intensity was calibrated by measuring the light power with a power meter (PM100 and S130A, Thorlabs) and dividing by the illuminated area. The maximum light intensities tested were 0.4, 1.5, and 1.5 mW/mm^2 for 143-, 29-, and 15-mm^2 large circular areas, respectively.

We assessed defibrillation success rates by conducting multiple defibrillation attempts per heart using 2 different protocols as follows. (a) Single-light-pulse protocol (Supplemental Figure 1B): VT/VF episodes were allowed to stabilize for 3, 5, or 10 seconds after induction. Subsequently, 1 single light pulse (1 second, 0.4 mW/mm^2, 143 mm^2) was applied, and we determined whether it terminated the arrhythmia within 4 seconds after the start of illumination (green box in Supplemental Figure 1B); otherwise, rescue defibrillation was performed. Spontaneous termination rate was analyzed during the same time period but without illumination (Figure 1B, black). (b) Four-light-pulse protocol (Supplemental Figure 1C): VT/VF episodes were allowed to stabilize for 3–15 seconds after induction. Subsequently, 4 light pulses with identical illumination parameters were applied with a 1- to 5-second delay in between, and we determined whether the arrhythmias were terminated between the onset of the first light pulse and 3–10 seconds after the last illumination (green box in Supplemental Figure 1C); otherwise rescue defibrillation was performed. For control experiments, the longest illumination protocols were applied to hearts from transgenic mice expressing EGFP under the control of the chicken β-actin promoter (5) and from CD1 WT mice (Figure 1C, green, red). The rate of spontaneous termination in ChR2 mice was assessed during the maximum duration of the 4-light-pulse protocol (Figure 1C, black) but without illumination. The efficacy of the different illumination parameters (pulse duration, illuminated area, and intensity; Figure 1, D and E) was analyzed using the 4-light-pulse protocol with identical illumination parameters for each of the 4 pulses.

The rescue defibrillation procedure included sequential or simultaneous application of high-intensity illumination (145 mm^2, 0.4 to 0.9 mW/mm^2, >3 seconds), mechanical force applied to the ventricles by tweezers, and/or electrical antitachycardia pacing (50 Hz, >20 pulses). If this procedure did not terminate the arrhythmia, the heart was temporarily perfused with normal Tyrode's solution and, if this restored normal rhythm, optogenetic defibrillation experiments were reattempted.

Acute myocardial infarction. The left anterior descending coronary artery of explanted hearts was ligated with a Prolene 8-0 thread (Ethicon). Ventricular arrhythmias were induced as reported above, but during perfusion with standard Tyrode's solution. This induced prolonged VT/VF episodes (>10 seconds) in 6 of 12 hearts. In these hearts, optogenetic defibrillation was tested 5 seconds after induction using the single-light-pulse protocol (Supplemental Figure 1B), as described above. To verify complete artery ligation, hearts were coronary-perfused after the experiment with the food dye Patent Blue V E131 (Brauns-Heitmann), and macroscopic images were taken (see below).

AAV-based gene transfer and optical cardiac pacing. Systemic injection of AAV was performed as reported earlier (6). Briefly, the AAV9-CAG-hChR2(H134R)-mCherry virus consisting of AAV9 virus capsid and AAV2 virus DNA was obtained from the Penn Vector Core (University of Pennsylvania) and injected into the jugular vein of WT mice anesthetized by inhalation of 1.5% isoflurane and O_2/N_2O (50%/50%). For this purpose, a 5-mm-long cervical incision was performed, 2×10^{11} AAV particles diluted in 100 μl of PBS were slowly (~10 seconds) injected, bleeding was stopped with forceps and surgical swabs, and the skin was sutured (Prolene C-1 13 mm 3/8c, Ethicon).

For optical cardiac pacing in vivo, mice were intubated and ventilated with 1.5% to 2.5% isoflurane and O_2/N_2O (50%/50%) 16 months

after the virus injection. To expose the beating heart, the rib cage was carefully removed as reported earlier (5, 6). Cardiac ECGs were recorded from a needle electrode placed at the right front leg and a spoon placed below the heart for stabilization using the bio-amplifier recording system (see above). Heart rates were adjusted to 350 to 450 bpm by varying isoflurane concentration. Optical pacing of the epicardial surface of the left ventricle was performed at a constant frequency 30 to 50 bpm above basal heart rate using the macroscope and LED system (see above). At each light intensity, a train of 40 light pulses was applied, and the threshold for optical pacing was defined as the minimal light intensity required to achieve 1:1 stimulation for the last 20 pulses. After in vivo optical pacing, hearts were explanted during anesthesia and perfused in Langendorff configuration. Optogenetic defibrillation was then tested as described above.

Histology and immunofluorescence. High-resolution macroscopic images were recorded from explanted and perfused hearts with an AxioZoom.V16 macroscope equipped with a PlanApoZ ×1.0 objective lens, a 43 HE filter set, and an AxioCam MRm camera with ZEN 2012 software (all Zeiss). Images of the curved epicardium were generated using Z-stacks and the extended focus module (Zeiss). Hearts were fixated by perfusion with 4% paraformaldehyde, dehydrated in 20% sucrose, cryopreserved, and sectioned in 10-μm-thick slices with a cryotome (Cryostat CM3050 S, Leica). Heart slices were permeabilized with 0.2% Triton X (Sigma-Aldrich) for 20 minutes. Nuclear staining was performed with 0.1% Hoechst 33342 (Sigma-Aldrich) for 1 hour at room temperature. Microscopic pictures were taken with inverted fluorescence microscopes (Axiovert 200M) equipped with the Apotome section module, a ×20 or ×40 Plan-Apochromat objective, AxioCam MRc or MRm camera, ZEN 2012 or AxioVision software, a 64 HE filter set (all Zeiss), and an mCherry filter set (F46-008, AHF Analysentechnik).

Geometrical model of the diseased human ventricles. We used a computational model of the diseased human ventricles reconstructed from clinical late gadolinium-enhanced MRI (LGE-MRI) scans of a patient with post–myocardial infarction VT (33). The modeling approach has been previously validated in infarct-related VT inducibility studies (12, 34, 35). Our laboratory pipeline for cardiac model reconstruction has been described in detail in previous work (12, 34–37). Briefly, anatomical landmark points on the epicardial and endocardial walls were identified manually in each LGE-MRI slice. These points were used as input data for previously described interpolation software, which was used to recreate a 3D rendering of the cardiac surfaces. To represent the patient's infarct geometry, tissue within the ventricular contours on each 2-dimensional LGE-MRI slice was classified as diseased or healthy via signal thresholding. Diseased tissue was then classified as either peri-infarct zone (PIZ) or infarct using a validated full-width half-maximum approach (38). 3D boundaries between the 3 tissue regions were reconstructed using a shape-based interpolation approach (39) that has been validated for use in characterizing myocardial scar (40). We then combined infarct and PIZ contours with the rendering of ventricular geometry and used a fully automatic octree-based technique (41) to generate a boundary-fitted, locally refined, smoothed, and conformal 3D mesh (Supplemental Figure 2) suitable for finite element modeling of cardiac electrophysiology. The ventricular mesh had 2,110,030 points and 2,687,615 volumetric elements. Finally, myocardial fiber orientations were assigned throughout this mesh using a previously validated rules-based approach (42).

Simulation of cardiac electrophysiology and numerical methods. Electrophysiology of normal and diseased human cardiac tissue was represented using an extensively validated approach (35). Briefly, cell- and tissue-scale properties were assigned to all 3 regions in the ventricular mesh: normal myocardium, PIZ, and infarct. At the cell scale, the infarcted region was modeled as electrically passive. In the PIZ and normal myocardium, action potential dynamics were represented via a validated human-specific model (43). In the PIZ, specific modifications to this model were incorporated to represent electrophysiological remodeling observed in patch-clamped myocytes harvested from the infarct border zone: fast sodium current (I_{Na}) was decreased by 62% (44), L-type calcium current ($I_{Ca,L}$) was decreased by 68% (45), and delayed rectifier potassium currents (I_{Kr} and I_{Ks}) were decreased by 80% and 70%, respectively (46). Consequently, the PIZ action potential differed from that in the normal myocardium: +16.1% duration, –42.2% upstroke velocity, and –42.8% amplitude. These changes were consistent with previously reported values (47, 48). At the tissue scale, the infarcted region was modeled as nonconductive. In normal myocardium, longitudinal and transverse intracellular conductivity values were scaled to 0.255 and 0.0775 S/m, respectively. This resulted in longitudinal and transverse conduction velocities (CV_L = 59.9 and CV_T = 33.5 cm/s, respectively) consistent with values measured in experiments with human ventricular tissue (49, 50). In the PIZ, transverse intracellular conductivity was reduced by 90% to represent connexin-43 remodeling observed in the infarct border zone (51). Because of this change and differences in cell-level electrophysiology (as described above), PIZ conduction velocities were lower than in normal myocardium (CV_L = 49.2 cm/s, CV_T = 4.16 cm/s) and had a larger anisotropy ratio (11.8:1 vs. 1.79:1). Excitation propagation in the ventricular model was modeled via the monodomain formulation as implemented in the CARP software (Johns Hopkins University, Université de Bordeaux, Medizinische Universität Graz) (52, 53). As described previously (52), a leapfrogging approach was used to couple the monodomain partial differential equation with the system of ordinary differential equations that modeled cell-level phenomena. Our previous studies have described rigorous validation of this computational framework against experimental measurements (14, 34, 54–56). All simulations were executed on 24 Intel Haswell CPUs (2.5 GHz) on the parallel computing resource at the Maryland Advanced Research Computing Center. The total wall time required to simulate 1 second of electrophysiological activity in the ventricular model was about 1 hour 40 minutes.

Simulation of channelrhodopsin expression and illumination. To simulate optogenetic transduction of the human ventricles via viral gene delivery, we used our previously validated computational modeling framework (13, 14, 57). Channelrhodopsin expression was modeled by incorporation of a photocycle model (15) in 58.2% of myocardial nodes (normal + PIZ) with a diffuse spatial pattern (Supplemental Figure 4). This value corresponded to the reported average percentage of ChR2-expressing cardiomyocytes in mouse hearts after systemic AAV injection (6). The ChR2 channel conductance parameter was calibrated to 0.17 mS/cm^2, resulting in a peak photocurrent of 5.04 pA/pF when a simulated myocyte clamped to V_m = –52 mV was subjected to blue illumination (5 mW/mm^2). This value matched (<1% error) recorded peak photocurrent in patch-clamped ChR2-positive myocytes from our earlier study (6). ChR2 light sensitivity was adjusted to the CatCh variant (17, 19) by increasing the model rate parameters controlling the dark- and light-adapted transitions between closed and

open states (i.e., *k1* and *k2* in the Williams et al. model; ref. 15) by 2.2-fold. This resulted in a half-maximal optogenetic activation level (i.e., threshold irradiance to elicit 50% of maximal I_{ChR2}) of 0.4 mW/mm^2, which was consistent with the reported value for CatCh (58). The expression for ChR2 photocurrent was:

$$I_{ChR2} = g_{ChR2}(O_1 + \gamma O_2)(V_m - E_{ChR2})$$

(Equation 1)

where g_{ChR2} was the maximal channel conductance (0.17 mS/cm^2), $\gamma = 0.1$ was the conductance ratio between dark- and light-adapted open channel states (O_1 and O_2, respectively), and $E_{ChR2} = 0$ mV was the ChR2 reversal potential. The ordinary differential equations controlling light- and voltage-dependent rates of change in O_1, O_2, and other model state variables can be found in previous publications (13, 15, 57). At the organ scale, we used a finite element approximation of the steady-state photon diffusion equation to model light attenuation due to scattering and energy absorption in the ventricular myocardium (13, 57). The corresponding partial differential equation, which assumes isotropic absorption and homogenous scattering, is given by:

$$D\nabla^2 E_e(r) - \mu_a E_e(r) = -w(r)$$

(Equation 2)

where E_e and w are, respectively, the distributions of irradiance and photon sources at each point r; ∇^2 is the Laplace operator; D is the diffusivity of light in cardiac tissue; and μ_a is the light absorption rate. As described previously (57), w is set to zero and the equation is solved with Dirichlet boundary conditions derived from the placement of simulated light sources. We validated this approach in earlier work concerned with simulation of optical mapping experiments (20). Optical parameters of myocardium were derived from experimentally measured values for cardiac tissue (59) and depended on whether the applied illumination was blue ($\lambda = 488$ nm, $D = 0.18$ mm, $\mu_a = 0.52$ mm^{-1}) or red ($\lambda = 669$ nm, $D = 0.34$ mm, $\mu_a = 0.10$ mm^{-1}). As shown in Supplemental Figure 5, this resulted in significantly deeper light penetration for red stimuli (approximate exponential decay rate $\delta = 1.84$ mm) compared with blue stimuli ($\delta = 0.588$ mm).

Additional calculations were performed to analyze how optical energy requirements for optogenetic defibrillation would be affected if red light were applied to the outer surface of the pericardium instead of directly to the epicardium. This illumination configuration was modeled by assuming the heart was surrounded by a layer of adipose tissue (i.e., epicardial fat) and a fibrous sac filled with fluid (i.e., visceral and parietal pericardial membranes plus pericardial fluid). Both layers were assumed to have uniform thickness based on nominal measurements from human patients: 1.7 mm for the pericardium (21) and 4.1 mm for the epicardial fat layer (22). To quantify how variability in the extent of epicardial fat would affect the light energy required for optogenetic defibrillation, we considered a range of possible adipose layer thicknesses (0 to 8 mm) and calculated, for each case, the applied pericardial E_e necessary to ensure that light with a particular $E_{e,0}$ value was able to reach the epicardial surface based on the exponential decay approximation:

$$E_e(x) = E_{e,0}e^{-x/\delta}$$

(Equation 3)

Optical decay rates (δ) for nonmyocardial layers were obtained from the available literature, with optical diffusivity values derived from absorption and scattering coefficients (μ_a and μ_s', respectively) using the following formulas:

$$D = \frac{1}{3(\mu_a + \mu_s')}$$

(Equation 4)

$$\delta = \sqrt{\left(\frac{D}{\mu_a}\right)}$$

(Equation 5)

For the epicardial fat layer, we used parameter values for red light (669 nm) illumination of subcutaneous adipose tissue ($\mu_a = 0.0134$ mm^{-1} and $\mu_s' = 1.13$ mm^{-1}, $D = 0.292$ mm, $\delta = 4.66$ mm) (60). Relevant measurements of the mammalian pericardium were not found in the literature; thus, for the pericardium in our model, we used optical parameters reported for the human peritoneum ($\mu_a = 0.0270$ mm^{-1}, $\mu_s' = 1.83$ mm^{-1}, $D = 0.180$ mm, $\delta = 2.56$ mm) (61, 62).

Protocol for initiation and optogenetic defibrillation of VT. Sustained arrhythmia (≥5 seconds of self-sustained re-entrant activity) was initiated by a rapid pacing sequence resembling the clinical protocol for electrophysiological study in VT patients (59). A train of six 10-ms-long electrical stimuli (S1) was delivered to the ventricular apex at a cycle length of 350 ms. This was followed by a premature stimulus (S2, coupling interval = 270 ms), which induced sustained VT (Figure 4A, Supplemental Figure 3, and Supplemental Video 1). Three unique simulations were conducted with different optogenetic configurations: control (no illumination), blue illumination (488 nm), and red illumination (669 nm). For the latter 2 cases, light stimulation (10 mW/mm^2) was applied to the entire epicardial surface for 1 second. Light pulse onset time was at $t = 4$ seconds, approximately 2 seconds after the delivery of the S2 stimulus.

Pseudo-ECGs. Extracellular potential from 2 points approximately 1 cm away from the left and right ventricular surfaces (φ_{LV} and φ_{RV}, respectively; black dots in Supplemental Figure 3) was calculated using an approach we have used in previous studies (63, 64). Pseudo-ECG signals (Figure 4, A and B, Supplemental Figure 6B, and Supplemental Video 2), analogous to clinical lead I (i.e., left arm minus right arm), were obtained by subtraction of φ_{RV} from φ_{LV}.

Analysis of diastolic depolarization and Na$^+$ current inactivation. To characterize minimal diastolic transmembrane voltage (V_m) values within the free ventricular walls (without the septum) during illumination (Figure 5D), 3D maps of V_m were output at high temporal resolution (1-ms time step) for the interval during which stimulation was applied ($t = 4$–5 seconds). Data within the first 100 ms (i.e., $t = 4$–4.1 seconds) were excluded from analysis to ensure that these values were not biased toward either fast upstrokes associated with the initial response to optogenetic stimulation (i.e., directly light-induced action potentials) or low preillumination resting potentials. The threshold for

90% inactivation of Na^+ current (dashed line in Figure 5D) was derived by identification of the specific value (V_m = –65.8 mV) for which h_∞ was equal to 0.1 in the human ventricular action potential model (43).

Statistics. Because of the exploratory nature of this study, effect sizes could not be predicted, and thus prior power analysis to determine the sample sizes could not be performed. Randomization and blinding for mouse strains were not applicable because the light pulse–induced stimulation is disclosing the ChR2 genotype. For statistical comparison (Figure 1, B–F, and Figure 2C), we considered only experiments in which at least 5 defibrillation attempts could be evaluated for each displayed parameter. For each mouse heart, the average termination rate for a given illumination parameter was calculated, displayed as 1 data point in the graphs, and used for subsequent statistical analysis as 1 biological replicate. Because of the non-normal distribution and the unequal variances of average arrhythmia termination rates, the following nonparametric tests were used: the Friedman test to estimate the influences of illumination parameters (Figure 1, D–F), the 1-way ANOVA Kruskal-Wallis with Dunn's multiple-comparison post-test for comparison between different mouse lines (Figure 1C), and the Wilcoxon matched pairs *t* test for comparison between protocols with and without illumination in ChR2-expressing hearts (Figure 1B and Figure 2C). Statistics were calculated with GraphPad Prism (GraphPad Software). *P* values less than 0.05 were considered statistically significant and are indicated by $^*P \le 0.05$, $^{**}P \le 0.01$, and $^{***}P \le 0.001$ in the figures. Data are shown as mean ± SEM unless otherwise indicated.

Study approval. All animal procedures were performed in accordance with the *Guide for the Care and Use of Laboratory Animals* published by the National Institutes of Health (8th edition, revised 2011) and were authorized by the local ethics review board (Landesamt für Natur, Umwelt und Verbraucherschutz Nordrhein-Westfalen, Germany, 84-02.04.2011.A292).

Author contributions

TB, PMB, BKF, NAT, and PS designed the study. TB, CCV, and PS performed the experiments in mice and analyzed the experimental data. HJA developed the human VT model. TVK and PMB performed and analyzed the simulations of the human VT model. TB, PMB, TVK, BKF, NAT, and PS wrote the manuscript.

Acknowledgments

We thank F. Holst for technical assistance and Penn Vector Core, Gene Therapy Program (University of Pennsylvania), for providing the AAV9-CAG-hChR2(H134R)-mCherry.WPRE.SV40 virus vector. This work was supported by the German Research Foundation (SA 1785/5-1, SA 1785/7-1 and Research Training Group 1873 to P. Sasse); the BONFOR Program, Medical Faculty, University of Bonn (O-162.0011 to P. Sasse); and the NIH (DP1 HL123271, R01 HL105216, R01 HL103428, and R01 HL126802 to N.A. Trayanova).

Address correspondence to: Philipp Sasse, Institute of Physiology I, University of Bonn, Life and Brain Center, Sigmund-Freud-Strasse 25, 53127 Bonn, Germany. Phone: 49.228.6885.200; E-mail: philipp.sasse@uni-bonn.de.

1. Marcus GM, Chan DW, Redberg RF. Recollection of pain due to inappropriate versus appropriate implantable cardioverter-defibrillator shocks. *Pacing Clin Electrophysiol*. 2011;34(3):348–353.
2. Reynolds MR, et al. The frequency and incremental cost of major complications among medicare beneficiaries receiving implantable cardioverter-defibrillators. *J Am Coll Cardiol*. 2006;47(12):2493–2497.
3. Sohail MR, Henrikson CA, Braid-Forbes MJ, Forbes KF, Lerner DJ. Mortality and cost associated with cardiovascular implantable electronic device infections. *Arch Intern Med*. 2011;171(20):1821–1828.
4. Larsen GK, Evans J, Lambert WE, Chen Y, Raitt MH. Shocks burden and increased mortality in implantable cardioverter-defibrillator patients. *Heart Rhythm*. 2011;8(12):1881–1886.
5. Bruegmann T, et al. Optogenetic control of heart muscle in vitro and in vivo. *Nat Methods*. 2010;7(11):897–900.
6. Vogt CC, et al. Systemic gene transfer enables optogenetic pacing of mouse hearts. *Cardiovasc Res*. 2015;106(2):338–343.
7. Nussinovitch U, Gepstein L. Optogenetics for in vivo cardiac pacing and resynchronization therapies. *Nat Biotechnol*. 2015;33(7):750–754.
8. Arrenberg AB, Stainier DY, Baier H, Huisken J. Optogenetic control of cardiac function. *Science*. 2010;330(6006):971–974.
9. Zipes DP, Fischer J, King RM, Nicoll A deB, Jolly WW. Termination of ventricular fibrillation in dogs by depolarizing a critical amount of myocardium. *Am J Cardiol*. 1975;36(1):37–44.
10. Burton RA, et al. Optical control of excitation waves in cardiac tissue. *Nat Photonics*. 2015;9(12):813–816.
11. Bingen BO, et al. Light-induced termination of spiral wave arrhythmias by optogenetic engineering of atrial cardiomyocytes. *Cardiovasc Res*. 2014;104(1):194–205.
12. Maguire CT, Wakimoto H, Patel VV, Hammer PE, Gauvreau K, Berul CI. Implications of ventricular arrhythmia vulnerability during murine electrophysiology studies. *Physiol Genomics*. 2003;15(1):84–91.
13. Boyle PM, Williams JC, Ambrosi CM, Entcheva E, Trayanova NA. A comprehensive multiscale framework for simulating optogenetics in the heart. *Nat Commun*. 2013;4:2370.
14. Ambrosi CM, Boyle PM, Chen K, Trayanova NA, Entcheva E. Optogenetics-enabled assessment of viral gene and cell therapy for restoration of cardiac excitability. *Sci Rep*. 2015;5:17350.
15. Williams JC, et al. Computational optogenetics: empirically-derived voltage- and light-sensitive channelrhodopsin-2 model. *PLoS Comput Biol*. 2013;9(9):e1003220.
16. Karathanos TV, Bayer JD, Wang D, Boyle PM, Trayanova NA. Opsin spectral sensitivity determines the effectiveness of optogenetic termination of ventricular fibrillation in the human heart: a simulation study [published online ahead of print March 4, 2016]. *J Physiol*. doi:10.1113/JP271739.
17. Klapoetke NC, et al. Independent optical excitation of distinct neural populations. *Nat Methods*. 2014;11(3):338–346.
18. Lin JY, Knutsen PM, Muller A, Kleinfeld D, Tsien RY. ReaChR: a red-shifted variant of channelrhodopsin enables deep transcranial optogenetic excitation. *Nat Neurosci*. 2013;16(10):1499–1508.
19. Kleinlogel S, et al. Ultra light-sensitive and fast neuronal activation with the Ca^{2+}-permeable channelrhodopsin CatCh. *Nat Neurosci*. 2011;14(4):513–518.
20. Bishop MJ, Rodriguez B, Eason J, Whiteley JP, Trayanova N, Gavaghan DJ. Synthesis of voltage-sensitive optical signals: application to panoramic optical mapping. *Biophys J*. 2006;90(8):2938–2945.
21. Sechtem U, Tscholakoff D, Higgins CB. MRI of the normal pericardium. *AJR Am J Roentgenol*. 1986;147(2):239–244.
22. Flüchter S, et al. Volumetric assessment of epicardial adipose tissue with cardiovascular magnetic resonance imaging. *Obesity (Silver Spring)*. 2007;15(4):870–878.
23. Pezhouman A, et al. Molecular Basis of Hypokalemia-Induced Ventricular Fibrillation. *Circulation*. 2015;132(16):1528–1537.
24. Glukhov AV, Flagg TP, Fedorov VV, Efimov IR, Nichols CG. Differential K(ATP) channel pharmacology in intact mouse heart. *J Mol Cell Cardiol*. 2010;48(1):152–160.
25. Billman GE. The cardiac sarcolemmal ATP-sensitive potassium channel as a novel target for anti-arrhythmic therapy. *Pharmacol Ther*. 2008;120(1):54–70.
26. Zipes DP, Wellens HJ. Sudden cardiac death. *Circulation*. 1998;98(21):2334–2351.
27. Arevalo HJ, et al. Arrhythmia risk stratification of patients after myocardial infarction using person-

alized heart models. *Nat Commun*. 2016;7:11437.
28. Kim TI, et al. Injectable, cellular-scale optoelectronics with applications for wireless optogenetics. *Science*. 2013;340(6129):211–216.
29. Xu L, et al. 3D multifunctional integumentary membranes for spatiotemporal cardiac measurements and stimulation across the entire epicardium. *Nat Commun*. 2014;5:3329.
30. Zacchigna S, Zentilin L, Giacca M. Adeno-associated virus vectors as therapeutic and investigational tools in the cardiovascular system. *Circ Res*. 2014;114(11):1827–1846.
31. Werfel S, et al. Rapid and highly efficient inducible cardiac gene knockout in adult mice using AAV-mediated expression of Cre recombinase. *Cardiovasc Res*. 2014;104(1):15–23.
32. Nagel G, Brauner M, Liewald JF, Adeishvili N, Bamberg E, Gottschalk A. Light activation of channelrhodopsin-2 in excitable cells of Caenorhabditis elegans triggers rapid behavioral responses. *Curr Biol*. 2005;15(24):2279–2284.
33. Prakosa A, et al. Methodology for image-based reconstruction of ventricular geometry for patient-specific modeling of cardiac electrophysiology. *Prog Biophys Mol Biol*. 2014;115(2–3):226–234.
34. Deng D, et al. Accuracy of prediction of infarct-related arrhythmic circuits from image-based models reconstructed from low and high resolution MRI. *Front Physiol*. 2015;6:282.
35. Ashikaga H, et al. Feasibility of image-based simulation to estimate ablation target in human ventricular arrhythmia. *Heart Rhythm*. 2013;10(8):1109–1116.
36. Arevalo H, Plank G, Helm P, Halperin H, Trayanova N. Tachycardia in post-infarction hearts: insights from 3D image-based ventricular models. *PLoS One*. 2013;8(7):e68872.
37. Vadakkumpadan F, et al. Image-based models of cardiac structure with applications in arrhythmia and defibrillation studies. *J Electrocardiol*. 2009;42(2):157.e1–157.10.
38. Schmidt A, et al. Infarct tissue heterogeneity by magnetic resonance imaging identifies enhanced cardiac arrhythmia susceptibility in patients with left ventricular dysfunction. *Circulation*. 2007;115(15):2006–2014.
39. Raya SP, Udupa JK. Shape-based interpolation of multidimensional objects. *IEEE Trans Med Imaging*. 1990;9(1):32–42.
40. McDowell KS, et al. Methodology for patient-specific modeling of atrial fibrosis as a substrate for atrial fibrillation. *J Electrocardiol*. 2012;45(6):640–645.
41. Prassl AJ, et al. Automatically generated, anatomically accurate meshes for cardiac electrophysiology problems. *IEEE Trans Biomed Eng*. 2009;56(5):1318–1330.
42. Bayer JD, Blake RC, Plank G, Trayanova NA. A novel rule-based algorithm for assigning myocardial fiber orientation to computational heart models. *Ann Biomed Eng*. 2012;40(10):2243–2254.
43. ten Tusscher KH, Panfilov AV. Alternans and spiral breakup in a human ventricular tissue model. *Am J Physiol Heart Circ Physiol*. 2006;291(3):H1088–H1100.
44. Pu J, Boyden PA. Alterations of Na^+ currents in myocytes from epicardial border zone of the infarcted heart. A possible ionic mechanism for reduced excitability and postrepolarization refractoriness. *Circ Res*. 1997;81(1):110–119.
45. Dun W, Baba S, Yagi T, Boyden PA. Dynamic remodeling of K^+ and Ca^{2+} currents in cells that survived in the epicardial border zone of canine healed infarcted heart. *Am J Physiol Heart Circ Physiol*. 2004;287(3):H1046–H1054.
46. Jiang M, Cabo C, Yao J, Boyden PA, Tseng G. Delayed rectifier K currents have reduced amplitudes and altered kinetics in myocytes from infarcted canine ventricle. *Cardiovasc Res*. 2000;48(1):34–43.
47. Decker KF, Rudy Y. Ionic mechanisms of electrophysiological heterogeneity and conduction block in the infarct border zone. *Am J Physiol Heart Circ Physiol*. 2010;299(5):H1588–H1597.
48. Cabo C, Boyden PA. Electrical remodeling of the epicardial border zone in the canine infarcted heart: a computational analysis. *Am J Physiol Heart Circ Physiol*. 2003;284(1):H372–H384.
49. Taggart P, et al. Inhomogeneous transmural conduction during early ischaemia in patients with coronary artery disease. *J Mol Cell Cardiol*. 2000;32(4):621–630.
50. Glukhov AV, et al. Transmural dispersion of repolarization in failing and nonfailing human ventricle. *Circ Res*. 2010;106(5):981–991.
51. Yao JA, Hussain W, Patel P, Peters NS, Boyden PA, Wit AL. Remodeling of gap junctional channel function in epicardial border zone of healing canine infarcts. *Circ Res*. 2003;92(4):437–443.
52. Vigmond EJ, Weber dos Santos R, Prassl AJ, Deo M, Plank G. Solvers for the cardiac bidomain equations. *Prog Biophys Mol Biol*. 2008;96(1–3):3–18.
53. Vigmond EJ, Hughes M, Plank G, Leon LJ. Computational tools for modeling electrical activity in cardiac tissue. *J Electrocardiol*. 2003;36(suppl):69–74.
54. Rodríguez B, Li L, Eason JC, Efimov IR, Trayanova NA. Differences between left and right ventricular chamber geometry affect cardiac vulnerability to electric shocks. *Circ Res*. 2005;97(2):168–175.
55. Bishop MJ, Rodriguez B, Qu F, Efimov IR, Gavaghan DJ, Trayanova NA. The role of photon scattering in optical signal distortion during arrhythmia and defibrillation. *Biophys J*. 2007;93(10):3714–3726.
56. Rantner LJ, Arevalo HJ, Constantino JL, Efimov IR, Plank G, Trayanova NA. Three-dimensional mechanisms of increased vulnerability to electric shocks in myocardial infarction: altered virtual electrode polarizations and conduction delay in the peri-infarct zone. *J Physiol (Lond)*. 2012;590(18):4537–4551.
57. Boyle PM, Karathanos TV, Entcheva E, Trayanova NA. Computational modeling of cardiac optogenetics: Methodology overview & review of findings from simulations. *Comput Biol Med*. 2015;65:200–208.
58. Mattis J, et al. Principles for applying optogenetic tools derived from direct comparative analysis of microbial opsins. *Nat Methods*. 2012;9(2):159–172.
59. Wellens HJ, Brugada P, Stevenson WG. Programmed electrical stimulation of the heart in patients with life-threatening ventricular arrhythmias: what is the significance of induced arrhythmias and what is the correct stimulation protocol? *Circulation*. 1985;72(1):1–7.
60. Bashkatov AN, Genina ÉA, Kochubey VI, Tuchin VV. Optical properties of the subcutaneous adipose tissue in the spectral range 400–2500 nm. *Opt Spectrosc*. 2005;99(5):836–842.
61. Sandell JL, Zhu TC. A review of in-vivo optical properties of human tissues and its impact on PDT. *J Biophotonics*. 2011;4(11–12):773–787.
62. Wang HW, et al. Broadband reflectance measurements of light penetration, blood oxygenation, hemoglobin concentration, and drug concentration in human intraperitoneal tissues before and after photodynamic therapy. *J Biomed Opt*. 2005;10(1):14004.
63. Boyle PM, Veenhuyzen GD, Vigmond EJ. Fusion during entrainment of orthodromic reciprocating tachycardia is enhanced for basal pacing sites but diminished when pacing near Purkinje system end points. *Heart Rhythm*. 2013;10(3):444–451.
64. Boyle PM, Massé S, Nanthakumar K, Vigmond EJ. Transmural IK(ATP) heterogeneity as a determinant of activation rate gradient during early ventricular fibrillation: mechanistic insights from rabbit ventricular models. *Heart Rhythm*. 2013;10(11):1710–1717.

Supplemental information for

Optogenetic defibrillation of ventricular arrhythmia in mouse hearts and human simulations

T. Bruegmann, P.M. Boyle, C.C. Vogt, T.V. Karathanos, H.J. Arevalo, B.K. Fleischmann, N.A. Trayanova, P. Sasse

Legends to Supplemental Movies 1-3:

Supplemental Movie 1: Induction of VT via pacing from the apex of the human ventricular model.
V_m is rendered on the 3-dimensional surface using the same color scale as in Figure 4C. Normal (left) and cutaway (right) views are shown. Pink spheres in the left-hand panel indicate locations at which extracellular potential was recovered to reconstruct the pseudo-ECGs.

Supplemental Movie 2: Simulation of optogenetic defibrillation in the human ventricles.
V_m propagation in the 3-dimensional human ventricular model in cutaway view (top) and corresponding pseudo-ECGs (bottom) for three configurations corresponding to Figure 4A, Supplemental Figure 6B and Figure 4B: no stimulus (left), blue light (middle), and red light (right). Same color scale as Figure 4C. Blue and red auras indicate timing of optogenetic stimuli. In pseudo-ECGs, the black boxes indicate the beginning and end of the interval shown in the movie and the dashed pink link indicates progress over time.

Supplemental Movie 3: Dynamics of reentrant wavefront interaction with tissue subjected to optogenetic stimulation.
V_m propagation in the 3-dimensional human ventricular model in a zoomed-in cutaway view for blue light (left) and red light (right), corresponding to Supplemental Figure 6C and Figure 5E, respectively. Same color scale as Figure 4C. Blue and red auras indicate timing of optogenetic stimuli. Arrows appear during the movie to highlight reentrant wavefront propagation into the endocardial layer of the right ventricular free wall (blue light, left) and reentrant wavefront conduction block induced by optogenetic depolarization (red light, right).

Supplemental Figure 1

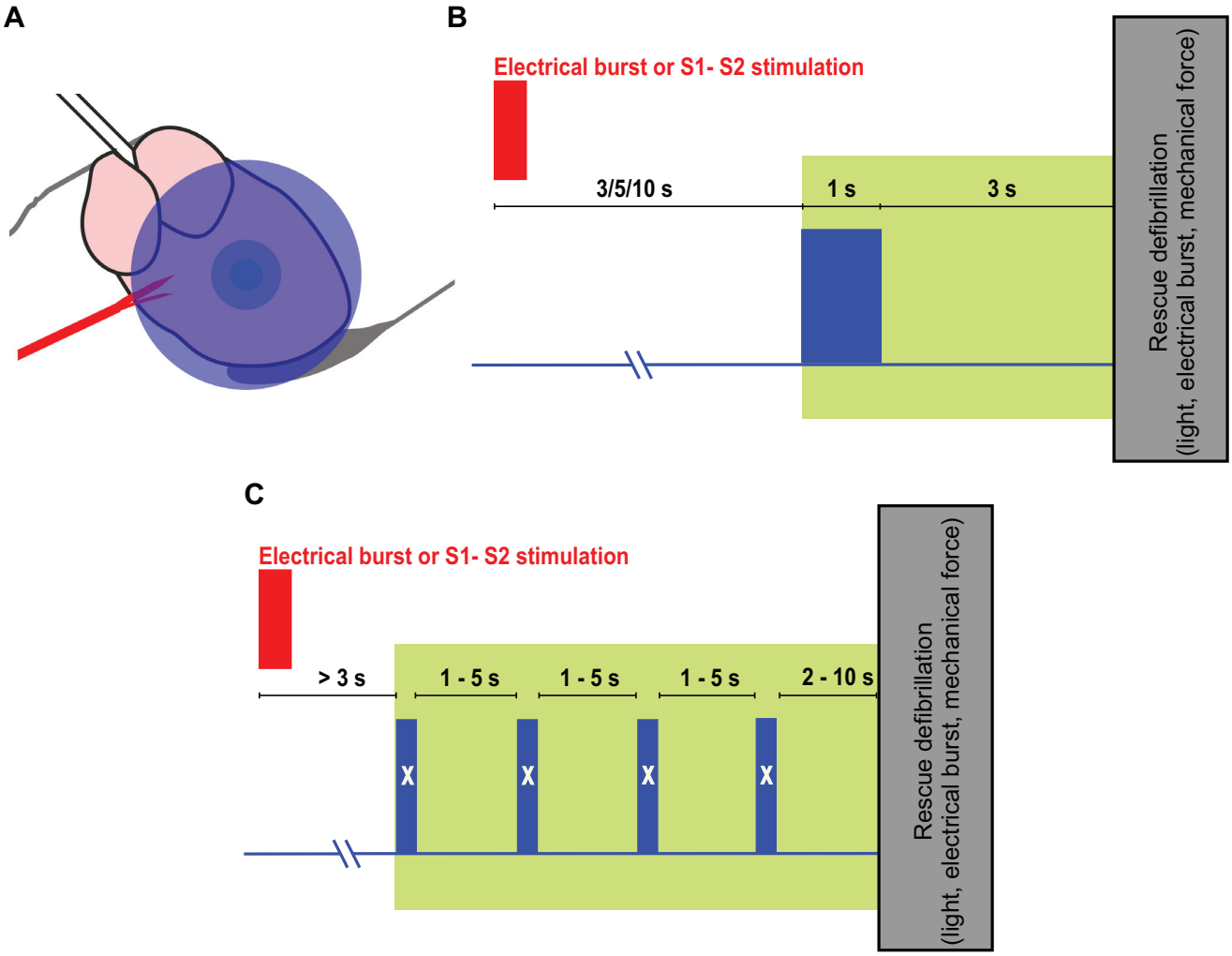

Supplemental Figure 1: Experimental setup and protocols for optogenetic defibrillation. (**A**) Explanted hearts were retrogradely perfused and the ECG was recorded with electrodes placed at the right atrium and the ventricular apex (gray). Ventricular arrhythmia was induced by electrical stimulation with two silver chloride electrodes (red). Optogenetic defibrillation was tested by illuminating the anteroseptal epicardium with light stimuli covering 15, 29, or 143 mm^2 areas (blue circles). (**B**) Schematic illustrating the one light pulse protocol: Electrical burst or S1/S2 stimulation was used to induce ventricular arrhythmia and 3, 5 or 10 s later one 1 s long light pulse (0.4 mW/mm^2, 143 mm^2) was applied. Optogenetic defibrillation was classified as successful if arrhythmia terminated within 4 s after start of the illumination (green box). If arrhythmia persisted, the attempt was classified as a failure and a rescue defibrillation procedure was performed (see Methods). (**C**) Schematic illustrating the four light pulse protocol: Arrhythmia was allowed to stabilize for 3-15 s after induction and four identical light stimuli were applied with 1 to 5 s delay in-between. Optogenetic defibrillation was classified as successful if arrhythmia terminated between the start of illumination and a predefined period of 2-10 s after the last light pulse (time period indicated by green box). If arrhythmia persisted, the attempt was classified as a failure and a rescue defibrillation procedure was performed. For control experiments in ChR2 expressing hearts without illumination and in hearts without ChR2 expression, spontaneous arrhythmia termination was assessed in a time window (green boxes in A and B) using the longest times indicated.

Supplemental Figure 2

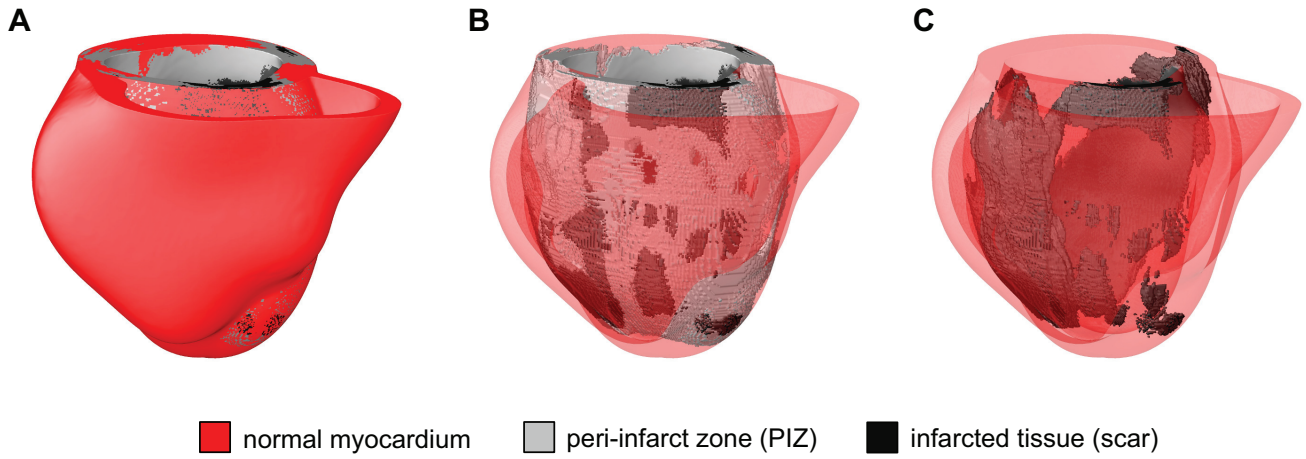

Supplemental Figure 2: Image-based model of the diseased human ventricles.
Different renderings of the model with (**A**) surface views of all three tissue types and translucent normal myocardium with (**B**) or without (**C**) the peri-infarct zone.

Supplemental Figure 3

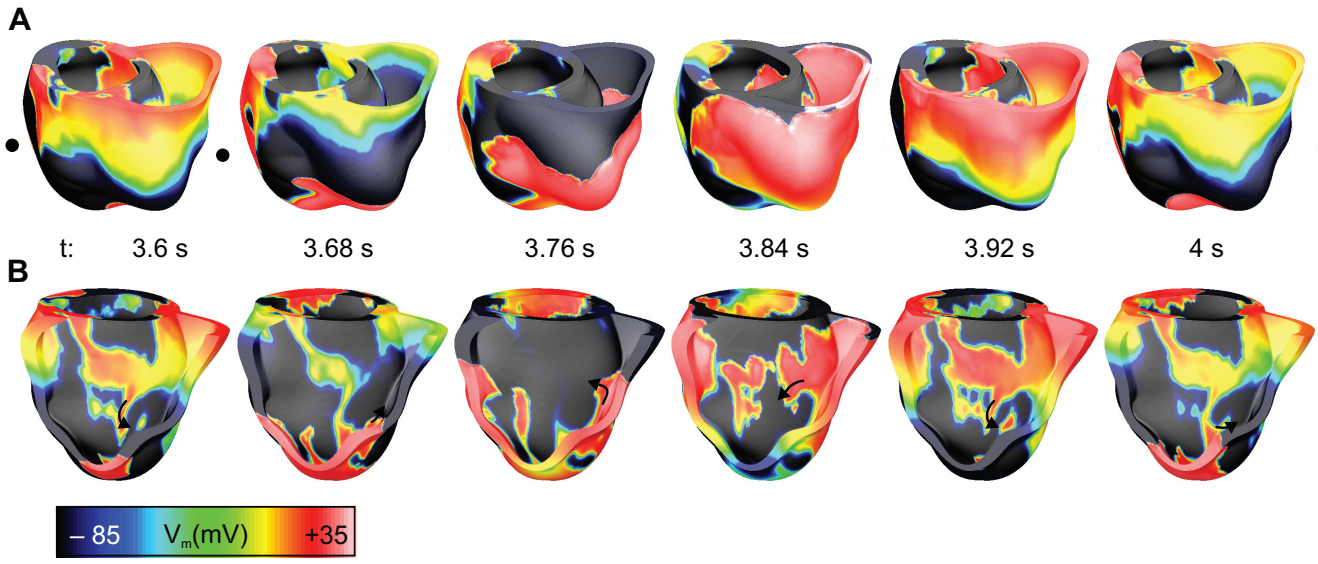

Supplemental Figure 3: Snapshots of V_m distribution during simulated VT in the diseased human heart model.
(**A**) Whole-heart view. Black dots in left-most panel show locations near left and right ventricles where extracellular potentials were recorded to generate pseudo-ECG signals in Figures 4A,B and Supplemental Figure 6B. (**B**) Cutaway view with free wall of right ventricle removed for visualization. Black arrows indicate the direction of the propagating reentrant wavefront that perpetuated VT.

Supplemental Figure 4

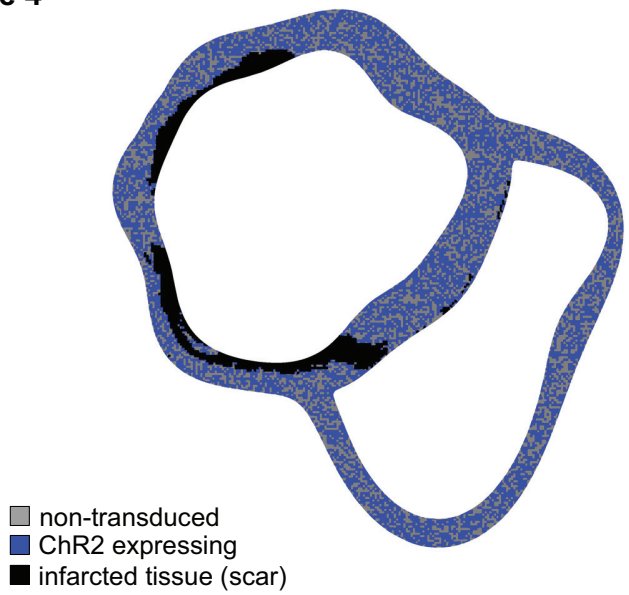

Supplemental Figure 4: ChR2 distribution in the ventricular model.
2D slice showing distribution of the ChR2 expressing cardiomyocytes in the normal myocardium and peri-infarct zone of the human ventricular model.

Supplemental Figure 5

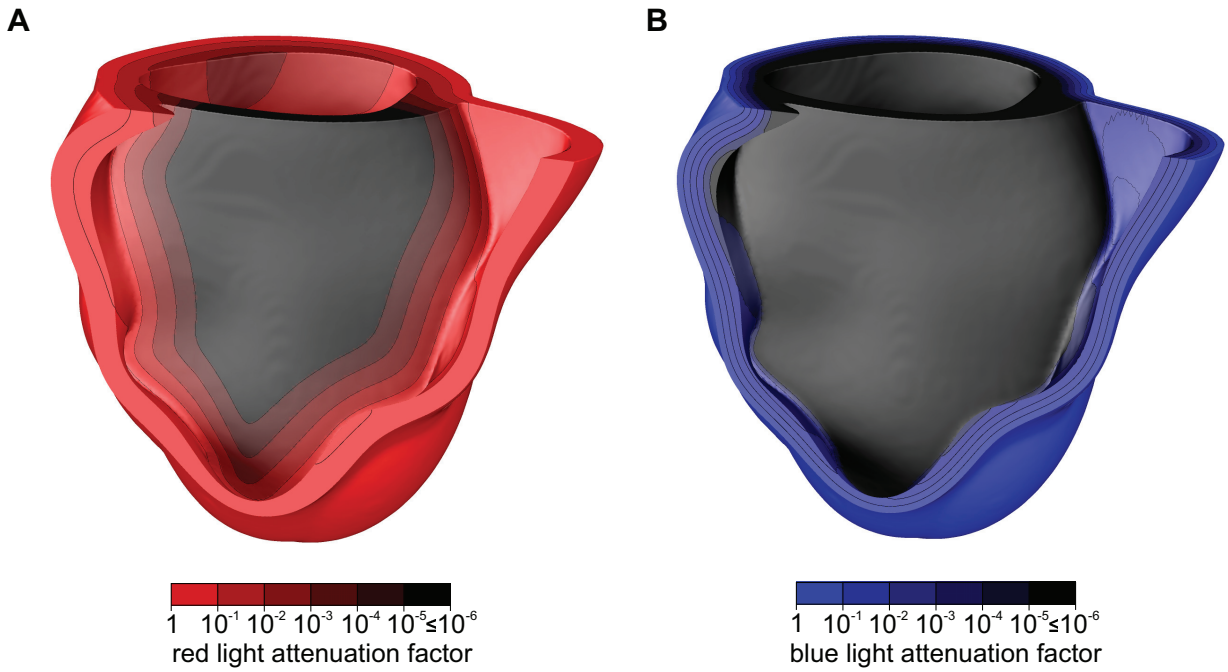

Supplemental Figure 5: Light attenuation characteristics in the human ventricular model.
3D map showing light attenuation during uniform illumination of the epicardial surface with red light (669 nm, **A**) and blue light (488 nm, **B**). The right ventricular free wall is cut away to facilitate visualization. Scale bars for light attenuation factor are logarithmic.

Supplemental Figure 6

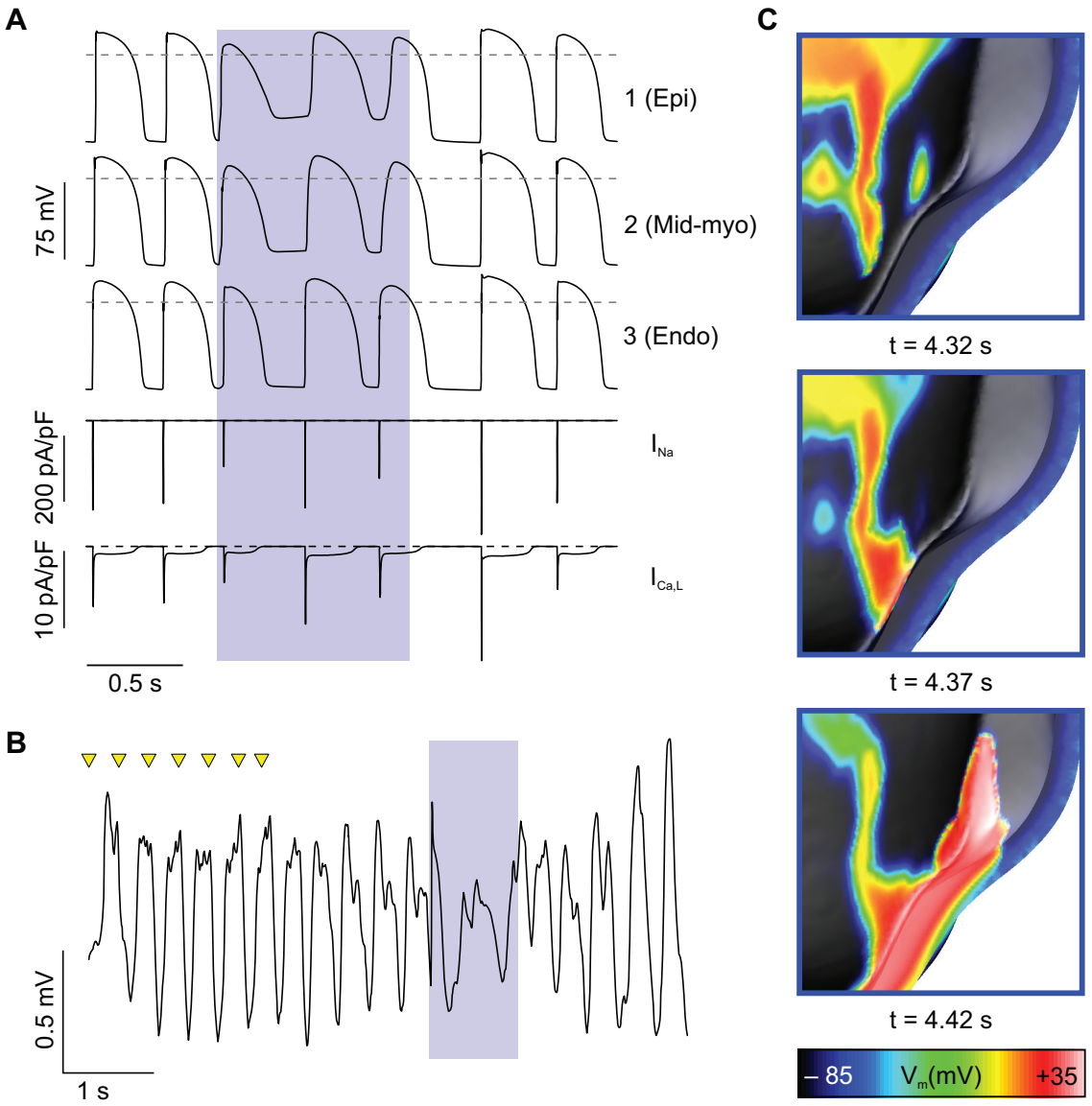

Supplemental Figure 6: Optogenetic defibrillation failure using epicardial illumination with blue light.

(**A**) Top: V_m-traces from sites 1-3 in Figure 5A during epicardial illumination with blue light. Bottom: Ionic Na^+ (I_{Na}) and L-type Ca^{2+} ($I_{Ca,L}$) currents underlying V_m from site 3. (**B**) Pseudo-ECG signals for the model configurations with epicardial illumination with blue light. Timing of blue illumination (488 nm, 1 s, 10 mW/mm^2) is indicated by blue boxes (A and B). (**C**) Zoomed-in snapshots of V_m distribution during the illumination at the indicated time points (from start of simulation). Snapshots were taken from the region shown in Figure 5A top by black rectangle.

Supplemental Figure 7

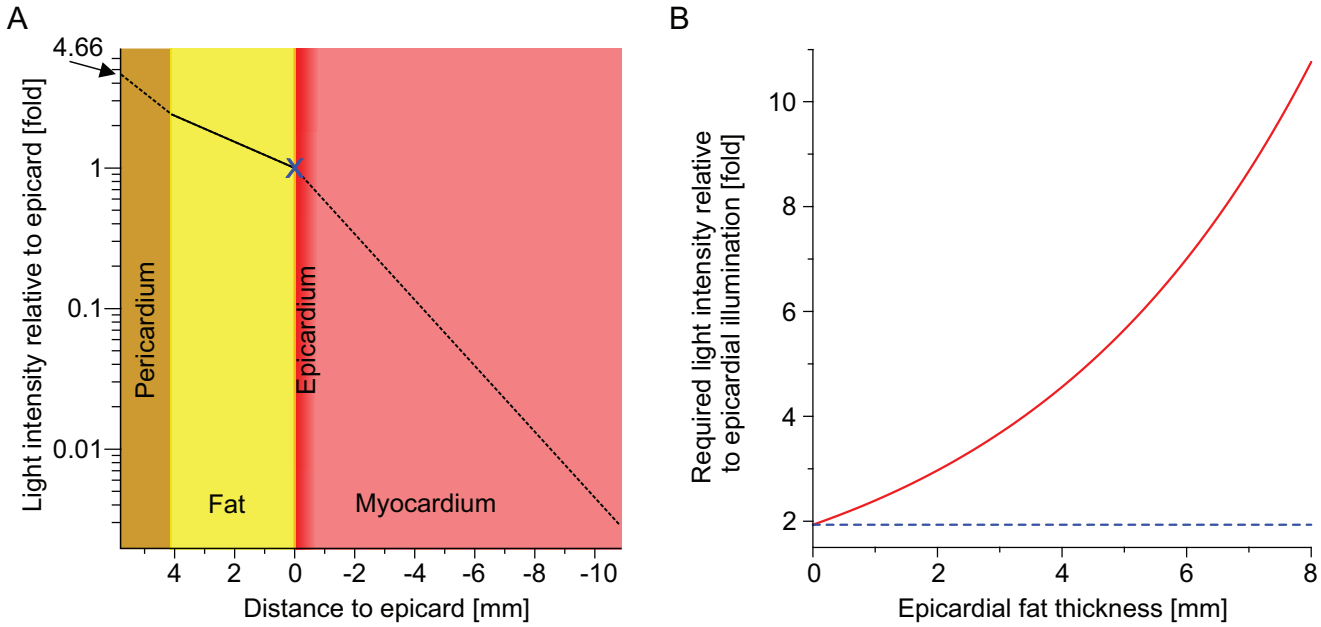

Supplemental Figure 7: Requirements for optogenetic defibrillation for illumination from the pericardium.
(**A**) Required increase in optical stimulus intensity due to light attenuation in epicardial fat tissue (yellow, 4.1 mm) and the pericardium (brown, 1.7 mm) relative to the light intensity reaching the epicardium (blue x) using global illumination with red light (669 nm). (**B**) Required increase in light intensity (red line) for pericardial illumination for different epicardial fat layer thickness values. Dashed blue line indicates increase in required light intensity due to light attenuation by the 1.7 mm-thick pericardium only.

3.3 Epilogue

This publication was the first report proving the termination of ventricular arrhythmia with optogenetic depolarization in intact hearts. The combination of experiments in mouse hearts and *in silico* simulations of an infarcted patient heart revealed a completely new mechanism to terminate arrhythmia. We propose that optogenetic stimulation allows transmural depolarization to block the excitation wave travelling into the illuminated region. Importantly, because illumination and optogenetic depolarization can be sustained for seconds until the arrhythmia is terminated, this principle could be much safer compared to brief electrical shocks. Furthermore, light generation does not require charging of capacitators for electrical shocks, which allows fast repetition of illumination until the arrhythmias have been successfully terminated.

The ability to use optogenetic stimulation to understand to improve current treatment options was shown shortly after our publication.[166] In this publication, the authors used patterned light stimulation and thereby were able to reduce the required light energy compared to global illumination. However, this approach was only tested in one type of ventricular tachycardia with a specific reentrant wave front. Therefore it remains to be determined how effective this patterned light stimulation is for other arrhythmia types or how the light pattern could be defined individually in patients. Recently, the feasibility of optogenetic defibrillation was demonstrated in rats after AAV-based gene transfer of ChRs.[167] The authors suggested continuous illumination would prolong the AP and thereby terminated the ventricular tachycardia. However, the AP prolongation was only seen in the last AP during the illumination and did not happen directly after onset of the illumination. Therefore it can be questioned whether the observed AP prolongation is causing or caused by the arrhythmia termination.

In conclusion, optogenetic defibrillation based on gene transfer of ChRs to cardiomyocytes in combination with implantable light emitting devices could become a novel treatment option for patients with recurrent ventricular arrhythmia. Because the required gene transfer might put patients at risk, the patient cohort would have to be very carefully chosen. Patients suffering from electrical storm (generation of at least 3 episodes of ventricular arrhythmia requiring electrical defibrillation per day) or patients with many inappropriate shocks would have probably the greatest benefit of implantable optogenetic defibrillators. Furthermore optogenetic technologies are well suited to investigate the mechanism of defibrillation by electrical shocks and might thereby improve current therapeutic strategies.

4. Optogenetic stimulation of skeletal muscle

4.1 Prologue

Direct stimulation of intact mammalian skeletal muscles with optogenetic methods has not been demonstrated but could be very useful to study electrophysiology and excitation-contraction coupling in skeletal muscle fibers. Aim of this part was not only to establish direct optogenetic stimulation of skeletal muscle but also to carefully characterize the underlying biophysical principles and to point out the advantages and limitations of this technology.

In addition, I explored whether direct optogenetic stimulation of skeletal muscles could be suited for therapeutic applications. Because electrical stimulation is restricted in clinics to indirect stimulation via motor neurons, optogenetics could provide new treatment options when direct stimulation of skeletal muscles is required. Examples for this scenario are peripheral nerve injuries and pathologies or diseases affecting the neuromuscular synapses, such as amyotrophic lateral sclerosis or myasthenia gravis. In addition, indirect electrical muscle stimulation of the nerve is impaired if the nerve fibers within one nerve innervates different skeletal muscle groups. In the human larynx, the recurrent laryngeal nerve innervates all skeletal muscles involved in opening the vocal cords to allow air passage into the lung during breathing and closing the vocal cords for phonation and protection from aspiration. Bilateral recurrent nerve paralysis is a severe complication of neck surgery, tumors or central neurological diseases[168] and results in a fixed paramedian position of the vocal cords and eventually life-threatening dyspnea. Current treatment options are the surgical removal of one vocal cord, which severely impairs phonation and increases the risk of aspiration or alternatively permanent tracheotomy, which leads to high stigmatization, alteration of voice and frequent infections. Although electrical stimulation of the posterior cricoarytenoid muscle within the larynx has been shown to enable opening of the vocal cords in animals and humans,[169-175] severe side-effects prevent the routine clinical application. These include corrosion or encapsulation of the electrode tip reducing the efficiency of stimulation, discomfort due to the activation of sensory nerves, and co-stimulation of antagonistic muscles, which requires in some patients the selective silencing of antagonistically acting muscle groups by repetitive botulinum toxin injections.[171,172] To propose optogenetic stimulation as alternative to restore laryngeal functions, I tested the advantage of the high spatial resolution of light for specific stimulation of intralaryngeal muscles.

4.2 Original publication

nature COMMUNICATIONS

ARTICLE

Received 12 Feb 2015 | Accepted 13 Apr 2015 | Published 2 Jun 2015

DOI: 10.1038/ncomms8153 OPEN

Optogenetic control of contractile function in skeletal muscle

Tobias Bruegmann[1,2], Tobias van Bremen[3], Christoph C. Vogt[1], Thorsten Send[3], Bernd K. Fleischmann[1] & Philipp Sasse[1]

Optogenetic stimulation allows activation of cells with high spatial and temporal precision. Here we show direct optogenetic stimulation of skeletal muscle from transgenic mice expressing the light-sensitive channel Channelrhodopsin-2 (ChR2). Largest tetanic contractions are observed with 5-ms light pulses at 30 Hz, resulting in 84% of the maximal force induced by electrical stimulation. We demonstrate the utility of this approach by selectively stimulating with a light guide individual intralaryngeal muscles in explanted larynges from ChR2-transgenic mice, which enables selective opening and closing of the vocal cords. Furthermore, systemic injection of adeno-associated virus into wild-type mice provides sufficient ChR2 expression for optogenetic opening of the vocal cords. Thus, direct optogenetic stimulation of skeletal muscle generates large force and provides the distinct advantage of localized and cell-type-specific activation. This technology could be useful for therapeutic purposes, such as restoring the mobility of the vocal cords in patients suffering from laryngeal paralysis.

[1] Institute of Physiology I, University of Bonn, Life and Brain Center, Sigmund-Freud-Strasse 25, 53127 Bonn, Germany. [2] Research Training Group 1873, University of Bonn, 53127 Bonn, Germany. [3] Department of Otorhinolaryngology/Head and Neck Surgery, University Hospital of Bonn, Sigmund-Freud-Strasse 25, 53127 Bonn, Germany. Correspondence and requests for materials should be addressed to P.S. (email: philipp.sasse@uni-bonn.de) or to T.B. (email: tbruegmann@uni-bonn.de).

In contrast to electrical stimulation, optogenetic methods allow cell-type-specific stimulation with high spatial and temporal precision of excitable cells by expressing light-sensitive proteins such as the light-gated nonselective cation channel Channelrhodopsin-2 (ChR2)[1–3]. This technology has been used to evoke contractions in innervated skeletal muscle by indirect stimulation of either the secondary motor cortex[3] or of peripheral motor neurons[4–6], whereas direct optogenetic stimulation of skeletal muscle cells was so far shown only in nematodes[7] and in immortalized myotubes *in vitro*[8]. These as well as earlier studies in heart muscle[9,10] do not allow to predict the feasibility and efficacy of direct optogenetic stimulation of intact mammalian skeletal muscle. This is because maximal force generation in intact skeletal muscle depends on the recruitment of electrically isolated muscle fibres, which is potentially challenging when using direct optogenetic stimulation of skeletal muscle because of the high concentration of light-absorbing myoglobin. Furthermore, maximal and sustained force can only be generated by Ca^{2+} accumulation during tetanic high-frequency stimulation, which is in contrast to the non-tetanic heart.

Because of these specific features of skeletal muscle physiology, we explore herein the biophysical basics of direct optogenetic stimulation of intact mammalian skeletal muscle. Muscle-specific expression of ChR2 would allow the spatially controlled and pain-free stimulation of skeletal muscle, and therefore we test also the applicability of optogenetic stimulation of individual intralaryngeal muscles to illustrate as a proof-of-concept the functional recovery of paralysed larynges.

Results

Direct optogenetic stimulation of isolated muscle fibres. We used transgenic mice expressing the ChR2(H134R) mutant in fusion with enhanced yellow fluorescent protein (EYFP) under the control of the chicken-β-actin promotor[10], which is strongly active in muscle cells[11], and found bright EYFP signals in single flexor digitorum brevis (FDB) fibres located within the plasma membrane and in the t-tubulus system (Fig. 1a). Illumination of isolated single FDB fibres with short light flashes (470 nm, 1 ms, 8 mW mm^{-2}) induced contractions (Supplementary Movie 1) proving the direct activation of muscle because isolated single FDB fibres do not contain neuromuscular synapses.

Light-induced isometric force in intact soleus muscles. To quantify the potency of optogenetic stimulation in intact skeletal muscles, isometric force was measured in explanted soleus muscles, which showed EYFP expression (Fig. 1b) in α-actinin-positive muscle fibres (Fig. 1c). Stimulation with light pulses as short as 2 ms and as low as 0.35 mW mm^{-2} induced contractions and force gradually increased with higher light intensities (Fig. 1d left). When using 25-ms-long pulses, force generation saturated at low light intensities (0.5 mW mm^{-2}; Fig. 1d right). Importantly, with high light intensity (1.4 mW mm^{-2}) force could be increased by prolongation of light pulses from 1 to 50 ms, whereas longer light pulses did not further increase force generation (Fig. 1e). Comparison of all light intensities and pulse durations highlighted their interdependence, and longer light pulses led to a saturation of force at lower light intensities (Fig. 1f). Overall, the maximal force of light-induced single twitches was 53.2 ± 2.4 mN ($n = 5$) using 100-ms-long light pulses at 0.35 mW mm^{-2}.

In order to obtain maximal force in skeletal muscle, sustained contractions are required. Interestingly, continuous illumination resulted in non-sustained force generation with an initial peak followed by a decline to basal levels (Fig. 2a) highlighting the importance of pulsed stimulation. To determine the most effective pulsed illumination, we tested a broad range of repetition rates (10–70 Hz) and pulse durations (2–20 ms) and analysed the average force during these stimulations. Using low repetition rates (10 Hz), soleus muscles showed incomplete tetanic contractions with short relaxations between the light pulses; however, repetition rates above 30 Hz led to complete and uniform tetanic contractions (Fig. 2a). Overall optical stimulation with 5 ms at 30 Hz generated the highest average force with 94.3 ± 5.6 mN and the average force per cross-sectional area amounts to 140.1 ± 8.4 kN m^{-2} ($n = 6$; Fig. 2b). This value was close (84.0 ± 4.7%) to the maximal force induced by the most effective electrical stimulation. To analyse the force–frequency relationship of optical compared with electrical stimulation, we normalized for each muscle the respective force on optical stimulation with the maximal force induced by electrical stimulation (Fig. 2c). At low repetition rates (< 30 Hz), pulsed illumination was superior to electrical stimulation in generating force; however, the efficacy of optical stimulation decreased at repetition rates above 40 Hz (Fig. 2c). In order to determine the mechanism underlying this effect, we measured the membrane potential of muscle fibres within the intact soleus muscle using sharp electrodes. We found that the action potential duration was strongly dependent on the duration of light pulses (Fig. 3a), and repolarization was delayed after termination of illumination (Fig. 3b). This can be explained by the slow off-kinetics (time constant of deactivation ∼20 ms) of ChR2(H134R)[7]. Thus, at higher repetition rates, repolarization did not occur leading to continuous depolarization (Fig. 3c).

Muscle fatigue was not different between optical (5 ms, 30 Hz, 1.4 mW mm^{-2}) and electrical stimulation (20 V, 0.1 ms, biphasic, 100 Hz; Fig. 4). Importantly, isometric force measurements with soleus muscles from control mice expressing EGFP did not reveal any light-induced contractions (Fig. 5) confirming the specificity of optogenetic stimulation.

Optogenetic stimulation of explanted larynges. One clear advantage of the optogenetic stimulation approach could be the selective activation of individual agonistic and antagonistic muscles located in close vicinity. In contrast, electrical stimulation lacks this spatial precision and indirect stimulation through motoric nerves is also impossible in case that both muscle groups are innervated by the same nerve. The mammalian larynx is a good example because the recurrent laryngeal nerve innervates all skeletal muscles that control the position of the vocal cords (Fig. 6a). Contraction of the posterior cricoarytenoid muscle opens the vocal cords allowing air passage into the lung during breathing, whereas the other intralaryngeal muscles close the vocal cords for phonation and protection from aspiration[12,13]. We have taken advantage of optogenetic stimulation to demonstrate selective stimulation of individual intralaryngeal muscles. For this purpose, an *ex vivo* preparation of the larynx was used that reflects the physiological characteristics of a denervated larynx *in vivo* including paramedian position and physiological tension of the vocal cords as well as integrity and intact biomechanical movement of the intralaryngeal muscles and the arytenoid cartilage. In explanted larynges from the ChR2-transgenic mouse line, all muscles displayed bright and membrane-bound EYFP signals (Fig. 6b). Selective illumination of the posterior cricoarytenoid muscle was performed with a light-emitting diode (LED)-coupled small light guide (400-μm core diameter), and the most efficient stimulation pattern was determined using 4-s-long stimulations with a broad range of pulse durations (2–20 ms) and repetition rates (10–50 Hz). Illumination with low repetition rates (< 20 Hz) showed incomplete tetanic contractions with oscillating movements (Fig. 6c left), whereas rates above 30 Hz led to sustained opening of the vocal cords (Fig. 6c middle, Supplementary

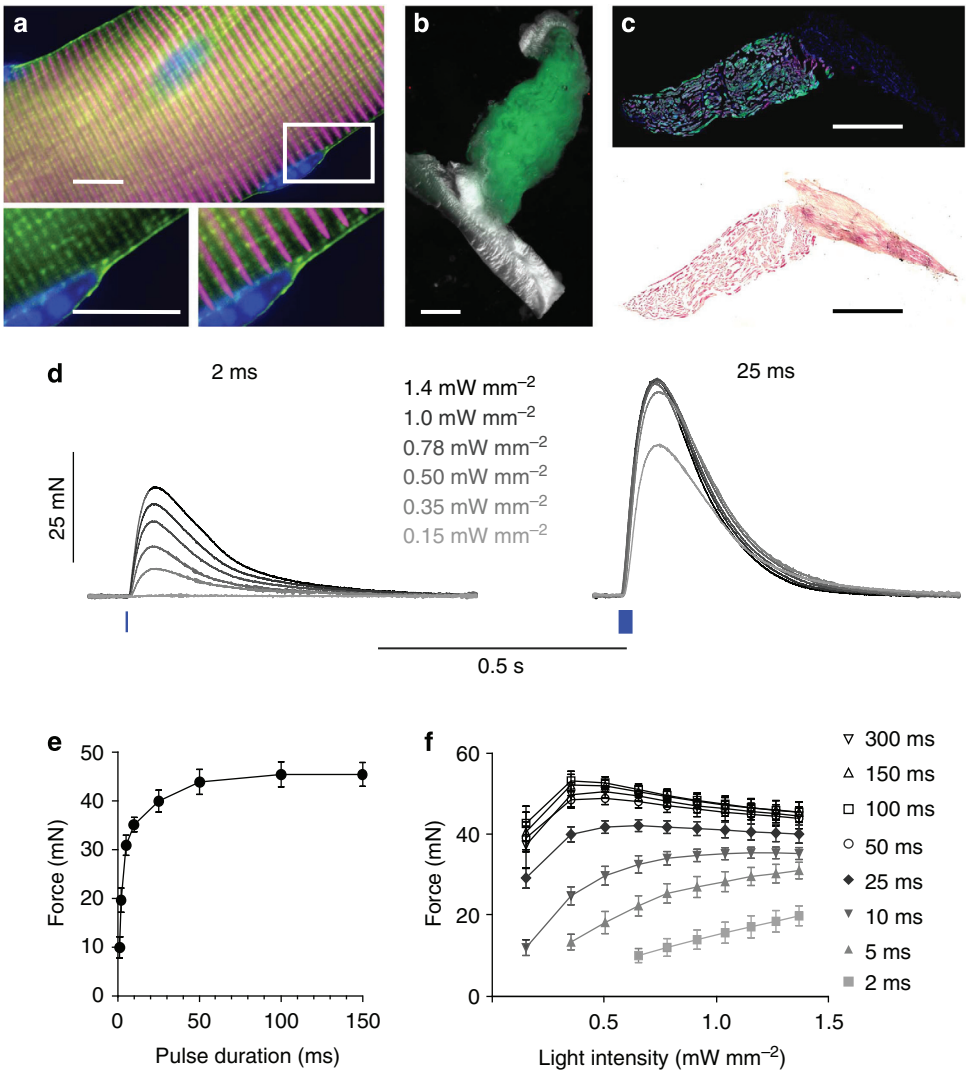

Figure 1 | Functional expression of ChR2 in skeletal muscle. (**a**–**c**) Expression of ChR2-EYFP in skeletal muscles. (**a**) Single fibres isolated from flexor digitorum brevis muscles showed bright ChR2-EYFP (green) signals with localization at the cell membrane including the t-tubulus system that surrounds the α-actinin (magenta) containing z-discs (enlargements in lower panels). (**b**,**c**) Bright ChR2-EYFP (green) signals were found in explanted soleus muscles (**b**) and were restricted to α-actinin (magenta) positive skeletal muscle cells (**c**, top). No expression was seen in the tendon identified with haematoxylin and eosin staining (**c**, bottom). (**d**–**f**) Light-induced single twitches in soleus muscles. (**d**) Representative examples of single twitches induced by 2- and 25-ms-long light pulses with increasing light intensities. (**e**) Relationship of pulse duration and maximal twitch force at high light intensity (1.4 mW mm^{-2}, $n=5$). (**f**) Overall comparison of the maximum twitch force induced by single light pulses of different durations and intensities ($n=5$). Error bars, s.e.m., nuclear staining in blue, scale bars, 10 μm (**a**), 1 mm (**b**,**c**).

Movie 2). Importantly, during continuous illumination we observed an initial opening with subsequent re-closure (Fig. 6c right) highlighting the importance of pulsed illumination. For quantification of vocal cord opening, we calculated the average of the area between the vocal cords at baseline and during illumination. Comparison of all tested stimulation patterns revealed that 10-ms-long light pulses at 40 Hz induced the maximum opening of the vocal cords leading to a change of the open area from 76 ± 19 to 344 ± 73 mm^2, which is an increase of 420 ± 131% ($n=5$; Fig. 6d). In order to take anatomical variations into account and to compare the effectiveness of different stimulation patterns, we normalized the respective openings to the maximal opening (Fig. 6e). Compared with the maximal opening obtained with 10-ms pulses at 40 Hz, we found that 12 other stimulation patterns had similar efficiency ($n\geq3$, $P>0.05$, repeated analysis of variance (ANOVA) test with Bonferroni multiple comparison post test). Among these, 2-ms-long pulses at 40 Hz had the lowest duty cycle (8%) and its use would therefore avoid possible photo damage. To further prove selectivity of optical stimulation, we moved the light guide in front of the superior cricoarytenoid muscle, which is responsible for closure of the vocal cords in mice. Illumination of this region led to a closing of the vocal cords (Supplementary Movie 3).

Gene transfer for optogenetic stimulation of wild-type mice. These proof-of-principle experiments were performed in a transgenic animal model, whereas for therapeutic purposes gene transfer of ChR2 into skeletal muscle is required. In order to demonstrate the feasibility of this approach for optogenetic control of larynx function in wild-type mice, we have systemically injected adeno-associated viruses (AAV) expressing ChR2(H134R) in fusion to mCherry with the capsid of serotype 9

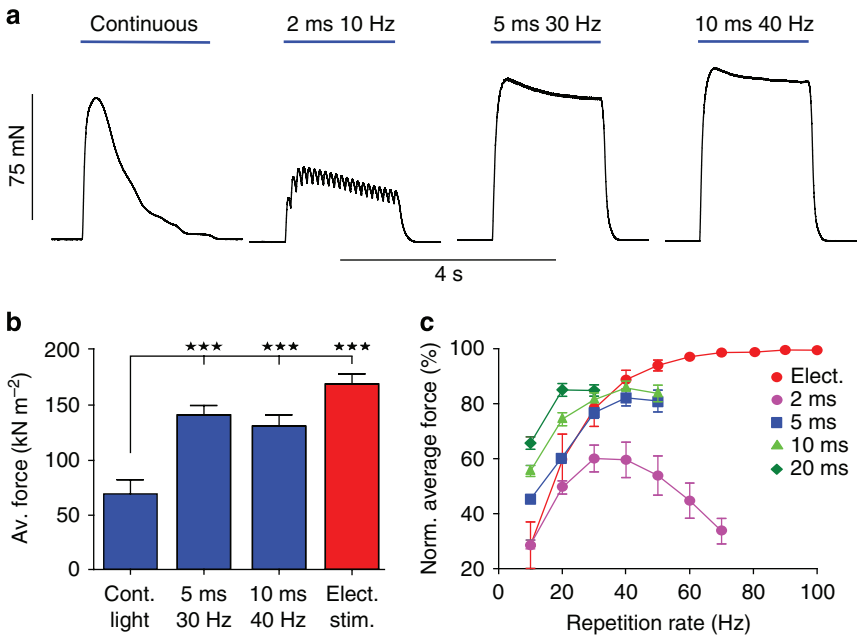

Figure 2 | Optogenetic generation of tetanic contractions. (**a**) Representative examples of sustained contractions generated by various 2-s-long illumination patterns. (**b**) Quantification of average force during optical stimulation in comparison with electrical stimulation (100 Hz, 20 V, 1 ms, biphasic) ($P<0.0001$, repeated Dunnett ANOVA test with continuous light stimulation as control, $n=6$). (**c**) Relationship between repetition rate and average force normalized to maximal electrical stimulation for different light pulse durations ($n=4$). Error bars, s.e.m. Av., average; cont., continuous; elect., electrical; norm., normalized; stim., stimulation.

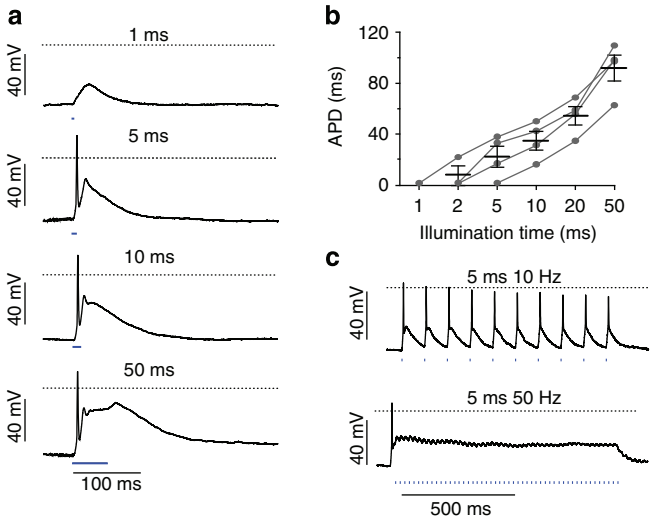

Figure 3 | Light-induced action potentials. (**a**) Light-induced depolarizations and action potentials using 1-, 5-, 10- and 50-ms-long light pulses (1.4 mW mm^{-2}). (**b**) Relationship between the duration of light pulses and action potential durations (APD, $n=4$). (**c**) Membrane potential change during tetanic stimulation (rate of 10 or 50 Hz) using 5-ms-long light pulses (1.4 mW mm^{-2}). Error bars, s.e.m.

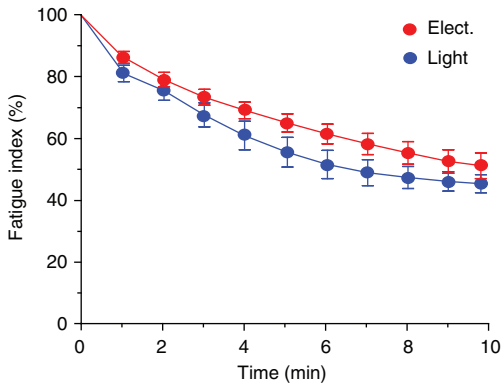

Figure 4 | Fatigue induction during optical and electrical stimulation. Fatigue development during 350-ms-long tetanic stimulation pattern (optical, 5 ms pulses, 30 Hz, 1.4 mW mm^{-2}, electrical, 0.1 ms, biphasic, 100 Hz, 20 V) over a time period of 10 min. Fatigue values were compared at each time point using a two-way, paired Student's *t*-test resulting in *P* values > 0.05 ($n=7$).

because this serotype has been reported to infect skeletal muscles in mice[14]. Four weeks after the injection, we could detect mCherry fluorescence in the posterior cricoarytenoid muscle (Fig. 7a) and detailed histological analysis revealed that in this muscle 10.2 ± 3.6% of the fibres ($n=3$) expressed the ChR2-mCherry fusion protein. Pulsed illumination (10 ms, 40 Hz) applied to the posterior cricoarytenoid muscle of explanted larynges from the AAV-treated mice led to an opening of the vocal cords (Fig. 7b and Supplementary Movie 4) with a change of the open area from 96 ± 14 mm^2 to a maximum of 227 ± 80 mm^2, which is an increase of 139 ± 66% ($n=4$). The opening was only transient and declined nearly to baseline during stimulation (Fig. 7b), indicating that AAV-based ChR2 expression must be improved for optogenetic induction of sustained tetanic contractions.

Discussion

We herein report direct optogenetic stimulation of intact mammalian skeletal muscle. Even though in skeletal muscle all of the electrically isolated fibres must be simultaneously stimulated for maximal force generation, optogenetic stimulation was found to induce 84% of the maximal force during electrical

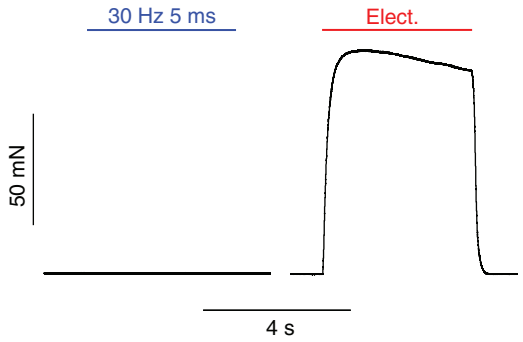

Figure 5 | Optical stimulation in CAG EGFP control mice. Representative recording ($n=4$) of isometric force measurements of soleus muscles from mice expressing only EGFP during optical stimulation with 5-ms-long pulses at 30 Hz (1.4 mW mm^{-2}) and electrical stimulation (10 mA, 1 ms, 100 Hz).

stimulation. In contrast to using brief electrical pulses, the ability to apply longer light pulses allowed the biophysical investigation of different depolarization patterns on skeletal muscle contraction, and the high spatial control enabled the selective stimulation of intralaryngeal muscles.

Using single light pulses of various duration and intensities we found increasing twitch forces either by applying higher light intensities or longer pulse durations. This can be explained with enhanced recruitment of muscle fibres from deeper layers by using higher intensities and by longer lasting ChR2 photocurrents both leading to action potential generation in more fibres. Interestingly, light pulses longer than 50 ms had no additional benefit, indicating that at this pulse duration all fibres are activated and excitation of the whole muscle is saturated. For higher and sustained forces, pulsed illumination was required because continuous illumination induced only a transient contraction, which highlights the importance of repolarization

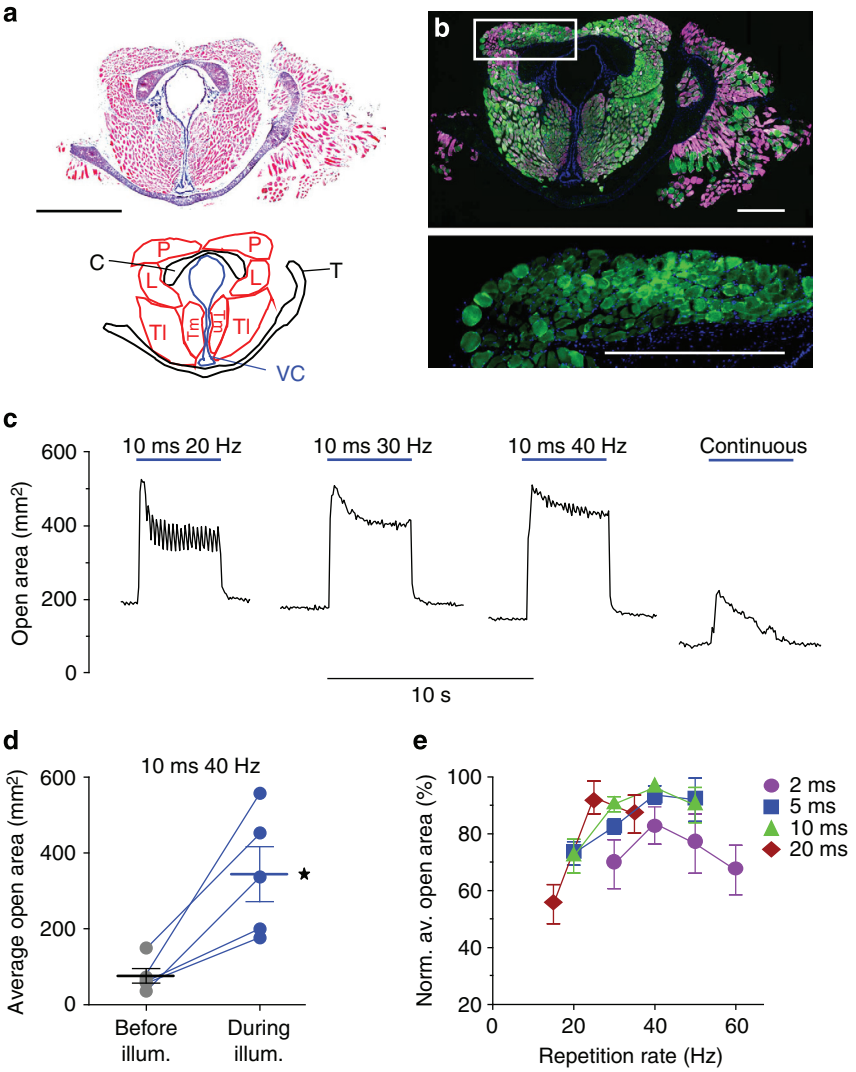

Figure 6 | Optogenetic opening of the vocal cords. (**a**) H&E staining of a section through the larynx (top) and schematic drawing displaying the different muscle groups and cartilages (bottom: P: posterior cricoarytenoid muscle; L, lateral cricoarytenoid muscle, C, cricoid cartilage; VC, vocal cords; T, thyroid cartilage; Tl, lateral cricothyroid muscle; Tm, medial cricothyroid muscle). (**b**) Membrane-bound ChR2-EYFP signals (green, enlargement in lower panel) overlaid with α-actinin staining (magenta) in a consecutive slice. (**c**) Representative examples of opening of the vocal cords induced by various 4-s-long illumination patterns. (**d**) Open area between the vocal cords calculated before and during illumination (10 ms light pulses, 35.7 mW mm^{-2}, 40 Hz repetition rate, $n=5$, two-way, paired Student's t-test, $P=0.0145$). (**e**) Relationship between repetition rate and average open area normalized to maximal opening for different light pulse durations (35.7 mW mm^{-2}, $n=3$). Error bars, s.e.m., nuclear staining in blue, scale bars, 1 mm (**a**), 500 μm (**b**).

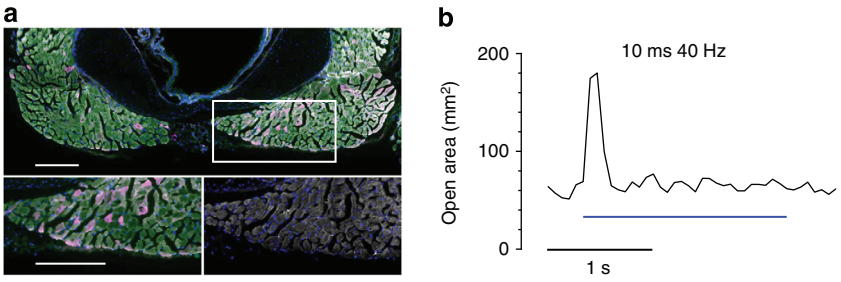

Figure 7 | Functional ChR2 expression in the larynx after AAV-based gene transfer. (**a**) mCherry expression (magenta) in α-actinin (white)-positive fibres of the posterior cricoarytenoid muscle (autofluorescence in green, enlargements in lower panels). (**b**) Representative example of the transient opening of the vocal cords during 2-s-long pulsed illumination (10 ms, 40 Hz, 35.7 mW mm^{-2}). Nuclear staining in blue, scale bar, 200 μm.

for proper tetanus induction in skeletal muscle. At low frequencies (<30 Hz), optogenetic stimulation was superior to electrical stimulation because it allowed longer pulse durations and hence the prolonged action potentials would result in longer Ca^{2+} transients and higher force generation. In contrast, at high repetition rates (>40 Hz), the slow off-kinetics of the ChR2(H134R) variant prevented the repolarization between pulses. This causes similar to constant illumination, refractoriness of L-type Ca^{2+} channels, impaired Ca^{2+} accumulation and attenuation of force[15]. Accordingly, short phases of repolarization are required for sustained tetanic contractions. Thus, in contrast to cardiac muscle, where this effect is not present because of the long action potentials and the inability to generate tetanus, larger contractile force in skeletal muscles could be generated by high-rate tetanus induction using ultrafast ChR2 variants with fast off-kinetics (time constant of deactivation ~5 ms) such as ChETA[16] or Chronos[17]. Furthermore, light attenuation by blood and muscle tissue could be decreased using ChR2 variants with red-shifted excitation spectra[18] because of higher light penetrance.

Our experiments also provide proof-of-concept for a translational approach. Bilateral recurrent nerve paralysis is a severe complication of various disease processes[19] and results in a fixed paramedian position of the vocal cords and life-threatening dyspnoea[20]. Current treatment options are surgical removal of one vocal cord or permanent tracheotomy; however, these treatment forms have severe side effects[21,22]. Alternatively, also electrical stimulation has been tested; however, this approach is seriously affected by corrosion or encapsulation of the electrode tip, discomfort due to the stimulation of sensory nerves and co-stimulation of antagonist muscles[20,23], preventing its clinical use. Our experiments prove the specific stimulation of small intralaryngeal muscles to selectively open and close the vocal cords. Given the anatomic and biomechanical similarities between larynges from mice and humans[24], this approach could be a potential therapeutic option for patients suffering from bilateral laryngeal paralysis.

AAVs would be a very promising tool for the expression of ChR2 because several clinical trials have already proven their efficacy and safety for therapeutic gene transfer into skeletal muscles in humans[25–27]. The transduction rate in the larynx could be enhanced by either using catheter-based intravascular injection into laryngeal vessels, or local intramuscular injection of AAV. Selective expression of ChR2 in skeletal muscle cells would enable pain-free optogenetic stimulation, and selective targeting of ChR2 to the most fatigue-resistant slow twitch muscle fibres could be used to reduce muscle fatigue. Moreover, direct optogenetic stimulation of muscle could be also applied in diseases that affect peripheral nerves or synaptic transmission, such as amyotrophic lateral sclerosis or myasthenia gravis in which the previously reported indirect optogenetic stimulation through peripheral nerves[4–6] would fail.

In summary, we demonstrate the feasibility and the biophysical basics of direct optogenetic stimulation in intact mammalian skeletal muscle. Its high efficacy as well as the advantage of site-specific and time-controlled excitation of skeletal muscle makes this an ideal approach to explore basic principles in muscle physiology and to develop this further towards translation.

Methods

Transgenic mouse model. Experiments were performed using the previously reported[10] transgenic mouse line expressing the ChR2 (H134R) variant under the control of the chicken-β-actin (CAG) promoter; in total, eight male mice (ages 2–8 months, median 2.5 months) and six females (ages 5–8 months, median 4.8 months) were used. Transgenic mice (three female mice, 7 months old) expressing EGFP under control of the CAG promoter[10] served as controls in Fig. 5. Both lines were backcrossed ≥10 generations on a CD1 genetic background. Animal experiments conformed with the Guide for the Care and Use of Laboratory Animals published by the US National Institutes of Health (eighth edition, revised 2011). For the harvesting of tissue, mice were killed by cervical dislocation and dissection of skeletal muscle was performed in ice-cold bicarbonate Tyrode solution containing (in mM) 118 NaCl, 3.4 KCl, 0.8 $MgSO_4$, 1.2 KH_2PO_4, 11.1 Glucose, 25 $NaHCO_3$ and 2.5 $CaCl_2$ gassed with 95% O_2 and 5% CO_2 at room temperature. Preparation of FDB muscles was performed in ice-cold Tyrode solution containing (in mM) 140 NaCl, 5.4 KCl, 1.8 $CaCl_2$, 2 $MgCl_2$, 10 glucose and 10 Hepes (pH 7.4, adjusted with NaOH) and preparation of explanted larynges was performed in ice-cold DPBS (Gibco, Life technologies).

Single FDB fibre preparation. To obtain single FDB fibres, FDB muscles were explanted and dissociated with 2 mg ml^{-1} collagenase B (Roche) in Tyrode solution for 1 h at 37 °C. Single FDB fibres were plated on glass coverslips coated with 100 μg ml^{-1} Laminin (Sigma-Aldrich) and incubated for 2–3 h at room temperature in Tyrode solution. Illumination (470 nm) was performed on an Axiovert 200 microscope (Zeiss) through a ×20 Fluar objective (numerical aperture: 0.75, Zeiss) with a temperature-controlled LED module (Omicron, LEDMOD LAB 470 nm, Omicron Laserage). Videos were recorded at 60 fps with a CMOS camera (Basler A602f) and the Fire-I Application 5.51 software (UniBrain).

Isometric force measurements. Soleus muscles were explanted and incubated in Bicarbonate Tyrode solution containing (in mM) 118 NaCl, 3.4 KCl, 0.8 $MgSO_4$, 1.2 KH_2PO_4, 11.1 Glucose, 25 $NaHCO_3$ and 2.5 $CaCl_2$ gassed with 95% O_2 and 5% CO_2 at room temperature. To measure isometric force, soleus muscles were mounted between a force transducer (KG 2, Scientific Instruments) and a fixed hook. For illumination, a temperature-controlled LED module (Omicron, LEDMOD LAB 470 nm, Omicron Laserage) was coupled to a plastic optical fibre (2 mm diameter, numerical aperture (NA) = 0.5) and directed into the window of the muscle recording chamber resulting in the illumination of the whole muscle. Light intensity was calibrated by measuring the power (PM100 powermeter with S130A sensor, Thorlabs) at the site of muscle placement within the recording chamber.

Control of LED and recording of force were performed with a Powerlab 8/30 recording system and the Chart 7.1 software (AD Instruments). Electrical stimuli were generated by a stimulator (Stim7, Scientific Instruments or stimulator 2100, AM Systems) connected to the force transducer and the hook. Soleus muscles were pre-stretched until single light stimuli (10 ms, 1.4 mW mm^{-2}) evoked maximal force generation. This optimal muscle length was multiplied by 0.85 to calculate the optimal fibre length as previously reported[28]. To confirm the viability of the skeletal muscle before the optical activation, soleus muscles were activated with a maximal electrical tetanus stimulation (20 V, 0.1 ms biphasic, 100 Hz, 2 s) and, only if this muscle yielded a maximum force generation above 70 mN, it was used for further experiments. Light-induced single twitches were evoked with at least 10-s

intervals between stimulations. Tetanic contractions induced by optical and electrical stimulation were 2 s long with an interval of 3 min between stimulations. Directly after force recording, tendons were removed and soleus muscles were blotted on tissue paper to remove the excess fluid and weighed. For quantification, maximal force was analysed for single twitch contractions and the average force during tetanic contractions was normalized to cross-sectional area that was calculated as weight/(optimal fibre length × density (1.06 mg mm^{-3}) as previously reported[28]. For the analysis of the force–frequency relationship (Fig. 2c), force was normalized to the maximal force induced by electrical stimulation (20 V, 1 ms, biphasic) to account for variation between muscles. To analyse fatigue induction, 350-ms-long tetanic optical or electrical stimulation pattern were applied every 3.7 s over a total period of 10 min similarly as reported before using the best optical (5 ms, 30 Hz, 1.4 mW mm^{-2}) and electrical (100 Hz, 20 V, 0.1 ms, biphasic) stimulation pattern[29].

Recording of membrane potential from intact skeletal muscles. For intracellular recording of membrane potential, soleus muscles were mounted, over-stretched to 110–130% of optimal length and 25 mM 2,3-Butanedione monoxime (Sigma) was added to the bicarbonate Tyrode solution in order to alleviate contractions. Sharp electrodes (filled with 3 M KCl, 50–150 MΩ) were impaled into the soleus muscle using a piezomanipulator (PM10, Maerzhaeuser Wetzlar) and membrane potential was recorded with a bridge amplifier (BA-03X, npi electronic), the Powerlab 8/30 recording system and the Chart 7.1 software (AD Instruments). Only cells with a resting membrane potential more negative than −50 mV and action potentials with overshoot above 0 mV were included into the analysis. Action potential duration was determined by measuring the time from the peak to repolarization to −35 mV.

Analysis of laryngeal function *ex vivo*. Explanted larynges were placed in bicarbonate Tyrode solution (for composition see above) gassed with 95% O_2 and 5% CO_2. For optical stimulation a light guide (Ø 400 µm, NA 0.48) was coupled to a 470-nm LED (M470F1, Thorlabs), controlled by a Powerlab 8/30 recording system and the Chart 7.1 software (AD Instruments) and placed directly in front of the posterior cricoarytenoid muscles or the superior cricoarytenoid muscles. Light intensity was calibrated at the tip of the light guide, and this might be therefore an overestimate. For visualization explanted larynges were illuminated from the top with white light from a cold-light source (Olympus KL2500LCD) and videos were recorded through a macroscope (MVX10, Olympus) equipped with a ×1 Objective (MVPLAPO1x, NA 0.25, Olympus) and a 542 ± 27-nm bandpass filter (F37-542, AHF Analysetechnik) to block the stimulation light. For each stimulation pattern, a single video file was recorded at 15 or 30 f.p.s. with a CMOS camera (Basler A602f) and the Fire-I Application 5.51 software (UniBrain). Videos of the same larynx were merged, and only videos in which the whole area between the vocal cords was darker than the surrounding tissue of the larynges could be used for the automatic analysis. Brightness adjustments and converting into binary images by threshold analysis was performed with the Virtual Dub video processing software. This conversion resulted in a video in which the area between the vocal cords was black and the surrounding tissue turned white. A custom-made, Lab-view-based area analysis software detected and calculated the black area between the vocal cords over time. Calibration of pixel size was used to determine the absolute areas (in mm^2). Traces of the open area between the vocal cords over time were further analysed using the Chart 7.1 software (AD Instruments). The average open area was analysed by determining the integral of the open area and was normalized to the maximal average opening of each muscle in order to take anatomical variations into account.

AAV injection and analysis of efficacy. Injection of AAV was approved by the local ethics review board. The AAV9-CAG-hChR2(H134R)-mCherry virus consisting of the AAV9 virus capsid and AAV2 virus DNA were ordered from the Penn Vector Core from the University of Pennsylvania. Ten-week-old female mice (CD1, Charles River) were anaesthetized by inhalation of 1.5% isoflurane and O_2/N_2O (50%/50%). Overall, 2×10^{11} genome copies of AAV diluted in 100 µl PBS were injected slowly (~10 s) through a 1-ml syringe (Insuline Syringe U-40, BD) connected to a sterile 33-gauge needle (200 µm diameter, Nanopass 33, Terumo) into the left jugular vein. Bleeding was carefully stopped using surgical swabs trapped in forceps, and the lesion was closed with a suture (Prolene C-1 13 mm 3/8c, Ethicon). Four weeks later, larynges were explanted and tested with the same set-up as described above using 2 or 4 s long, pulsed stimulation with a pulse duration of 10 ms and a repetition rate of 40 Hz, and the open area between the vocal cords was manually determined in individual frames using the area measurement tool of the ImageJ software (NIH).

Histology and immunofluorescence staining. Single FDB fibres, soleus muscles and explanted larynges were fixated with 4% paraformaldehyde (PFA). Cryopreserved muscles and larynges were sectioned with a cryotome (Cryostat CM3050 S, Leica) into 10-µm-thick slices. Slices of larynges were stained with haematoxylin and eosin (H&E) according to the standard protocols and consecutive slices were used for immunohistochemical stainings. All sections were permeabilized with 0.2% Triton X in PBS, and immunohistochemical stainings were performed in 5% donkey serum for 2 h at room temperature with a primary antibody to the α-actinin protein (1:400, Sigma-Aldrich). Cy3- or Cy5-conjugated secondary antibodies (1:400, Jackson ImmunoResearch) were diluted in Hoechst 33342 for nuclear staining. Pictures of native soleus muscles and laryngeal H&E sections were acquired with a stereomicroscope (AxioZoom.V16, Zeiss), and fluorescence pictures of laryngeal slices, soleus muscles and single FDB fibre were acquired with an inverted fluorescence microscope (Axio Imager, Zeiss). To analyse the percentage of muscle fibres with ChR2-mCherry expression after systemic AAV injection, fluorescence images were acquired with a mCherry filter set (F46-008, AHF Analysentechnik) and overlaid with native autofluorescence signals acquired with a Cy2 filter set and α-actinin staining using the Cy3 channel. The number of mCherry-positive muscle fibres was counted and normalized to all muscle fibres identified by α-actinin staining.

Statistics. Statistical data are shown as mean ± s.e.m. For comparison of different stimulation patterns, repeated ANOVA tests were performed using Dunnett's multiple comparison tests for isometric force measurements with continuous light stimulation as control (Fig. 2b) or Bonferroni multiple comparison test for opening of the vocal cords. For comparison of the average open area between vocal cords before and during illumination (Fig. 6d) a one-way, paired Student's *t*-test and for comparison of fatigue induction by optical and electrical stimulation (Fig. 4) a two-way paired Student's *t*-test was chosen. The *n* values in the legends indicate the number of independent experiments (muscles or larynges), and a $P<0.05$ was considered statistically significant.

References

1. Nagel, G. *et al.* Channelrhodopsin-2, a directly light-gated cation-selective membrane channel. *Proc. Natl Acad. Sci. USA* **100,** 13940–13945 (2003).
2. Boyden, E. S., Zhang, F., Bamberg, E., Nagel, G. & Deisseroth, K. Millisecond-timescale, genetically targeted optical control of neural activity. *Nat. Neurosci.* **8,** 1263–1268 (2005).
3. Gradinaru, V. *et al.* Targeting and readout strategies for fast optical neural control *in vitro* and *in vivo*. *J. Neurosci.* **27,** 14231–14238 (2007).
4. Llewellyn, M. E., Thompson, K. R., Deisseroth, K. & Delp, S. L. Orderly recruitment of motor units under optical control *in vivo*. *Nat. Med.* **16,** 1161–1165 (2010).
5. Bryson, J. B. *et al.* Optical control of muscle function by transplantation of stem cell-derived motor neurons in mice. *Science* **344,** 94–97 (2014).
6. Towne, C., Montgomery, K. L., Iyer, S. M., Deisseroth, K. & Delp, S. L. Optogenetic control of targeted peripheral axons in freely moving animals. *PLoS ONE* **8,** e72691 (2013).
7. Nagel, G. *et al.* Light activation of channelrhodopsin-2 in excitable cells of *Caenorhabditis elegans* triggers rapid behavioral responses. *Curr. Biol.* **15,** 2279–2284 (2005).
8. Asano, T., Ishizua, T. & Yawo, H. Optically controlled contraction of photosensitive skeletal muscle cells. *Biotechnol. Bioeng.* **109,** 199–204 (2012).
9. Arrenberg, A. B., Stainier, D. Y., Baier, H. & Huisken, J. Optogenetic control of cardiac function. *Science* **330,** 971–974 (2010).
10. Bruegmann, T. *et al.* Optogenetic control of heart muscle *in vitro* and *in vivo*. *Nat. Methods* **7,** 897–900 (2010).
11. Zhang, Q. *et al.* Temporally and spatially controlled expression of transgenes in embryonic and adult tissues. *Transgenic Res.* **19,** 499–509 (2010).
12. Martin-Oviedo, C. *et al.* Functional role of human laryngeal nerve connections. *Laryngoscope* **121,** 2338–2343 (2011).
13. McCulloch, T. M., Van Daele, D. & Ciucci, M. R. Otolaryngology head and neck surgery: an integrative view of the larynx. *Head Neck* **33,** S46–S53 (2011).
14. Xu, L. *et al.* Adeno-associated virus 9 mediated FKRP gene therapy restores functional glycosylation of alpha-dystroglycan and improves muscle functions. *Mol. Ther.* **21,** 1832–1840 (2013).
15. Robin, G. & Allard, B. Major contribution of sarcoplasmic reticulum $Ca2^+$ depletion during long-lasting activation of skeletal muscle. *J. Gen. Physiol.* **141,** 557–565 (2013).
16. Gunaydin, L. A. *et al.* Ultrafast optogenetic control. *Nat. Neurosci.* **13,** 387–392 (2010).
17. Klapoetke, N. C. *et al.* Independent optical excitation of distinct neural populations. *Nat. Methods* **11,** 338–346 (2014).
18. Lin, J. Y., Knutsen, P. M., Muller, A., Kleinfeld, D. & Tsien, R. Y. ReaChR: a red-shifted variant of channelrhodopsin enables deep transcranial optogenetic excitation. *Nat. Neurosci.* **16,** 1499–1508 (2013).
19. Seyed Toutounchi, S. J., Eydi, M., Golzari, S. E., Ghaffari, M. R. & Parvizian, N. Vocal cord paralysis and its etiologies: a prospective study. *J. Cardiovasc. Thorac. Res.* **6,** 47–50 (2014).
20. Zealear, D. L. *et al.* Reanimation of the paralyzed human larynx with an Implantable electrical stimulation device. *Laryngoscope* **113,** 1149–1156 (2003).
21. Plouin-Gaudon, I., Lawson, G., Jamart, J. & Remacle, M. Subtotal carbon dioxide laser arytenoidectomy for the treatment of bilateral vocal fold immobility: long-term results. *Ann. Otol. Rhinol. Laryngol.* **114,** 115–121 (2005).

22. Danker, H. *et al.* Social withdrawal after laryngectomy. *Eur. Arch. Otorhinolaryngol.* **267,** 593–600 (2010).
23. Nomura, K. *et al.* Bilateral motion restored to the paralyzed canine larynx with implantable stimulator. *Laryngoscope* **120,** 2399–2409 (2010).
24. Thomas, L. B., Stemple, J. C., Andreatta, R. D. & Andrade, F. H. Establishing a new animal model for the study of laryngeal biology and disease: an anatomic study of the mouse larynx. *J. Speech Lang. Hear. Res.* **52,** 802–811 (2009).
25. Wang, Z. J., Tapscott, S. J., Chamberlain, J. S. & Storb, R. Immunity and AAV-mediated gene therapy for muscular dystrophies in large animal models and human trials. *Front. Microbiol.* **2,** 201 (2011).
26. Bowles, D. E. *et al.* Phase 1 gene therapy for duchenne muscular dystrophy using a translational optimized AAV vector. *Mol. Ther.* **20,** 443–455 (2012).
27. Mendell, J. R. *et al.* Sustained alpha-sarcoglycan gene expression after gene transfer in limb-girdle muscular dystrophy, type 2D. *Ann. Neurol.* **68,** 629–638 (2010).
28. Tallis, J., James, R. S., Cox, V. M. & Duncan, M. J. The effect of physiological concentrations of caffeine on the power output of maximally and submaximally stimulated mouse EDL (fast) and soleus (slow) muscle. *J. Appl. Physiol.* **112,** 64–71 (2012).
29. Gonzalez, E. & Delbono, O. Age-dependent fatigue in single intact fast- and slow fibers from mouse EDL and soleus skeletal muscles. *Mech. Ageing Dev.* **122,** 1019–1032 (2001).

Acknowledgements

We thank F. Holst (University of Bonn) for technical assistance, H. Begerau (University Bonn) for designing and programming the area analysis software, D. Wenzel (University of Bonn) for help with isometric force measurements and A. Schroeck for technical advice on larynx preparation. This work was supported by the Bonfor programme (Medical Faculty, University Bonn) and the German Research Foundation (Research Training Group 1873).

Author contributions

T.B. and P.S. designed the study, T.B., T.v.B., C.C.V. and T.S. performed experiments and analysed the data, T.B., B.K.F. and P.S wrote the manuscript.

Additional information

Supplementary Information accompanies this paper at http://www.nature.com/naturecommunications

Competing financial interests: The authors declare no competing financial interests.

Reprints and permission information is available online at http://npg.nature.com/reprintsandpermissions/

How to cite this article: Bruegmann, T. *et al.* Optogenetic control of contractile function in skeletal muscle. *Nat. Commun.* 6:7153 doi: 10.1038/ncomms8153 (2015).

4.3 Epilogue

Light induced depolarization of ChR2 expressing skeletal muscles allows completely new experiments for the investigation of skeletal muscle physiology because it enables for the first time uniform control over the membrane potential in intact skeletal fibers and muscles. Importantly, this is neither possible with electrical intracellular stimulation due to loss-of-voltage control nor with extracellular electrical field stimulation as explained above. Focused illumination on different parts of the cell membrane could be used to search for hot spots of excitability which are predicted at the site of the neuromuscular endplate or to quantify the different propagation kinetics of the electrical excitation at the sarcolemma surface and within the t-tubular membrane.[138] Global illumination enables uniform depolarization of the whole myofiber and the level and duration can be fine-grain controlled by the light intensity and pulse duration. This allows novel investigations of excitation-contraction-coupling mechanism in greater detail than using nerval or electrical stimulation. In addition, optogenetic proteins can be specifically expressed only in skeletal muscles and even specifically in fast or slow myofiber types using appropriate promotors. This would allow investigations of retrograde feedback and forward-loops between skeletal muscle and motor neuron activity[176] as well as mimicking the physiological fiber recruitment and lower fatigue development if the slower muscle fiber become selectively activated.

Interestingly, our approach for direct optogenetic stimulation of skeletal muscles was recently confirmed and extended to *in vivo* stimulation in transgenic mice.[177] Furthermore, the authors used repetitive optogenetic stimulation over several days to attenuate atrophy generation in denervated fibers which supports the clinical prospects of direct optogenetic stimulation of skeletal muscles.

5. Conclusion

In my thesis, I focused on describing the feasibility and mechanistic advantages of optogenetic stimulation of striated muscle and it is based on two ground breaking publications in the respective fields. In the first publication, I was able to prove that the sustained optogenetic depolarization can be used to terminate ventricular arrhythmia in intact mouse hearts. Excitingly, I suggest that optogenetic defibrillation terminates arrhythmia by a completely different mechanism compared to electrical shocks which could add to the efficacy and thus safety in future clinical applications. Furthermore optogenetic depolarization will enable to better understand the mechanism underlying the termination of tachyarrhythmia by electrical shocks.

In the second publication, I showed the feasibility and characterized the biophysical principles of direct optogenetic stimulation of intact skeletal muscles. This proved distinct advantages over electrical stimulation. Importantly, optogenetic stimulation enables the precise spatial control of the membrane potential in the whole elongated myofiber. The fine grain control over duration and depolarization will allow investigation of the excitation-contraction coupling machinery in much greater detail and even in intact muscles. Furthermore, the feasibility to directly stimulate skeletal muscle with considerably low energy will raise hope for therapeutic applications in neuromuscular diseases which cannot be treated with electrical stimulation so far.

Therefore optogenetic stimulation of striated muscles is a unique tool to address open questions in basic research due to its unprecedented spatial precision and ability to control the membrane potential of cells in intact tissues. Importantly, the possibility to perform cell-specific stimulation allows a tantalizing outlook for therapeutic applications in heart and skeletal muscle pathologies.

6. References

1. Bers DM. Calcium cycling and signaling in cardiac myocytes. *Annu Rev Physiol* 2008;**70**:23-49.
2. O'Hara T, Virag L, Varro A, Rudy Y. Simulation of the undiseased human cardiac ventricular action potential: model formulation and experimental validation. *PLoS Comput Biol* 2011;**7**:e1002061.
3. Bartos DC, Grandi E, Ripplinger CM. Ion Channels in the Heart. *Compr Physiol* 2015;**5**:1423-1464.
4. Hopkins PM. Skeletal muscle physiology. *CEACCPain* 2006;**6**:1-6.
5. Bottinelli R, Reggiani C. Human skeletal muscle fibres: molecular and functional diversity. *Prog Biophys Mol Biol* 2000;**73**:195-262.
6. Duval A, Leoty C. Comparison between the delayed outward current in slow and fast twitch skeletal muscle in the rat. *J Physiol* 1980;**307**:43-57.
7. Bretag AH. Muscle chloride channels. *Physiol Rev* 1987;**67**:618-724.
8. Cajavilca C, Varon J, Sternbach GL. Resuscitation great. Luigi Galvani and the foundations of electrophysiology. *Resuscitation* 2009;**80**:159-162.
9. Sakmann B, Neher E. Patch clamp techniques for studying ionic channels in excitable membranes. *Annu Rev Physiol* 1984;**46**:455-472.
10. Huser J, Lipp P, Niggli E. Confocal microscopic detection of potential-sensitive dyes used to reveal loss of voltage control during patch-clamp experiments. *Pflugers Arch* 1996;**433**:194-199.
11. Hernandez-Ochoa EO, Schneider MF. Voltage clamp methods for the study of membrane currents and SR Ca(2+) release in adult skeletal muscle fibres. *Prog Biophys Mol Biol* 2012;**108**:98-118.
12. Belles B, Malecot CO, Hescheler J, Trautwein W. "Run-down" of the Ca current during long whole-cell recordings in guinea pig heart cells: role of phosphorylation and intracellular calcium. *Pflugers Arch* 1988;**411**:353-360.
13. Merrill DR, Bikson M, Jefferys JG. Electrical stimulation of excitable tissue: design of efficacious and safe protocols. *J Neurosci Methods* 2005;**141**:171-198.
14. Tung L, Borderies JR. Analysis of electric field stimulation of single cardiac muscle cells. *Biophys J* 1992;**63**:371-386.
15. Wagenaar DA, Potter SM. Real-time multi-channel stimulus artifact suppression by local curve fitting. *J Neurosci Methods* 2002;**120**:113-120.
16. Corbin LV, 2nd, Scher AM. The canine heart as an electrocardiographic generator. Dependence on cardiac cell orientation. *Circ Res* 1977;**41**:58-67.
17. Roberts DE, Hersh LT, Scher AM. Influence of cardiac fiber orientation on wavefront voltage, conduction velocity, and tissue resistivity in the dog. *Circ Res* 1979;**44**:701-712.
18. Poelzing S, Akar FG, Baron E, Rosenbaum DS. Heterogeneous connexin43 expression produces electrophysiological heterogeneities across ventricular wall. *Am J Physiol Heart Circ Physiol* 2004;**286**:H2001-2009.
19. Wikswo JP, Jr., Wisialowski TA, Altemeier WA, Balser JR, Kopelman HA, Roden DM. Virtual cathode effects during stimulation of cardiac muscle. Two-dimensional in vivo experiments. *Circ Res* 1991;**68**:513-530.
20. Akar FG, Roth BJ, Rosenbaum DS. Optical measurement of cell-to-cell coupling in intact heart using subthreshold electrical stimulation. *Am J Physiol Heart Circ Physiol* 2001;**281**:H533-542.
21. Sambelashvili AT, Nikolski VP, Efimov IR. Nonlinear effects in subthreshold virtual electrode polarization. *Am J Physiol Heart Circ Physiol* 2003;**284**:H2368-2374.
22. Bishop MJ, Connolly A, Plank G. Structural heterogeneity modulates effective refractory period: a mechanism of focal arrhythmia initiation. *PLoS One* 2014;**9**:e109754.
23. Lieber RL, Roberts TJ, Blemker SS, Lee SSM, Herzog W. Skeletal muscle mechanics, energetics and plasticity. *J Neuroeng Rehabil* 2017;**14**:108.
24. Bryson JB, Machado CB, Lieberam I, Greensmith L. Restoring motor function using optogenetics and neural engraftment. *Curr Opin Biotechnol* 2016;**40**:75-81.

25. Hultman E, Sjoholm H, Jaderholm-Ek I, Krynicki J. Evaluation of methods for electrical stimulation of human skeletal muscle in situ. *Pflugers Arch* 1983;**398**:139-141.
26. Rushton WA. Identification of Lucas's alpha excitability. *J Physiol* 1932;**75**:445-470.
27. Gregory CM, Bickel CS. Recruitment patterns in human skeletal muscle during electrical stimulation. *Phys Ther* 2005;**85**:358-364.
28. Bickel CS, Gregory CM, Dean JC. Motor unit recruitment during neuromuscular electrical stimulation: a critical appraisal. *Eur J Appl Physiol* 2011;**111**:2399-2407.
29. Sideris S, Archontakis S, Dilaveris P, Gatzoulis KA, Trachanas K, Sotiropoulos I, Arsenos P, Tousoulis D, Kallikazaros I. Leadless Cardiac Pacemakers: Current status of a modern approach in pacing. *Hellenic J Cardiol* 2017.
30. Brignole M, Auricchio A, Baron-Esquivias G, Bordachar P, Boriani G, Breithardt OA, Cleland J, Deharo JC, Delgado V, Elliott PM, Gorenek B, Israel CW, Leclercq C, Linde C, Mont L, Padeletti L, Sutton R, Vardas PE, Guidelines ESCCfP, Zamorano JL, Achenbach S, Baumgartner H, Bax JJ, Bueno H, Dean V, Deaton C, Erol C, Fagard R, Ferrari R, Hasdai D, Hoes AW, Kirchhof P, Knuuti J, Kolh P, Lancellotti P, Linhart A, Nihoyannopoulos P, Piepoli MF, Ponikowski P, Sirnes PA, Tamargo JL, Tendera M, Torbicki A, Wijns W, Windecker S, Document R, Kirchhof P, Blomstrom-Lundqvist C, Badano LP, Aliyev F, Bansch D, Baumgartner H, Bsata W, Buser P, Charron P, Daubert JC, Dobreanu D, Faerestrand S, Hasdai D, Hoes AW, Le Heuzey JY, Mavrakis H, McDonagh T, Merino JL, Nawar MM, Nielsen JC, Pieske B, Poposka L, Ruschitzka F, Tendera M, Van Gelder IC, Wilson CM. 2013 ESC Guidelines on cardiac pacing and cardiac resynchronization therapy: the Task Force on cardiac pacing and resynchronization therapy of the European Society of Cardiology (ESC). Developed in collaboration with the European Heart Rhythm Association (EHRA). *Eur Heart J* 2013;**34**:2281-2329.
31. Meller ST, Gebhart GF. A critical review of the afferent pathways and the potential chemical mediators involved in cardiac pain. *Neuroscience* 1992;**48**:501-524.
32. Lau EW. Technologies for Prolonging Cardiac Implantable Electronic Device Longevity. *Pacing Clin Electrophysiol* 2017;**40**:75-96.
33. Priori SG, Blomstrom-Lundqvist C, Mazzanti A, Blom N, Borggrefe M, Camm J, Elliott PM, Fitzsimons D, Hatala R, Hindricks G, Kirchhof P, Kjeldsen K, Kuck KH, Hernandez-Madrid A, Nikolaou N, Norekval TM, Spaulding C, Van Veldhuisen DJ. 2015 ESC Guidelines for the management of patients with ventricular arrhythmias and the prevention of sudden cardiac death: The Task Force for the Management of Patients with Ventricular Arrhythmias and the Prevention of Sudden Cardiac Death of the European Society of Cardiology (ESC). Endorsed by: Association for European Paediatric and Congenital Cardiology (AEPC). *Eur Heart J* 2015;**36**:2793-2867.
34. Zipes DP, Fischer J, King RM, Nicoll Ad, Jolly WW. Termination of ventricular fibrillation in dogs by depolarizing a critical amount of myocardium. *Am J Cardiol* 1975;**36**:37-44.
35. Marcus GM, Chan DW, Redberg RF. Recollection of pain due to inappropriate versus appropriate implantable cardioverter-defibrillator shocks. *Pacing Clin Electrophysiol* 2011;**34**:348-353.
36. Glikson M, Friedman PA. The implantable cardioverter defibrillator. *Lancet* 2001;**357**:1107-1117.
37. Daubert JP, Zareba W, Cannom DS, McNitt S, Rosero SZ, Wang P, Schuger C, Steinberg JS, Higgins SL, Wilber DJ, Klein H, Andrews ML, Hall WJ, Moss AJ, Investigators MI. Inappropriate implantable cardioverter-defibrillator shocks in MADIT II: frequency, mechanisms, predictors, and survival impact. *J Am Coll Cardiol* 2008;**51**:1357-1365.
38. Versteeg H, Theuns DA, Erdman RA, Jordaens L, Pedersen SS. Posttraumatic stress in implantable cardioverter defibrillator patients: the role of pre-implantation distress and shocks. *Int J Cardiol* 2011;**146**:438-439.
39. Ripplinger CM, Krinsky VI, Nikolski VP, Efimov IR. Mechanisms of unpinning and termination of ventricular tachycardia. *Am J Physiol Heart Circ Physiol* 2006;**291**:H184-192.
40. Eysmann SB, Marchlinski FE, Buxton AE, Josephson ME. Electrocardiographic changes after cardioversion of ventricular arrhythmias. *Circulation* 1986;**73**:73-81.

41. Larsen GK, Evans J, Lambert WE, Chen Y, Raitt MH. Shocks burden and increased mortality in implantable cardioverter-defibrillator patients. *Heart Rhythm* 2011;**8**:1881-1886.
42. Stein RB, Chong SL, James KB, Kido A, Bell GJ, Tubman LA, Belanger M. Electrical stimulation for therapy and mobility after spinal cord injury. *Prog Brain Res* 2002;**137**:27-34.
43. Stevens JE, Mizner RL, Snyder-Mackler L. Neuromuscular electrical stimulation for quadriceps muscle strengthening after bilateral total knee arthroplasty: a case series. *J Orthop Sports Phys Ther* 2004;**34**:21-29.
44. Lewek M, Stevens J, Snyder-Mackler L. The use of electrical stimulation to increase quadriceps femoris muscle force in an elderly patient following a total knee arthroplasty. *Phys Ther* 2001;**81**:1565-1571.
45. Strollo PJ, Soose RJ, Maurer JT, de Vries N, Cornelius J, Froymovich O, Hanson RD, Padhya TA, Steward DL, Gillespie MB, Woodson BT, Van de Heyning PH, Goetting MG, Vanderveken OM, Feldman N, Knaack L, Strohl KP, Grp ST. Upper-Airway Stimulation for Obstructive Sleep Apnea. *New Engl J Med* 2014;**370**:139-149.
46. Testelmans D, Nafteux P, Van Cromphaut S, Vrijsen B, Vos R, De Leyn P, Decaluwe H, Van Raemdonck D, Verleden GM, Buyse B. Feasibility of diaphragm pacing in patients after bilateral lung transplantation. *Clin Transplant* 2017.
47. Zemelman BV, Lee GA, Ng M, Miesenbock G. Selective photostimulation of genetically chARGed neurons. *Neuron* 2002;**33**:15-22.
48. Hegemann P, Nagel G. From channelrhodopsins to optogenetics. *EMBO Mol Med* 2013;**5**:173-176.
49. Braun FJ, Hegemann P. Two light-activated conductances in the eye of the green alga Volvox carteri. *Biophys J* 1999;**76**:1668-1678.
50. Oesterhelt D, Stoeckenius W. Rhodopsin-like protein from the purple membrane of Halobacterium halobium. *Nat New Biol* 1971;**233**:149-152.
51. Bamberg E. Rhodopsin and other proteins in artificial lipid membranes. *Biophys Struct Mech* 1977;**3**:39-42.
52. Herrmann TR, Rayfield GW. A measurement of the proton pump current generated by bacteriorhodopsin in black lipid membranes. *Biochim Biophys Acta* 1976;**443**:623-628.
53. Schmies G, Engelhard M, Wood PG, Nagel G, Bamberg E. Electrophysiological characterization of specific interactions between bacterial sensory rhodopsins and their transducers. *Proc Natl Acad Sci U S A* 2001;**98**:1555-1559.
54. Nagel G, Mockel B, Buldt G, Bamberg E. Functional expression of bacteriorhodopsin in oocytes allows direct measurement of voltage dependence of light induced H+ pumping. *Febs Lett* 1995;**377**:263-266.
55. Nagel G, Ollig D, Fuhrmann M, Kateriya S, Musti AM, Bamberg E, Hegemann P. Channelrhodopsin-1: a light-gated proton channel in green algae. *Science* 2002;**296**:2395-2398.
56. Nagel G, Szellas T, Huhn W, Kateriya S, Adeishvili N, Berthold P, Ollig D, Hegemann P, Bamberg E. Channelrhodopsin-2, a directly light-gated cation-selective membrane channel. *Proc Natl Acad Sci U S A* 2003;**100**:13940-13945.
57. Kane MA, Chen N, Sparks S, Napoli JL. Quantification of endogenous retinoic acid in limited biological samples by LC/MS/MS. *Biochem J* 2005;**388**:363-369.
58. Boyden ES, Zhang F, Bamberg E, Nagel G, Deisseroth K. Millisecond-timescale, genetically targeted optical control of neural activity. *Nat Neurosci* 2005;**8**:1263-1268.
59. Ishizuka T, Kakuda M, Araki R, Yawo H. Kinetic evaluation of photosensitivity in genetically engineered neurons expressing green algae light-gated channels. *Neurosci Res* 2006;**54**:85-94.
60. Li X, Gutierrez DV, Hanson MG, Han J, Mark MD, Chiel H, Hegemann P, Landmesser LT, Herlitze S. Fast noninvasive activation and inhibition of neural and network activity by vertebrate rhodopsin and green algae channelrhodopsin. *Proc Natl Acad Sci U S A* 2005;**102**:17816-17821.

61. Nagel G, Brauner M, Liewald JF, Adeishvili N, Bamberg E, Gottschalk A. Light activation of channelrhodopsin-2 in excitable cells of Caenorhabditis elegans triggers rapid behavioral responses. *Curr Biol* 2005;**15**:2279-2284.
62. Bi A, Cui J, Ma YP, Olshevskaya E, Pu M, Dizhoor AM, Pan ZH. Ectopic expression of a microbial-type rhodopsin restores visual responses in mice with photoreceptor degeneration. *Neuron* 2006;**50**:23-33.
63. Zhang F, Wang LP, Brauner M, Liewald JF, Kay K, Watzke N, Wood PG, Bamberg E, Nagel G, Gottschalk A, Deisseroth K. Multimodal fast optical interrogation of neural circuitry. *Nature* 2007;**446**:633-639.
64. Mattis J, Tye KM, Ferenczi EA, Ramakrishnan C, O'Shea DJ, Prakash R, Gunaydin LA, Hyun M, Fenno LE, Gradinaru V, Yizhar O, Deisseroth K. Principles for applying optogenetic tools derived from direct comparative analysis of microbial opsins. *Nat Methods* 2011;**9**:159-172.
65. Wietek J, Wiegert JS, Adeishvili N, Schneider F, Watanabe H, Tsunoda SP, Vogt A, Elstner M, Oertner TG, Hegemann P. Conversion of channelrhodopsin into a light-gated chloride channel. *Science* 2014;**344**:409-412.
66. Berndt A, Lee SY, Ramakrishnan C, Deisseroth K. Structure-guided transformation of channelrhodopsin into a light-activated chloride channel. *Science* 2014;**344**:420-424.
67. Govorunova EG, Sineshchekov OA, Janz R, Liu X, Spudich JL. NEUROSCIENCE. Natural light-gated anion channels: A family of microbial rhodopsins for advanced optogenetics. *Science* 2015;**349**:647-650.
68. Govorunova EG, Cunha SR, Sineshchekov OA, Spudich JL. Anion channelrhodopsins for inhibitory cardiac optogenetics. *Sci Rep* 2016;**6**:33530.
69. Bailes HJ, Milosavljevic N, Zhuang LY, Gerrard EJ, Nishiguchi T, Ozawa T, Lucas RJ. Optogenetic interrogation reveals separable G-protein-dependent and -independent signalling linking G-protein-coupled receptors to the circadian oscillator. *BMC Biol* 2017;**15**:40.
70. Bailes HJ, Zhuang LY, Lucas RJ. Reproducible and sustained regulation of Galphas signalling using a metazoan opsin as an optogenetic tool. *PLoS One* 2012;**7**:e30774.
71. Beiert T, Bruegmann T, Sasse P. Optogenetic activation of Gq signalling modulates pacemaker activity of cardiomyocytes. *Cardiovasc Res* 2014;**102**:507-516.
72. Karunarathne WK, Giri L, Kalyanaraman V, Gautam N. Optically triggering spatiotemporally confined GPCR activity in a cell and programming neurite initiation and extension. *Proc Natl Acad Sci U S A* 2013;**110**:E1565-1574.
73. Masseck OA, Rubelowski JM, Spoida K, Herlitze S. Light- and drug-activated G-protein-coupled receptors to control intracellular signalling. *Exp Physiol* 2011;**96**:51-56.
74. Masseck OA, Spoida K, Dalkara D, Maejima T, Rubelowski JM, Wallhorn L, Deneris ES, Herlitze S. Vertebrate cone opsins enable sustained and highly sensitive rapid control of Gi/o signaling in anxiety circuitry. *Neuron* 2014;**81**:1263-1273.
75. Spoida K, Eickelbeck D, Karapinar R, Eckhardt T, Mark MD, Jancke D, Ehinger BV, Konig P, Dalkara D, Herlitze S, Masseck OA. Melanopsin Variants as Intrinsic Optogenetic On and Off Switches for Transient versus Sustained Activation of G Protein Pathways. *Curr Biol* 2016;**26**:1206-1212.
76. Jansen V, Alvarez L, Balbach M, Strunker T, Hegemann P, Kaupp UB, Wachten D. Controlling fertilization and cAMP signaling in sperm by optogenetics. *Elife* 2015;**4:**05161.
77. Jansen V, Jikeli JF, Wachten D. How to control cyclic nucleotide signaling by light. *Curr Opin Biotechnol* 2017;**48**:15-20.
78. Gao S, Nagpal J, Schneider MW, Kozjak-Pavlovic V, Nagel G, Gottschalk A. Optogenetic manipulation of cGMP in cells and animals by the tightly light-regulated guanylyl-cyclase opsin CyclOp. *Nat Commun* 2015;**6**:8046.
79. Scheib U, Stehfest K, Gee CE, Korschen HG, Fudim R, Oertner TG, Hegemann P. The rhodopsin-guanylyl cyclase of the aquatic fungus Blastocladiella emersonii enables fast optical control of cGMP signaling. *Sci Signal* 2015;**8**:rs8.

80. Kim T, Folcher M, Doaud-El Baba M, Fussenegger M. A synthetic erectile optogenetic stimulator enabling blue-light-inducible penile erection. *Angew Chem Int Ed Engl* 2015;**54**:5933-5938.
81. Gasser C, Taiber S, Yeh CM, Wittig CH, Hegemann P, Ryu S, Wunder F, Moglich A. Engineering of a red-light-activated human cAMP/cGMP-specific phosphodiesterase. *Proc Natl Acad Sci U S A* 2014;**111**:8803-8808.
82. Konermann S, Brigham MD, Trevino A, Hsu PD, Heidenreich M, Cong L, Platt RJ, Scott DA, Church GM, Zhang F. Optical control of mammalian endogenous transcription and epigenetic states. *Nature* 2013;**500**:472-476.
83. Hughes RM, Freeman DJ, Lamb KN, Pollet RM, Smith WJ, Lawrence DS. Optogenetic apoptosis: light-triggered cell death. *Angew Chem Int Ed Engl* 2015;**54**:12064-12068.
84. Deisseroth K. Optogenetics: 10 years of microbial opsins in neuroscience. *Nat Neurosci* 2015;**18**:1213-1225.
85. Feldbauer K, Zimmermann D, Pintschovius V, Spitz J, Bamann C, Bamberg E. Channelrhodopsin-2 is a leaky proton pump. *Proc Natl Acad Sci U S A* 2009;**106**:12317-12322.
86. Kato HE, Zhang F, Yizhar O, Ramakrishnan C, Nishizawa T, Hirata K, Ito J, Aita Y, Tsukazaki T, Hayashi S, Hegemann P, Maturana AD, Ishitani R, Deisseroth K, Nureki O. Crystal structure of the channelrhodopsin light-gated cation channel. *Nature* 2012;**482**:369-374.
87. Guo Y, Beyle FE, Bold BM, Watanabe HC, Koslowski A, Thiel W, Hegemann P, Marazzi M, Elstner M. Active site structure and absorption spectrum of channelrhodopsin-2 wild-type and C128T mutant. *Chem Sci* 2016;**7**:3879-3891.
88. Zhang F, Prigge M, Beyriere F, Tsunoda SP, Mattis J, Yizhar O, Hegemann P, Deisseroth K. Red-shifted optogenetic excitation: a tool for fast neural control derived from Volvox carteri. *Nat Neurosci* 2008;**11**:631-633.
89. Lin JY, Lin MZ, Steinbach P, Tsien RY. Characterization of engineered channelrhodopsin variants with improved properties and kinetics. *Biophys J* 2009;**96**:1803-1814.
90. Deisseroth K, Hegemann P. The form and function of channelrhodopsin. *Science* 2017;**357**.
91. Bruegmann T, Malan D, Hesse M, Beiert T, Fuegemann CJ, Fleischmann BK, Sasse P. Optogenetic control of heart muscle in vitro and in vivo. *Nat Methods* 2010;**7**:897-900.
92. Kleinlogel S, Feldbauer K, Dempski RE, Fotis H, Wood PG, Bamann C, Bamberg E. Ultra light-sensitive and fast neuronal activation with the Ca(2)+-permeable channelrhodopsin CatCh. *Nat Neurosci* 2011;**14**:513-518.
93. Gunaydin LA, Yizhar O, Berndt A, Sohal VS, Deisseroth K, Hegemann P. Ultrafast optogenetic control. *Nat Neurosci* 2010;**13**:387-392.
94. Klapoetke NC, Murata Y, Kim SS, Pulver SR, Birdsey-Benson A, Cho YK, Morimoto TK, Chuong AS, Carpenter EJ, Tian Z, Wang J, Xie Y, Yan Z, Zhang Y, Chow BY, Surek B, Melkonian M, Jayaraman V, Constantine-Paton M, Wong GK, Boyden ES. Independent optical excitation of distinct neural populations. *Nat Methods* 2014;**11**:338-346.
95. Berndt A, Yizhar O, Gunaydin LA, Hegemann P, Deisseroth K. Bi-stable neural state switches. *Nat Neurosci* 2009;**12**:229-234.
96. Yizhar O, Fenno LE, Prigge M, Schneider F, Davidson TJ, O'Shea DJ, Sohal VS, Goshen I, Finkelstein J, Paz JT, Stehfest K, Fudim R, Ramakrishnan C, Huguenard JR, Hegemann P, Deisseroth K. Neocortical excitation/inhibition balance in information processing and social dysfunction. *Nature* 2011;**477**:171-178.
97. Bamann C, Gueta R, Kleinlogel S, Nagel G, Bamberg E. Structural guidance of the photocycle of channelrhodopsin-2 by an interhelical hydrogen bond. *Biochemistry-Us* 2010;**49**:267-278.
98. Klapoetke NC, Murata Y, Kim SS, Pulver SR, Birdsey-Benson A, Cho YK, Morimoto TK, Chuong AS, Carpenter EJ, Tian Z, Wang J, Xie Y, Yan Z, Zhang Y, Chow BY, Surek B, Melkonian M, Jayaraman V, Constantine-Paton M, Wong GK, Boyden ES. Independent optical excitation of distinct neural populations. *Nat Methods* 2014;**11**:338-346.
99. Lin JY, Knutsen PM, Muller A, Kleinfeld D, Tsien RY. ReaChR: a red-shifted variant of channelrhodopsin enables deep transcranial optogenetic excitation. *Nat Neurosci* 2013;**16**:1499-1508.

100. Govorunova EG, Spudich EN, Lane CE, Sineshchekov OA, Spudich JL. New channelrhodopsin with a red-shifted spectrum and rapid kinetics from Mesostigma viride. *MBio* 2011;**2**:e00115-00111.
101. Bishop MJ, Rodriguez B, Eason J, Whiteley JP, Trayanova N, Gavaghan DJ. Synthesis of voltage-sensitive optical signals: application to panoramic optical mapping. *Biophys J* 2006;**90**:2938-2945.
102. Gradinaru V, Thompson KR, Zhang F, Mogri M, Kay K, Schneider MB, Deisseroth K. Targeting and readout strategies for fast optical neural control in vitro and in vivo. *J Neurosci* 2007;**27**:14231-14238.
103. Iyer SM, Montgomery KL, Towne C, Lee SY, Ramakrishnan C, Deisseroth K, Delp SL. Virally mediated optogenetic excitation and inhibition of pain in freely moving nontransgenic mice. *Nat Biotechnol* 2014;**32**:274-278.
104. Tkatch T, Greotti E, Baranauskas G, Pendin D, Roy S, Nita LI, Wettmarshausen J, Prigge M, Yizhar O, Shirihai OS, Fishman D, Hershfinkel M, Fleidervish IA, Perocchi F, Pozzan T, Sekler I. Optogenetic control of mitochondrial metabolism and Ca2+ signaling by mitochondria-targeted opsins. *Proc Natl Acad Sci U S A* 2017;**114**:E5167-E5176.
105. Rost BR, Schneider F, Grauel MK, Wozny C, Bentz C, Blessing A, Rosenmund T, Jentsch TJ, Schmitz D, Hegemann P, Rosenmund C. Optogenetic acidification of synaptic vesicles and lysosomes. *Nat Neurosci* 2015;**18**:1845-1852.
106. Oh E, Maejima T, Liu C, Deneris E, Herlitze S. Substitution of 5-HT1A receptor signaling by a light-activated G protein-coupled receptor. *J Biol Chem* 2010;**285**:30825-30836.
107. Entcheva E. Cardiac optogenetics. *Am J Physiol Heart Circ Physiol* 2013;**304**:H1179-1191.
108. Knollmann BC. Pacing lightly: optogenetics gets to the heart. *Nat Methods* 2010;**7**:889-891.
109. Xie Y, Sato D, Garfinkel A, Qu Z, Weiss JN. So little source, so much sink: requirements for afterdepolarizations to propagate in tissue. *Biophys J* 2010;**99**:1408-1415.
110. Zaglia T, Pianca N, Borile G, Da Broi F, Richter C, Campione M, Lehnart SE, Luther S, Corrado D, Miquerol L, Mongillo M. Optogenetic determination of the myocardial requirements for extrasystoles by cell type-specific targeting of ChannelRhodopsin-2. *Proc Natl Acad Sci U S A* 2015;**112**:E4495-4504.
111. Arrenberg AB, Stainier DY, Baier H, Huisken J. Optogenetic control of cardiac function. *Science* 2010;**330**:971-974.
112. Jia Z, Valiunas V, Lu Z, Bien H, Liu H, Wang HZ, Rosati B, Brink PR, Cohen IS, Entcheva E. Stimulating cardiac muscle by light: cardiac optogenetics by cell delivery. *Circ Arrhythm Electrophysiol* 2011;**4**:753-760.
113. Nussinovitch U, Shinnawi R, Gepstein L. Modulation of cardiac tissue electrophysiological properties with light-sensitive proteins. *Cardiovasc Res* 2014;**102**:176-187.
114. Boyle PM, Williams JC, Ambrosi CM, Entcheva E, Trayanova NA. A comprehensive multiscale framework for simulating optogenetics in the heart. *Nat Commun* 2013;**4**:2370.
115. Bruegmann T, Sasse P. Optogenetic cardiac pacemakers: science or fiction? *Trends Cardiovasc Med* 2015;**25**:82-83.
116. Boyle PM, Karathanos TV, Trayanova NA. "Beauty is a light in the heart": the transformative potential of optogenetics for clinical applications in cardiovascular medicine. *Trends Cardiovasc Med* 2015;**25**:73-81.
117. Kirkton RD, Badie N, Bursac N. Spatial profiles of electrical mismatch determine vulnerability to conduction failure across a host-donor cell interface. *Circ Arrhythm Electrophysiol* 2013;**6**:1200-1207.
118. Williams JC, Xu J, Lu Z, Klimas A, Chen X, Ambrosi CM, Cohen IS, Entcheva E. Computational optogenetics: empirically-derived voltage- and light-sensitive channelrhodopsin-2 model. *PLoS Comput Biol* 2013;**9**:e1003220.
119. Bingen BO, Engels MC, Schalij MJ, Jangsangthong W, Neshati Z, Feola I, Ypey DL, Askar SF, Panfilov AV, Pijnappels DA, de Vries AA. Light-induced termination of spiral wave arrhythmias by optogenetic engineering of atrial cardiomyocytes. *Cardiovasc Res* 2014;**104**:194-205.

120. Hacein-Bey-Abina S, Von Kalle C, Schmidt M, McCormack MP, Wulffraat N, Leboulch P, Lim A, Osborne CS, Pawliuk R, Morillon E, Sorensen R, Forster A, Fraser P, Cohen JI, de Saint Basile G, Alexander I, Wintergerst U, Frebourg T, Aurias A, Stoppa-Lyonnet D, Romana S, Radford-Weiss I, Gross F, Valensi F, Delabesse E, Macintyre E, Sigaux F, Soulier J, Leiva LE, Wissler M, Prinz C, Rabbitts TH, Le Deist F, Fischer A, Cavazzana-Calvo M. LMO2-associated clonal T cell proliferation in two patients after gene therapy for SCID-X1. *Science* 2003;**302**:415-419.
121. Jessup M, Greenberg B, Mancini D, Cappola T, Pauly DF, Jaski B, Yaroshinsky A, Zsebo KM, Dittrich H, Hajjar RJ, Calcium Upregulation by Percutaneous Administration of Gene Therapy in Cardiac Disease I. Calcium Upregulation by Percutaneous Administration of Gene Therapy in Cardiac Disease (CUPID): a phase 2 trial of intracoronary gene therapy of sarcoplasmic reticulum Ca2+-ATPase in patients with advanced heart failure. *Circulation* 2011;**124**:304-313.
122. Jaski BE, Jessup ML, Mancini DM, Cappola TP, Pauly DF, Greenberg B, Borow K, Dittrich H, Zsebo KM, Hajjar RJ, Calcium Up-Regulation by Percutaneous Administration of Gene Therapy In Cardiac Disease Trial I. Calcium upregulation by percutaneous administration of gene therapy in cardiac disease (CUPID Trial), a first-in-human phase 1/2 clinical trial. *J Cardc Fail* 2009;**15**:171-181.
123. Zsebo K, Yaroshinsky A, Rudy JJ, Wagner K, Greenberg B, Jessup M, Hajjar RJ. Long-term effects of AAV1/SERCA2a gene transfer in patients with severe heart failure: analysis of recurrent cardiovascular events and mortality. *Circulation research* 2014;**114**:101-108.
124. Zincarelli C, Soltys S, Rengo G, Rabinowitz JE. Analysis of AAV serotypes 1-9 mediated gene expression and tropism in mice after systemic injection. *Mol Ther* 2008;**16**:1073-1080.
125. Pacak CA, Mah CS, Thattaliyath BD, Conlon TJ, Lewis MA, Cloutier DE, Zolotukhin I, Tarantal AF, Byrne BJ. Recombinant adeno-associated virus serotype 9 leads to preferential cardiac transduction in vivo. *Circ Res* 2006;**99**:e3-9.
126. Vogt CC, Bruegmann T, Malan D, Ottersbach A, Roell W, Fleischmann BK, Sasse P. Systemic gene transfer enables optogenetic pacing of mouse hearts. *Cardiovasc Res* 2015;**106**:338-343.
127. Nussinovitch U, Gepstein L. Optogenetics for in vivo cardiac pacing and resynchronization therapies. *Nat Biotechnol* 2015;**33**:750-754.
128. Vogt CC, Bruegmann T, Malan D, Ottersbach A, Roell W, Fleischmann BK, Sasse P. Systemic gene transfer enables optogenetic pacing of mouse hearts. *Cardiovasc Res* 2015;**106**:338-343.
129. Aravanis AM, Wang LP, Zhang F, Meltzer LA, Mogri MZ, Schneider MB, Deisseroth K. An optical neural interface: in vivo control of rodent motor cortex with integrated fiberoptic and optogenetic technology. *J Neural Eng* 2007;**4**:S143-156.
130. Alilain WJ, Li X, Horn KP, Dhingra R, Dick TE, Herlitze S, Silver J. Light-induced rescue of breathing after spinal cord injury. *J Neurosci* 2008;**28**:11862-11870.
131. Llewellyn ME, Thompson KR, Deisseroth K, Delp SL. Orderly recruitment of motor units under optical control in vivo. *Nat Med* 2010;**16**:1161-1165.
132. Towne C, Montgomery KL, Iyer SM, Deisseroth K, Delp SL. Optogenetic control of targeted peripheral axons in freely moving animals. *PLoS One* 2013;**8**:e72691.
133. Bryson JB, Machado CB, Crossley M, Stevenson D, Bros-Facer V, Burrone J, Greensmith L, Lieberam I. Optical control of muscle function by transplantation of stem cell-derived motor neurons in mice. *Science* 2014;**344**:94-97.
134. Liske H, Towne C, Anikeeva P, Zhao S, Feng G, Deisseroth K, Delp S. Optical inhibition of motor nerve and muscle activity in vivo. *Muscle Nerve* 2013;**47**:916-921.
135. Yaffe D, Saxel O. Serial passaging and differentiation of myogenic cells isolated from dystrophic mouse muscle. *Nature* 1977;**270**:725-727.
136. Blau HM, Pavlath GK, Hardeman EC, Chiu CP, Silberstein L, Webster SG, Miller SC, Webster C. Plasticity of the differentiated state. *Science* 1985;**230**:758-766.
137. Asano T, Ishizua T, Yawo H. Optically controlled contraction of photosensitive skeletal muscle cells. *Biotechnol Bioeng* 2012;**109**:199-204.

138. Sebille S, Ayad O, Chapotte-Baldacci CA, Cognard C, Bois P, Chatelier A. Optogenetic approach for targeted activation of global calcium transients in differentiated C2C12 myotubes. *Sci Rep* 2017;**7**:11108.
139. Asano T, Ishizuka T, Morishima K, Yawo H. Optogenetic induction of contractile ability in immature C2C12 myotubes. *Sci Rep* 2015;**5**:8317.
140. Sakar MS, Neal D, Boudou T, Borochin MA, Li Y, Weiss R, Kamm RD, Chen CS, Asada HH. Formation and optogenetic control of engineered 3D skeletal muscle bioactuators. *Lab Chip* 2012;**12**:4976-4985.
141. Raman R, Cvetkovic C, Uzel SG, Platt RJ, Sengupta P, Kamm RD, Bashir R. Optogenetic skeletal muscle-powered adaptive biological machines. *Proc Natl Acad Sci U S A* 2016;**113**:3497-3502.
142. Park SJ, Gazzola M, Park KS, Park S, Di Santo V, Blevins EL, Lind JU, Campbell PH, Dauth S, Capulli AK, Pasqualini FS, Ahn S, Cho A, Yuan H, Maoz BM, Vijaykumar R, Choi JW, Deisseroth K, Lauder GV, Mahadevan L, Parker KK. Phototactic guidance of a tissue-engineered soft-robotic ray. *Science* 2016;**353**:158-162.
143. Hernandez VH, Gehrt A, Reuter K, Jing Z, Jeschke M, Mendoza Schulz A, Hoch G, Bartels M, Vogt G, Garnham CW, Yawo H, Fukazawa Y, Augustine GJ, Bamberg E, Kugler S, Salditt T, de Hoz L, Strenzke N, Moser T. Optogenetic stimulation of the auditory pathway. *J Clin Invest* 2014;**124**:1114-1129.
144. Shao J, Xue S, Yu G, Yu Y, Yang X, Bai Y, Zhu S, Yang L, Yin J, Wang Y, Liao S, Guo S, Xie M, Fussenegger M, Ye H. Smartphone-controlled optogenetically engineered cells enable semiautomatic glucose homeostasis in diabetic mice. *Sci Transl Med* 2017;**9**.
145. Ye H, Daoud-El Baba M, Peng RW, Fussenegger M. A synthetic optogenetic transcription device enhances blood-glucose homeostasis in mice. *Science* 2011;**332**:1565-1568.
146. Park JH, Hong JK, Jang JY, An J, Lee KS, Kang TM, Shin HJ, Suh JF. Optogenetic Modulation of Urinary Bladder Contraction for Lower Urinary Tract Dysfunction. *Sci Rep* 2017;**7**:40872.
147. Lagali PS, Balya D, Awatramani GB, Munch TA, Kim DS, Busskamp V, Cepko CL, Roska B. Light-activated channels targeted to ON bipolar cells restore visual function in retinal degeneration. *Nat Neurosci* 2008;**11**:667-675.
148. Doroudchi MM, Greenberg KP, Liu J, Silka KA, Boyden ES, Lockridge JA, Arman AC, Janani R, Boye SE, Boye SL, Gordon GM, Matteo BC, Sampath AP, Hauswirth WW, Horsager A. Virally delivered channelrhodopsin-2 safely and effectively restores visual function in multiple mouse models of blindness. *Mol Ther* 2011;**19**:1220-1229.
149. Mace E, Caplette R, Marre O, Sengupta A, Chaffiol A, Barbe P, Desrosiers M, Bamberg E, Sahel JA, Picaud S, Duebel J, Dalkara D. Targeting channelrhodopsin-2 to ON-bipolar cells with vitreally administered AAV Restores ON and OFF visual responses in blind mice. *Mol Ther* 2015;**23**:7-16.
150. Sengupta A, Chaffiol A, Mace E, Caplette R, Desrosiers M, Lampic M, Forster V, Marre O, Lin JY, Sahel JA, Picaud S, Dalkara D, Duebel J. Red-shifted channelrhodopsin stimulation restores light responses in blind mice, macaque retina, and human retina. *EMBO Mol Med* 2016;**8**:1248-1264.
151. Sugano E, Isago H, Wang Z, Murayama N, Tamai M, Tomita H. Immune responses to adeno-associated virus type 2 encoding channelrhodopsin-2 in a genetically blind rat model for gene therapy. *Gene Ther* 2011;**18**:266-274.
152. Kim TI, McCall JG, Jung YH, Huang X, Siuda ER, Li Y, Song J, Song YM, Pao HA, Kim RH, Lu C, Lee SD, Song IS, Shin G, Al-Hasani R, Kim S, Tan MP, Huang Y, Omenetto FG, Rogers JA, Bruchas MR. Injectable, cellular-scale optoelectronics with applications for wireless optogenetics. *Science* 2013;**340**:211-216.
153. Montgomery KL, Yeh AJ, Ho JS, Tsao V, Mohan Iyer S, Grosenick L, Ferenczi EA, Tanabe Y, Deisseroth K, Delp SL, Poon AS. Wirelessly powered, fully internal optogenetics for brain, spinal and peripheral circuits in mice. *Nat Methods* 2015;**12**:969-974.
154. Scharf R, Tsunematsu T, McAlinden N, Dawson MD, Sakata S, Mathieson K. Depth-specific optogenetic control in vivo with a scalable, high-density muLED neural probe. *Sci Rep* 2016;**6**:28381.

155. Xu L, Gutbrod SR, Bonifas AP, Su Y, Sulkin MS, Lu N, Chung HJ, Jang KI, Liu Z, Ying M, Lu C, Webb RC, Kim JS, Laughner JI, Cheng H, Liu Y, Ameen A, Jeong JW, Kim GT, Huang Y, Efimov IR, Rogers JA. 3D multifunctional integumentary membranes for spatiotemporal cardiac measurements and stimulation across the entire epicardium. *Nat Commun* 2014;**5**:3329.
156. Gossler C, Bierbrauer C, Moser R, Kunzer M, Holc K, Pletschen W, Kohler K, Wagner J, Schwaerzle M, Ruther P, Paul O, Neef J, Keppeler D, Hoch G, Moser T, Schwarz UT. GaN-based micro-LED arrays on flexible substrates for optical cochlear implants. *J Phys D Appl Phys* 2014;**47:**205401.
157. Ideker RE, Chattipakorn TN, Gray RA. Defibrillation mechanisms: the parable of the blind men and the elephant. *J Cardiovasc Electrophysiol* 2000;**11**:1008-1013.
158. Dosdall DJ, Fast VG, Ideker RE. Mechanisms of defibrillation. *Annu Rev Biomed Eng* 2010;**12**:233-258.
159. KenKnight BH, Bayly PV, Gerstle RJ, Rollins DL, Wolf PD, Smith WM, Ideker RE. Regional capture of fibrillating ventricular myocardium. Evidence of an excitable gap. *Circ Res* 1995;**77**:849-855.
160. Sweeney RJ, Gill RM, Steinberg MI, Reid PR. Ventricular refractory period extension caused by defibrillation shocks. *Circulation* 1990;**82**:965-972.
161. Zipes DP, Fischer J, King RM, Nicoll Ad, Jolly WW. Termination of ventricular fibrillation in dogs by depolarizing a critical amount of myocardium. *Am J Cardiol* 1975;**36**:37-44.
162. Cheng Y, Mowrey KA, Van Wagoner DR, Tchou PJ, Efimov IR. Virtual electrode-induced reexcitation: A mechanism of defibrillation. *Circ Res* 1999;**85**:1056-1066.
163. Burton RAB, Klimas A, Ambrosi CM, Tomek J, Corbett A, Entcheva E, Bub G. Optical control of excitation waves in cardiac tissue. *Nat Photon* 2015;**advance online publication**.
164. Karathanos TV, Bayer JD, Wang D, Boyle PM, Trayanova NA. Opsin spectral sensitivity determines the effectiveness of optogenetic termination of ventricular fibrillation in the human heart: a simulation study. *J Physiol* 2016;**594**:6879-6891.
165. Bishop MJ, Rodriguez B, Eason J, Whiteley JP, Trayanova N, Gavaghan DJ. Synthesis of voltage-sensitive optical signals: application to panoramic optical mapping. *Biophys J* 2006;**90**:2938-2945.
166. Crocini C, Ferrantini C, Coppini R, Scardigli M, Yan P, Loew LM, Smith G, Cerbai E, Poggesi C, Pavone FS, Sacconi L. Optogenetics design of mechanistically-based stimulation patterns for cardiac defibrillation. *Sci Rep* 2016;**6**:35628.
167. Nyns ECA, Kip A, Bart CI, Plomp JJ, Zeppenfeld K, Schalij MJ, de Vries AAF, Pijnappels DA. Optogenetic termination of ventricular arrhythmias in the whole heart: towards biological cardiac rhythm management. *Eur Heart J* 2017;**38**:2132-2136.
168. Seyed Toutounchi SJ, Eydi M, Golzari SE, Ghaffari MR, Parvizian N. Vocal cord paralysis and its etiologies: a prospective study. *J Cardiovasc Thorac Res* 2014;**6**:47-50.
169. Zealear DL, Rainey CL, Netterville JL, Herzon GD, Ossoff RH. Electrical pacing of the paralyzed human larynx. *Ann Oto Rhinol Laryn* 1996;**105**:689-693.
170. Zealear DL, Dedo HH. Control of Paralyzed Axial Muscles by Electrical-Stimulation. *T Am Acad Ophthalmol* 1977;**84**:310-310.
171. Zealear DL, Billante CR, Courey MS, Sant'anna GD, Netterville JL. Electrically stimulated glottal opening combined with adductor muscle botox blockade restores both ventilation and voice in a patient with bilateral laryngeal paralysis. *Ann Oto Rhinol Laryn* 2002;**111**:500-506.
172. Zealear DL, Billante CR, Courey MS, Netterville JL, Paniello RC, Sanders I, Herzon GD, Goding GS, Mann W, Ejnell H, Habets AMMC, Testerman R, Van de Heyning P. Reanimation of the paralyzed human larynx with an Implantable electrical stimulation device. *Laryngoscope* 2003;**113**:1149-1156.
173. Mueller AH, Hagen R, Foerster G, Grossmann W, Baumbusch K, Pototschnig C. Laryngeal pacing via an implantable stimulator for the rehabilitation of subjects suffering from bilateral vocal fold paralysis: A prospective first-in-human study. *Laryngoscope* 2016;**126**:1810-1816.

174. Foerster G, Arnold D, Bischoff S, Boltze K, Scholle HC, Schubert H, Mueller AH. Pre-clinical evaluation of a minimally invasive laryngeal pacemaker system in mini-pig. *Eur Arch Oto-Rhino-L* 2016;**273**:151-158.
175. Cheetham J, Perkins JD, Jarvis JC, Cercone M, Maw M, Hermanson JW, Mitchell LM, Piercy RJ, Ducharme NG. Effects of Functional Electrical Stimulation on Denervated Laryngeal Muscle in a Large Animal Model. *Artif Organs* 2015;**39**:876-885.
176. van Bremen T, Send T, Sasse P, Bruegmann T. Spot light on skeletal muscles: optogenetic stimulation to understand and restore skeletal muscle function. *J Muscle Res Cell Motil* 2017.
177. Magown P, Shettar B, Zhang Y, Rafuse VF. Direct optical activation of skeletal muscle fibres efficiently controls muscle contraction and attenuates denervation atrophy. *Nat Commun* 2015;**6**:8506.

7. Publications

7.1 Research articles, Reviews and Editorials

1. **Improved heart repair upon myocardial infarction: Combination of magnetic nanoparticles and tailored magnets strongly increases engraftment of myocytes**
Annika Ottersbach, Olga Mykhaylyk, Alexandra Heidsieck, Dietmar Eberbeck, Sarah Rieck, Katrin Zimmermann, Martin Breitbach, Britta Engelbrecht, Tobias Brügmann, Michael Hesse, Armin Welz, Philipp Sasse, Daniela Wenzel, Christian Plank, Bernhard Gleich, Michael Hölzel, Wilhelm Bloch, Alexander Pfeifer, Bernd K. Fleischmann & Wilhelm Roell.
Biomaterials 2017; 10.1016/j.biomaterials.2017.11.012

2. **Spot light on skeletal muscles: optogenetic stimulation to understand and restore skeletal muscle function**
Tobias van Bremen T, Thorsten Send, Philipp Sasse* & Tobias Bruegmann*
Journal of Muscle Research and Cell Motility 2017; 10.1007/s10974-017-9481-9

3. **Frequency-dependent drug screening using optogenetic stimulation of human iPSC-derived cardiomyocytes**
Hendrik Lapp,* Tobias Bruegmann,* Daneila Malan, Stephanie Friedrichs, Carsten Kilgus, Alexandra Heidsieck & Philipp Sasse
Scientific Reports 2017;7:9629.

4. **Synchronization of excitable cardiac cultures of different origin**
Nadezda N. Agladze, Oleh V. Halaidych, Valeriya A. Tsvelaya, Tobias Bruegmann, Carsten Kilgus, Philipp Sasse & Konstantine I. Agladze 2017.
Biomaterials Science 2017; 10.1039/c7bm00171a.

5. **Optogenetic defibrillation terminates ventricular arrhythmia in mouse hearts and human simulations**
Tobias Bruegmann*, Patrick M. Boyle*, Christoph C. Vogt, Thomas V. Karathanos, Hermenegild J. Arevalo, Bernd K. Fleischmann, Natalya A. Trayanova & Philipp Sasse
Journal of Clinical Investigation 2016; 126:3894-3904

6. **Optogenetic control of contractile function in skeletal muscle**
Tobias Bruegmann, Tobias van Bremen, Christoph C. Vogt, Thorsten Send, Bernd K. Fleischmann & Philipp Sasse
Nature Communications 2015; 10.1038/ncomms8153

7. **Systemic gene transfer enables optogenetic pacing of mouse hearts**
Christoph C. Vogt*, Tobias Bruegmann*, Daniela Malan, Annika Ottersbach, Wilhelm Roell, Bernd K. Fleischmann & Philipp Sasse
Cardiovascular Research 2015; 106:338-343

8. **Optogenetic activation of G_q-signalling modulates pacemaker activity of cardiomyocytes**
Thomas Beiert, Tobias Bruegmann & Philipp Sasse
Cardiovascular Research 2014; 102:507-516.

9. **Optogenetic cardiac pacemakers: Science or fiction?**
Tobias Bruegmann & Philipp Sasse
Trends in Cardiovascular Medicine 2014; S1050-1738(14)00194-7

10. **Optogenetic control of heart muscle *in vitro* and *in vivo***
Tobias Bruegmann, Daniela Malan, Michael Hesse, Thomas Beiert, Christoph J. Fuegemann, Bernd K. Fleischmann & Philipp Sasse
Nature Methods 2010; 7: 897-900

*these authors contributed equally

7.2 Talks and Poster presentations

Talks:

Optogenetische Cardioversion/Defibrillation und optogenetischer Larynxschrittmacher: Warum, wie und was gibt es noch zu tun?
Innovationsforum Optogenetik, Hannover 2017

Optogenetic stimulation of muscle cells: Shining new light on (patho-) physiology and illuminating new treatment options
Fortbildungsveranstaltung der pädiatrische Kardiologie, Intensivmedizin und EMAH der MHH Hannover, 2017

Optogenetic termination of atrial fibrillation in the mouse heart
Annual Conference of the German Genetics Society, Bochum 2017

Optogenetic stimulation for the heart: Shining new light on (patho-) physiology and illuminating new treatment options
Seminar des Internationalen Graduiertenkollegs 1816, Göttingen 2017

Optogenetics in muscle cells: shining light on excitation of skeletal and cardiac muscle for laryngeal pacemaking, cardioversion and defibrillation
Veterinärmedizinisches Kolloquium der Universität Leipzig, 2017

Optogenetic stimulation of muscle cells: Shining new light on physiology and illuminating new treatment options
Award Lecture of the Du Bois-Reymond Prize, 96. Jahrestagung der Deutschen Physiologischen Gesellschaft 2017, Greifswald

Optogenetic termination of atrial fibrillation in the mouse heart
96. Jahrestagung der Deutschen Physiologischen Gesellschaft 2017, Greifswald

Optogenetic termination of atrial fibrillation in the mouse heart
Gordon Research Seminar on “Cardiac Arrhythmia Mechanisms” 2017, Ventura, USA

Optogenetic control of laryngeal muscles
Neurolaryngology workshop for experts, Jena 2016

Optogenetic termination of atrial fibrillation in the mouse heart
40th Official Meeting of the European Working Group on Cardiac Cellular Electrophysiology 2016, Glasgow, Schottland

Understanding and treating cardiac arrhythmia - from mice and goat to man
(zusammen mit Ulrich Schotten, Maastricht University),
95. Jahrestagung der Deutschen Physiologischen Gesellschaft 2016, Lübeck

Optogenetics in muscle cells: shining light on excitation and intracellular signaling of smooth, skeletal and cardiac muscle.
1st Workshop Brazil Germany Cardiac regeneration and electrophysiology 2014, Rio de Janeiro, Brasilien

Optogenetic defibrillation of ventricular tachycardia in the murine heart
4. Symposium der Jungen Physiologen, Leipzig

Optogenetics in cells and whole hearts
Cardiostim 2014, Nizza, Frankreich

Optogenetics in muscle cells: A new tool for light-induced depolarization in muscle cells
5th Basel muscle symposium on skeletal muscle 2013, Basel, Schweiz

Optogenetische Kontrolle über Gefäßkontraktion - Einsatz von Kanalrhodopsin 2 in glatter Muskulatur der Gefäße
1. Symposium der Jungen Physiologen 2011, Leipzig

Channelrhodopsin expression in cardiomyocytes: A new tool for light-induced depolarization with high spatio-temporal resolution *in vitro* and *in vivo*
40. Jahrestagung der DGTHG 2011, Stuttgart

Lichtinduzierte Depolarisation von Channelrhodopsin 2 exprimierenden Kardiomyozyten
BONFORsymposium 2010, Bonn

Channelrhodopsin expression in cardiomyocytes: A new tool for light-induced depolarization with high spatio-temporal resolution *in vitro* and *in vivo*
Joint Meeting of the Scandinavian and German Physiological Societies 2010, Kopenhagen, Dänemark

<u>Poster presentations:</u>

Frequency-dependent multi-well cardiotoxicity screening enabled by optogenetic stimulation
41st Meeting of the European Working Group on Cardiac Cellular Electrophysiology im Rahmen des EHRA Europace 2017, Wien, Österreich

Optogenetic termination of atrial fibrillation in the mouse heart
Gordon Research Conference on “Cardiac Arrhythmia Mechanisms” 2017
Ventura, USA

Terminating ventricular arrhythmia by optogenetic hyperpolarisation
ESC Congress 2016, Rom, Italien

Optogenetic defibrillation of ventricular tachycardia in the murine heart
Gordon Research Seminar and Conference: “Cardiac Arrhythmia Mechanisms” 2015, Lucca, Italien

Optogenetic control of skeletal muscle: a new method to treat laryngeal paralysis
93. Jahrestagung der Deutschen Physiologischen Gesellschaft 2014, Mainz

Optogenetic stimulation of skeletal muscles
Biophysical Society 58th Annual Meeting 2014, San Francisco, USA

Optogenetic control of vascular tone with high temporal resolution
Biophysical Society 57th Annual Meeting 2013, Philadelphia, USA

Optogenetics in cardiovascular research: a new tool for light-induced depolarization of cardiomyocytes and vascular smooth muscle cells *in vitro* and *in vivo*
ESC Congress 2011, Paris, Frankreich

Optogenetic control of vascular contraction
90. Jahrestagung der Deutschen Physiologischen Gesellschaft 2011, Regensburg

Light-induced depolarization to stimulate cardiomyocytes with high spatio-temporal resolution and to modulate their differentiation *in vitro*
Biophysical Society 54th Annual Meeting 2010, San Francisco, USA

8. Danksagung

Mein besonderer Dank gilt meinem Doktorvater Professor Philipp Saße für die intensive Betreuung und das Vertrauen in meine Fähigkeiten. Ich danke Ihm vor allem dafür, dass ich meine eigenen Ideen verwirklichen konnte und für die erfolgreiche Zusammenarbeit über die vielen Jahren seit meinem ersten Praktikum im Februar 2008. Bei Professor Bernd K. Fleischmann möchte ich mich für seine Unterstützung und wertvolle Beratung während der ganzen Zeit bedanken. Des Weiteren bedanke ich mich bei meinem Zweitbetreuer Professor Klaus Mohr, der die Verantwortung der Betreuung gegenüber der naturwissenschaftlichen Fakultät übernommen hat, und bei Professorin Christa Müller und Professor Stefan Herlitze, die sofort zugestimmt haben, der Prüfungskommission beizusitzen.

Bei dem Graduiertenkolleg 1873 und insbesondere dessen Vorsitzenden Professor Alexander Pfeifer sowie dem BONFOR Förderprogramm bedanke ich mich für die finanzielle Unterstützung. Dabei möchte ich besonders hervorheben, dass beide Seiten von Anfang an der Idee einer naturwissenschaftlichen Promotion eines Humanmediziners offen gegenüber gestanden haben und diese gefördert haben. Ohne diese Förderung wäre diese Dissertation sicher nicht zu Stande gekommen.

Für die Verwirklichung der beiden Projekte war die Zusammenarbeit mit Dr. med. Tobias van Bremen, Dr. med. Thorsten Send, PD Dr. med. Andreas Schröck und Professor Friedrich Bootz aus der Klinik für Hals-/Nasen/Ohrenheilkunde und Chirurgie und Dr. Patrick Boyle, Thomas Karathanos und Professorin Natalya Trayanova vom Johns Hopkins Institut essentiell. Ich bedanke mich für die zahlreichen interessanten Diskussionen und ihren wissenschaftlichen Input. Ein ganz herzlicher Dank geht an alle aktuellen und ehemaligen Labormitglieder, mit denen ich zusammengearbeitet habe, für die Hilfe, das angenehme Arbeitsklima und die gute Zusammenarbeit. Ich möchte hier besonders Dr. rer. nat. Daniela Malan, Christoph Vogt und Frank Holst hervorheben, die nicht nur tolle Kollegen waren, sondern auch entscheidend zu den Projekten beigetragen haben.

Besonders dankbar bin ich auch meiner Familie. Meine Frau Grethe muss viel Verständnis für den hohen Zeitaufwand inklusive der zahlreiche Reisen aufbringen und hat mich trotzdem in allen Phasen dieser Arbeit unterstützt und motiviert. Mein besonderer Dank gilt meinen Eltern, auf die ich mich immer verlassen kann und die mich in meinem Werdegang bedingungslos unterstützt und gefördert haben. Außerdem möchte ich meinen Großvater Dr. med. Dr. rer. nat. Eberhard Brügmann erwähnen, der mit seinen zwei Doktortiteln als Vorbild gedient hat, aber leider meine beiden Promotionen nicht mehr miterleben kann.